Models for adaptive feeding and population dynamics in plankton

Sofia Piltz

Linacre College

University of Oxford

A thesis submitted for the degree of

Doctor of Philosophy

Trinity Term 2014

Acknowledgements

First and foremost, I would like to thank Mason and Philip for all their advice, assistance, and guidance, I have had the best combination of supervisors I could have ever imagined. I am grateful to all those who have helped me with the work in this thesis, and to the Osk. Huttunen Foundation and the Life Sciences Interface Doctoral Training Centre for their financial support. In particular, I am grateful to Mike Jeffrey, Chris Klausmeier, Christian Kuehn, Øystein Varpe, and Frits Veerman for numerous helpful discussions and comments. I would also like to thank Ursula Gaedke for useful discussions and sending us the data. I would like to express my special thanks to Elspeth Garman for her help and support. Finally, I owe a debt of gratitude to Azim, Francis, Mikko, Philip, Stephen, and ä&i for their unwavering encouragement.

Abstract

Traditionally, differential-equation models for population dynamics have considered organisms as "fixed" entities in terms of their behaviour and characteristics. However, there have been many observations of adaptivity in organisms, both at the level of behaviour and as an evolutionary change of traits, in response to the environmental conditions. Taking such adaptiveness into account alters the qualitative dynamics of traditional models and is an important factor to be included, for example, when developing reliable model predictions under changing environmental conditions. In this thesis, we consider piecewise-smooth and smooth dynamical systems to represent adaptive change in a 1 predator-2 prey system.

First, we derive a novel piecewise-smooth dynamical system for a predator switching between its preferred and alternative prey type in response to prey abundance. We consider a linear ecological trade-off and discover a novel bifurcation as we change the slope of the trade-off. Second, we reformulate the piecewise-smooth system as two novel 1 predator-2 prey smooth dynamical systems. As opposed to the piecewise-smooth system that includes a discontinuity in the vector fields and assumes that a predator switches its feeding strategy instantaneously, we relax this assumption in these systems and consider continuous change in a predator trait.

We use plankton as our reference organism because they serve as an important model system. We compare the model simulations with data from Lake Constance on the German-Swiss-Austrian border and suggest possible mechanistic explanations for cycles in plankton concentrations in spring.

Contents

List of Figures

Chapter 1

Introduction

1.1 Overview

1.1.1 Models of predator-prey population dynamics

The modelling of predator-prey dynamics is a long-established subdiscipline in mathematical biology [97]. Indeed, mathematical biology is often introduced with an example describing biomass or population density growth on resources. Since the pioneering Lotka-Volterra equations for the temporal evolution of interacting predator and population densities [85, 137], exploiter-resource interactions described via coupled systems of differential equations have also provided a versatile modelling approach for applications other than ecology [57]. These examples include epidemiological models for the interaction between immune system and viruses, or infectious and susceptible populations [13].

The Lotka-Volterra system was originally developed to explain the oscillatory behaviour of observed fish catches or of chemical concentrations in a chemical

reaction system [85,137]. For predator (z) and prey (p) density, the Lotka-Volterra model [85, 137] is given as follows:

$$\begin{aligned} \frac{dp}{dt} &= rp - \beta pz, \\ \frac{dz}{dt} &= e\beta pz - mz, \end{aligned} \tag{1.1}$$

where r is the growth rate of the prey, β is the death rate of the prey due to predation, e is the predator *conversion efficiency* (which describes what proportion of the prey eaten by the predator yields predator growth), and m is the predator death rate. The Lotka-Volterra model (1.1) exhibits periodic solutions for predator and prey populations. However, these solutions are not stable, in that a small perturbation from one solution can result in a huge difference in the amplitude of the oscillations. Although it is unrealistic, the Lotka-Volterra model has been useful for studying the mechanisms behind oscillatory population behaviour, thereby suggesting further directions to acquire deeper understanding of the observed phenomena [97].

In 1963, Rosenzweig and MacArthur introduced a modified version of the Lotka-Volterra model with logistic prey growth and a saturating predation term [109]:

$$\begin{aligned} \frac{dp}{dt} &= rp\left(1 - \frac{p}{K}\right) - c\frac{p}{p + k_p}z, \\ \frac{dz}{dt} &= ec\frac{p}{p + k_p}z - mz, \end{aligned} \tag{1.2}$$

where K is the prey carrying capacity, c is the maximum consumption rate, and k_p is the half-saturation constant for consumption (i.e., the concentration of p at which the predation rate of z reaches half of its maximum value). The Rosenzweig-

MacArthur model reproduces two types of behaviour: coexistence of predator and prey at a steady state and predator-prey stable limit cycles—periodic orbits in the predator-prey phase plane from which small perturbations tend to zero as time $t \to \infty$. Thus, the amplitude of the predator-prey cycles is independent of the initial conditions (unlike in the Lotka-Volterra model). We discuss these two models (1.1) and (1.2), and how they have been used to explain observed plankton dynamics in Section 1.3.1.

1.1.2 Models for population dynamics and adaptive feeding

The systems of equations (1.1) and (1.2) describe the population dynamics of organisms that are represented as "fixed entities"—that is, with constant (or periodically varying, as we discuss in Section 1.3.1) parameter values and fixed feeding behaviour. In addition, typical models of predator-prey interaction consider the time scale of adaptive change in traits, such as defence strategies against predators, to be extremely long compared to the time scale of the predator-prey interactions. However, there is increasing evidence that organisms can adapt to changing environmental conditions, such as prey availability, predation risk or temperature. They thus exhibit both *phenotypic plasticity*, in which the same genotype can express different phenotypes depending on the environment (see [63] for different definitions of phenotypic plasticity), and rapid adaptive change of traits [38], which are properties that affect how well an individual performs as an organism [91]. More experimental and observational studies are needed to determine the interactions between the two different forms of adaptation and ecological in-

teractions and mathematical modelling can play an important role in explaining the dependencies between adaptation and ecological dynamics [38].

Adaptive feeding behaviour can be incorporated into a smooth dynamical system by considering a more sophisticated functional response than in (1.1) or (1.2) (see Section 1.4), whereas adaptive change of traits has been previously implemented in models of population dynamics by representing a trait value as a system variable instead of as a parameter (see Section 1.3.2). However, there are problems with these two approaches. First, it is not clear which smooth functional response best describes adaptive feeding or adaptive change of traits. Second, considering traits as system variables increases the dimensionality of the system. Consequently, the analysis of the resulting system can become increasingly challenging when more species or other aspects, such as trade-offs between traits, are taken into account. This is problematic for a full analysis of the resulting equations, which may be necessary to provide a deep mechanistic understanding of the dynamical behaviour exhibited by the model. This mechanistic understanding can then be used in developing models with predictive power.

In this thesis, we consider an alternative dynamical systems approach—that is, *piecewise-smooth dynamical systems*—to include adaptive feeding, manifested as a change in behaviour or a functional trait, into models for predator-prey population dynamics. We do not expect the analysis in this alternative framework to be any less challenging than that of a typical model for predator-prey interaction (i.e., such as (1.1) or (1.2) constructed for more than one predator-prey pair) that takes adaptivity into account. However, to maximise analytical tractability, we start from the simplest case and construct the piecewise-smooth dynamical system that describes adaptive feeding between a predator and two prey. We choose two prey

in order to model adaptive feeding interaction between a predator and multiple prey with the lowest possible dimension. We investigate how adaptive feeding can be modelled within this framework, which is not as common as smooth dynamical systems in theoretical ecology. Nevertheless, it has considerable potential utility for modelling adaptivity in predator-prey interaction (see Section 1.4). In the second part of this thesis, we reformulate the piecewise-smooth system as a smooth dynamical system in two different ways. Piecewise-smooth and their smooth analogs are related to one another, however, there does not yet exist a standard theory for transiting between them. Thus, we aim to, not only increase the understanding of the underlying mechanisms behind adaptivity and population dynamics, but also contribute to the knowledge of the relation between a piecewise-smooth system and its smooth analog constructed by using either hyperbolic tangent functions or adding an extra dimension to the system.

1.1.2.1 Piecewise-smooth dynamical systems

Piecewise-smooth dynamical systems are a class of discontinuous systems—they describe behaviour using smooth evolution of variables alternating with abrupt events [15, 23]. These events can be caused by friction, collisions, impacts, or by components such as relays that make a system switch from one behaviour to another in a short time [23]. In addition to such engineering applications, piecewise-smooth dynamical systems have also been used in some applications in biology. In theoretical ecology, piecewise-smooth dynamical systems have given insight into adaptive feeding of an optimal forager that maximises its growth [70, 74–77]. Piecewise-smooth dynamical systems have also been used to describe limitations

on harvesting a species when it is rare [22, 73], different behavioural stages of ruminants [122], and to approximate a sigmoid function in gene regulatory networks [14,45] or a Heaviside function in the behaviour of ion channel gates [5]. We discuss previous studies of piecewise-smooth predator-prey models with adaptive feeding in Section 1.4.2.

1.1.3 Plankton as a model system

We have chosen plankton as our example organism for models of predator-prey interaction and adaptive feeding for the following principal reasons. Plankton are small but important organisms with a short lifespan. These characteristics make it possible to obtain field and experimental data on plankton. Because plankton have a large population size and are often found in the well-mixed upper part of the water column [78], one can study the temporal/spatiotemporal evolution of plankton distribution using a continuum description and deterministic ordinary or partial differential equations (ODE or PDE) models. In addition, plankton have considerable diversity, which motivates the use of community-integrated parameters instead of species-specific parameters [93] and thereby models based on low-dimensional differential equations. However, similar models can also be formulated for any other predator-prey interaction in which it is viable to assume a large population size, well-mixed environment, and the use of community-integrated parameters.

A simple and intuitive phytoplankton-zooplankton food web with a diverse community of species enables a comparison between the model result and the observed data, which in turn helps to assess the validity and suitability of the model.

Accordingly, plankton food webs can serve as model systems for larger and more complex ecosystems. Moreover, studying plankton populations can yield results that are applicable to other complex systems [83]. For example, universal indicators of critical shifts in system behaviour, such as species extinction or economic collapse, have been studied by using plankton populations as the example system [24]. Indeed, the understanding of the dynamics of ecological food webs can be used directly in quantitative economics by developing analogous models for "financial ecosystems" to give more insight into the stability of a network composed of complex financial instruments that are operated by individual banks and investment funds [51].

1.2 Plankton data

1.2.1 A short introduction to plankton

Plankton are aquatic organisms varying from less than 0.2 μm to over 2 cm in size that are principally transported by currents. They are thus "planktonic"[1]. Phytoplankton (from 0.2 μm to 2 mm in size) produce organic compounds from inorganic compounds. They are analogous to land plants: they photosynthesise and require CO_2, sunlight, and nutrients for growth. The required nutrients are supplied from river outputs or deeper waters and are transported by tides, wind, mixing and upwelling, which are influenced by water temperature [78].

Phytoplankton contribute less than 1% of the Earth's photosynthetic biomass

[1]The word *plankton* comes from the Greek adjective for "wandering". We have chosen to follow this generally accepted convention instead of *planktic*, which is the correct adjective.

but are responsible for roughly half of the Earth's net production of organic compounds [27] and half of the Earth's carbon fixation [107]. Thus, they have a biogeochemically important role in the Earth's carbon cycle. Because plankton are sensitive to the conditions in their environment (e.g., an increase in water temperature affects the ability of phytoplankton to capture CO_2 [107]), they function as an indicator of the health and environmental change of the seas [24, 25, 78]. Phytoplankton can cause harmful algal blooms, which range in classification from non-toxic nuisance to high toxicity to humans and marine organisms. They thus impact both aquaculture and tourism [107].

Phytoplankton and the zooplankton (i.e., small crustaceans and marine worms and juvenile forms of larger animals, such as crabs, fish, or starfish) that graze upon them constitute the basis of aquatic food webs. Thus, the abundance, species composition, and timing of plankton blooms affect the abundance of other organisms on higher levels of aquatic food webs—all the way up to fish and marine mammals [25,78]. A crucial link in this chain of energy transportation from the bottom to the top are *ciliates*—that is, small eukaryotic single cells with animal-like behaviour that propel themselves using an undulating movement that is generated by small hair-like protuberances (called *cilia*)—that feed on small phytoplankton and are grazed by small zooplankton [78]. Thus, studying predator-prey dynamics in plankton is important for decision-making in the fishing industry and for the world's fish production [25], of which 80% is consumed by humans. Fish production is a globally important factor for ensuring food security and provides livelihood for more than 600 million people [30].

Recent studies based on processing and analysis of historical data sets arrived at contradictory conclusions documenting both a decline [12] and an in-

crease [87, 92, 110] in phytoplankton growth in warm seas. The disagreement was reported widely in the media [9,108] and reflects not only the importance of reliable long-term data collection but also the scientific insufficiency of relying only on descriptive studies without the modelling of underlying mechanisms. Turning conceptual ideas such as the adaptive feeding behaviour in a phytoplankton-zooplankton food web into mathematical models leads to quantitative understanding that can be used to (1) explain mechanisms underlying the observed behaviour, (2) assess the importance of each of these mechanisms, (3) propose experiments to test hypotheses, (4) predict how system behaviour changes under perturbations such as climate change, and (5) adjust decisions that directly or indirectly affect aquatic ecosystems. Because of the important role that plankton play in climate change, and especially in the aquatic food chain, increased qualitative and quantitative understanding of plankton dynamics is crucial for directing policy [25, 107].

1.2.2 Lake Constance data

In Section 3.4.7, we will compare our model simulations with data from observations for ciliate-predators and their algal prey collected from Lake Constance on the German-Swiss-Austrian border [125, 127]. These data, which were provided by Prof. Ursula Gaedke (University of Potsdam, Germany), are an observational data set for phytoplankton, small eukaryotic organisms that feed on phytoplankton, and herbivorous and carnivorous zooplankton collected between 1979 and 1999. Situated in the northern Alps, Lake Constance is a freshwater lake with a surface area of 536 km^2. It has been under scientific study for decades, and hourly records for weather conditions—such as temperature, surface irradiance,

and wind speed—have been collected since 1979. In addition to such abiotic factors, weekly data on biomass of several phytoplankton and zooplankton species are also available [6].

The Lake Constance data refer to abundance (individuals or cells per ml) and biomass (units of carbon per m^2) of a species obtained at least once in a sample of a few ml to a litre of water in Lake Constance between March 1979 and December 1999. When unavailable, the abundance or the biomass were calculated from each other using size of the species as a conversion factor [125, 127]. Each sample was collected from a water column with an area of 1 m^2 and a depth of 20 m. The full data set includes over 23,000 observations of 205 different phytoplankton species.

As we discuss in Section 1.3, the Plankton Ecological Group (PEG) model describes verbally the relative importance of forces (i.e., abiotic, top-down, or bottom-up control mechanisms) that drive the observed seasonal patterns in plankton biomass. According to the PEG model, in a lake with only a few nutrients, nutrient limitation is a more important regulator of algal growth than predation. In contrast, in a lake with a large quantity of nutrients, predation has been suggested to control phytoplankton growth more than nutrient limitation [116, 117]. In its natural state, Lake Constance would be categorised as a lake with a low level of productivity if there were no excess nutrients from agricultural and other sources of human population in its catchment area. Lake Constance was categorised as a lake with an intermediate level of productivity (as measured in terms of abundance of nutrients such as nitrogen and phosphorus) when the data were collected [128]. However, the increased sewage-water treatment since 1979 has reduced the amount of nutrients that enter Lake Constance. Nowadays, Lake Constance is once again categorised as a lake with a low level of productivity [36].

In addition to the well-documented plankton seasonal cycle (i.e., increase in biomass in spring and decay in autumn; see Section 1.3), field observations of plankton in Lake Constance indicate that predators and multiple prey species coexist in spring when biomasses are high and the external conditions can be considered to be stable. Importantly, ciliates and their algal prey populations also vary at shorter-than-seasonal scales. The biomass and the properties at the community level have been observed to fluctuate less than those at the level of individual species. During years, such as 1991 and 1998 (see the data for two selected ciliate-predators and a group of their algal prey species in Figure 1.1), when the spring bloom lasts for several weeks (equivalent to 15 to 30 ciliate generations), phytoplankton and ciliate biomasses exhibit recurring patterns of increases followed by declines [126]. It has been suggested that a relatively constant community biomass, but highly variable biomasses of different species populations, results from alternation in the number of predator and prey groups of different functionality present at different times [128]. The different functionality can be manifested, for example, as different predator feeding preferences or predation mechanisms. Additionally, both predator and prey species can adapt to the prevailing situation by changing their diet [128].

There is experimental evidence of prey preference and selective feeding in predator behaviour in a laboratory experiment on ciliate-predator and phytoplankton-prey species found in Lake Constance [94]. Such adaptive feeding has been suggested to occur because different ciliate species benefit differently depending on the match between their feeding mode and the prey species that are abundant in the prey community. In the experiment, as well as in the field, ciliates have been observed to actively select against certain types of prey [128]. As a result, it has been suggested that the driving forces for the subseasonal temporal variability

observed in ciliate-algal dynamics lie in predator-prey interactions between diverse predator and prey plankton communities, particularly during periods of the year in which environmental conditions are relatively settled [128]. We discuss previous approaches to model adaptive feeding behaviour in predator-prey systems in Section 1.4.

Ciliates are known to have different modes of predator behaviour, and they can be categorised roughly in terms of being more or less selective [136]. To illustrate a predator that is more selective, some ciliate species such as *Balanion planctonicum* (see magenta asterisks in Figure 1.1) hunt as "interception feeders" that scavenge on food particles and intercept them directly. By contrast, ciliate "filter feeders", such as *Rimostrombidum lacustris* (see red asterisks in Figure 1.1), sieve suspended food particles and provide an example of less selective predators. Consequently, the prey community, on which the ciliate-predators feed, can roughly be divided into easily digested (i.e., preferred prey; see blue circles in Figure 1.1) types and less edible (i.e., alternative prey; see black circles in Figure 1.1) types on which ciliates feed but select against when offered a mixed diet of both easily digested and less edible prey [94]. Small diatoms (which are one of the most common phytoplankton species [80]), such as *Stephanodiscus parvus* (which have a hard silicate cover), or small and medium-size flagellates, such as Chlamydomonas *spp.* (i.e., green algae with two hair-like protuberances (called *flagella*) [80]), can be considered as the less edible prey type for ciliate-predators. By contrast, cryptomonads (a group of small algae [80]) can be related to the preferred prey type [128]. In addition, diatoms, flagellates, and cryptomonads are the dominant species groups in the phytoplankton community during spring bloom [126].

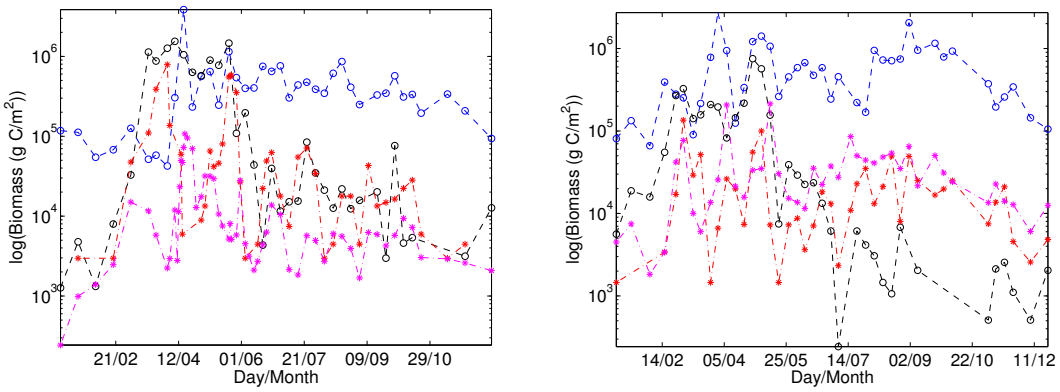

Figure 1.1: Biomass data for (asterisks) two ciliate-predator and (circles) two algal prey groups in Lake Constance in (left) 1991 and (right) 1998. During these years, the spring bloom lasted for several weeks (i.e., for 15 to 30 ciliate generations), and phytoplankton and ciliate biomasses exhibit recurring patterns of increases followed by declines [126]. Red denotes the unselective (i.e., filter feeder) predator group and is composed of data for *Rimostrombidum lacustris*, while magenta denotes the selective (i.e., interception feeder) predator group and is represented by data for *Balanion planctonicum*. Blue denotes the preferred (i.e., easily digested) prey group and is composed of data for *Cryptomonas ovata*, *Cryptomonas marssonii*, *Cryptomonas reflexa*, *Cryptomonas erosa*, *Rhodomonas lens*, and *Rhodomonas minuta*. Black denotes the alternative (i.e., less edible) prey group and is composed of data for small and medium-size *Chlamydomonas* spp. and *Stephanodiscus parvus*. These data, which were previously reported in [125, 127], were provided by Ursula Gaedke.

1.3 Models for the onset and succession of plankton blooms

Plankton form a community of high diversity, with different species present at different times and in different places [27, 78]. Plankton seasonal succession—that is, the sequence of different species appearing, disappearing, and reappearing—in fresh water systems is described verbally in the Plankton Ecological Group (PEG) model [117]: A rapid growth of diatoms (e.g., one of the three principal eukaryotic phytoplankton groups that have a silicate cover [27]) in spring is followed by extensive zooplankton predation and nutrient depletion. In summer, zooplankton decrease and diatoms are replaced by flagellates (e.g., eukaryotic phytoplankton that are armoured with cellulose plates and have tail-like flagella that propel the cell). In winter, both phytoplankton and zooplankton populations are low due to decreased light availability and low temperature [117]. The driving forces for such a succession are physical factors and internal dynamics of the food web, such as top-down control from higher levels or bottom-up control from lower levels of the web. For example, for phytoplankton, these control mechanisms correspond to predation by herbivorous zooplankton (top-down) and nutrient limitation (bottom-up) [78, 117].

1.3.1 Modifications of the Lotka-Volterra (1.1) and Rosenzweig-MacArthur (1.2) models

The Lotka-Volterra and Rosenzweig-MacArthur predator-prey models (in Equations (1.1) and (1.2), respectively) have inspired several extensions and modifications to explain the onset of plankton blooms and plankton seasonal succession using systems of coupled ODEs or PDEs. Modelling work suggests that both top-down and bottom-up mechanisms regulate the onset of a plankton bloom. In the former approach, the phytoplankton-zooplankton food web is considered as a nonlinear *excitable system* [130][2], where both an increase in the phytoplankton growth rate and in the initial density can perturb the system into a bloom that is controlled by zooplankton grazing (i.e., a top-down factor) [130]. In the latter approach, a bloom is triggered as the level of nutrients (i.e., the bottom-up control mechanism) exceeds a certain threshold [59]. However, it is unclear if it is feasible to draw a strong conclusion about the relative importance of the regulation mechanisms from such a simplified model without testing alternative hypotheses, such as phytoplankton competition and nutrient excretion by zooplankton [135].

To reproduce the plankton seasonal cycle, the top-down [130] and bottom-up [59] regulation mechanisms for the onset of a bloom have been extended to seasonally forced predator-prey models in [58] and [35,40], respectively. In addition, a multispecies system governed by a seasonally forced Rosenzweig-MacArthur model can reproduce the succession of different plankton species that occur seasonally and have variations in the species composition between different years. This has

[2] An excitable system possesses stable equilibria. Once the system is perturbed, the behaviour of these equilibria depends on the magnitude and nature of the perturbation. Importantly, an *excitable medium* is able to support a solitary excitation wave, return to its initial state, and generate a subsequent excitation after a certain amount of time has passed [97].

also been observed in data [20]. Moreover, seasonal succession of a phytoplankton bloom followed by a zooplankton peak has been observed to follow a latitudinal gradient (i.e., in temperate zones, there is a spring and an autumn bloom each year, whereas only one bloom appears in spring in the arctic [19]). The influence of the latitudinal gradient on plankton seasonal succession was studied in [103], where a forcing function was constructed from chlorophyll data collected by remote sensing. This model reproduced the more complex seasonal cycles of phytoplankton blooms in southern latitudes compared to northern latitudes [103]. In addition, a discrete approach, in which the observed annual cycle for plankton is divided into two distinctive intervals—the "good" season (i.e., when predator-prey dynamics are governed by a Rosenweig-MacArthur model) and the "bad" season (i.e., when both the predator and the prey experience exponential decay)—predicted that a longer good season would increase the chance of predator and prey coexisting and the peaks in population densities to appear early [65], which is in agreement with data from laboratory experiments [119].

As concerns lake environments, seasonality modelled as periodically varying parameters in a phytoplankton-zooplankton-fish system can generate the seasonal plankton pattern observed in lakes [111]. The model in [111], like many of the models presented above, makes unrealistic assumptions concerning the role of nutrient depletion in phytoplankton collapse after the bloom. In addition, the authors include seasonal forcing in the model using a sinusoidal periodic function that has the same phase and amplitude for parameters which represent rather different aspects of the model. Most importantly, the model deviates from observations, especially in the amplitude of the population oscillations [111].

1.3.2 Different modelling approaches for grouping similar plankton species together

Because plankton have high diversity (there are approximately $25,000$ morphologically defined forms of phytoplankton [27]), there have been several approaches to group similar species together to model plankton in oceanography. These include nutrient-phytoplankton-zooplankton (NPZ) [26] or nutrient-phytoplankton-zooplankton-detritus (NPZD) models [28], in which species that consume the same resources (i.e., that are on the same trophic level) are grouped together (see [33] for a review). To account for the high diversity in phytoplankton for their functioning as a biological pump for cycling CO_2 [27], different phytoplankton in plankton functional type (PFT) models are grouped together according to the similarity of their biogeochemical roles. PFT models are better than NPZ models at accounting for the diversity of the species composition, but they require reliable parameter values [55] that might not be yet known for every included species [4, 81].

Traits are properties of an organism that can be measured from individuals and compared against measurements from individuals in other species. For example, phytoplankton have traits that characterise their maximum growth or photosynthesis rate, their size, or their susceptibility to predation. Traits can also be constructed as functional traits because they affect how well an individual performs as an organism [91]. Additionally, performance in ecological function is constrained by limited resources. An organism that invests more energy in predation-defence mechanisms cannot invest as much energy in growth or other facets. This is an example of an ecological *trade-off*. In an environment that changes seasonally, trade-offs yield different optimal periods of time for different species. Thus, tem-

poral variation of environment and trade-offs result not only in species coexistence amidst limited resources but also in temporal variation exhibited within a community [66,84], such as cycles between ciliate-predators and their phytoplankton-prey during spring in Lake Constance (see Figure 1.1).

The coexistence of competing plankton species at high biomasses is one of the key phenomena observed in plankton that has been difficult to model [128]. Despite a dynamical-system analysis that can give a simple rule for checking whether a model exhibits coexistence [18], NPZ and PFT models are both examples of models of population dynamics that can easily become very complex. In particular, it can be difficult to experimentally determine parameter values and retain analytical tractability as more species or groups of species are added. As an alternative, trait-based models, in which plankton species that have similar traits are grouped together, provide an approach to study coexistence of species by keeping a model sufficiently simple while preserving the diversity of the species composition [91].

Because of the high diversity in phytoplankton species communities, phytoplankton can be studied using a trait-based modelling approach. In theory, this makes it possible to derive general principles of *community ecology*, which is the study of coexisting species at a certain time in a given place [91] (see [83] for review). In trait-based models, a community of species is usually represented by a continuous trait distribution. The mean trait value and the variance indicate, respectively, the characteristics of the most abundant species and the diversity present in a community. In this way, one gathers information on how the total biomass behaves instead of knowing what happens to a particular species [91]. The trait-value distribution is affected by factors such as the surrounding environmental conditions and species interaction (e.g., competition and predation) [91]. For

example, an increase in temperature can yield a shift in the species composition as species better suited to the new governing conditions become more abundant. This also justifies considering traits as state variables to account for their dynamic characteristics, as has been done in [93].

1.4 Models for population dynamics and adaptive feeding

As we discussed in Section 1.2.2, it has been suggested that the coexistence and variability in biomasses of different plankton species in spring results from the alternation in the number of predator and prey groups of different functionality, which manifests, for example, as different predator feeding preferences [128]. Additionally, both predator and prey species can adapt to the prevailing situation by changing their diet [128]. In the simplest case of a predator and two prey, two prey species (with limited growth) can coexist if they share a predator [54]. However, a standard Lotka-Volterra model for one predator and two prey (with unlimited prey growth) that allows diversity in the prey community, predicts extinction of the prey type that has a smaller capacity to survive [68]. Therefore, such a framework is inappropriate for investigations of ciliate-phytoplankton dynamics during spring, when predator-prey interaction—rather than nutrient limitation—seems to govern plankton dynamics [116, 128], and several predators and prey coexist. One way to resolve this discrepancy is to examine adaptive predator behaviour in response to changes in prey densities.

1.4.1 Prey switching

In ecology, *prey switching* refers to a predator's adaptive change of habitat or diet in response to prey abundance. In a system with at least one predator and multiple prey, prey switching is a way to describe the situation in which a predator expresses preference for more abundant prey [95]. However, in a 1 predator-1 prey system, prey switching refers to a change in predation as opposed to a predator alternating between different prey types. In smooth differential-equation models, such a change in predation of one type of prey can be modelled by, for example, using a Holling type-III functional response [53], in which predation is low at low prey densities but saturates quickly at a high value when prey is abundant. Such a functional response was observed in a system of protist (i.e., eukaryotic single cells with animal-like behaviour) predators and their yeast prey [42]. By considering a case with a predator and multiple prey, one can explicitly examine predator preference towards more abundant prey by constructing models in which the densities of the different prey are system variables. It has been demonstrated that prey switching can promote coexistence of competing prey species [124] or decrease prey competition due to a shared predator [2]. In addition, a prey-switching approach has been used when switching is independent of total prey density [104], for density-dependent switching [3], and using information on which prey type was last consumed when there are two [134] or more [133] prey. The result that flexible predator feeding behaviour affects the complexity and stability of food webs raises the question of why food networks with large numbers of species and complicated feeding or grazing interactions between them are commonly observed in nature, even though standard ecological theory suggests that they should not

persist (see [67] and references therein). Therefore, it has been suggested that adaptive prey-switching in a food web composed of several species is an important subject for research on modelling food webs [138].

1.4.2 Piecewise-smooth dynamical systems for prey switching

An alternative approach to studying prey switching is to posit that predators behave as *optimal foragers* instead of explicitly incorporating adaptive predator behaviour in response to changing prey densities. According to *optimal foraging theory*, a predator's choice to switch prey depends on prey abundances and which diet composition maximises its rate of energy intake [120]. Originally, optimal foraging theory is based on constant population densities, and it aims to predict when a predator will always feed on its preferred prey. An optimal forager also feeds on an alternative prey if doing so does not decrease its rate of energy intake [120]. When using the principle of optimal foraging to model changing population densities, a 1 predator-2 prey interaction can be represented as a piecewise-smooth dynamical system [70].

Using optimum foraging theory [120], Křivan [70] showed that an alternative prey can be part of an optimal forager's diet (such that the probability that the predator attacks the alternative prey is $p \in [0, 1]$). By contrast, the corresponding 1 predator-2 prey system in which the predator is not an optimal forager predicts that both prey coexist and that the predator becomes extinct. In the model proposed in [70], the predator always preys on one type of prey and also includes the alternative prey in the diet whenever the energy intake rate is not decreased

by doing so. How likely it is for the predator to eat the alternative prey depends on how much prey of the first type (i.e., its preferred prey) is available. Once the density of its preferred prey is below some threshold, the alternative prey type is included in the diet. As a result, depending on parameter choices and initial conditions, the predator can eat both prey, only one type of prey, or switch between the two prey types. A similar 1 predator-2 prey system, in which the diet decision is based on optimal foraging theory, was studied in [77]. This model focused on prey competition and coexistence of predator and prey. It was suggested that a predator behaving according to optimal foraging theory would promote coexistence [77]. In another follow-up article [75], the logistic prey growth used in the models in [70] and [77] was replaced by exponential prey growth, which allowed for further analysis of the system because of increased analytical tractability. It was shown that predation according to optimal foraging theory reduced the apparent prey competition and increased the probability of coexistence of all of the species.

It has also been suggested that optimal foraging reduces the amplitude of population-density oscillations compared to models with non-adaptive predators [11, 75, 77]. In [11], this occurs because a global attractor arises in piecewise-smooth systems and consists of stable Lotka-Volterra cycles. In other words, trajectories that start inside the attractor do not escape it and will eventually follow Lotka-Volterra-type dynamics. Trajectories that start outside the attractor either enter it or approach it [11]. In addition to the choice of whether to include or exclude an alternative prey, similar models of optimal behaviour in 1 predator-2 prey systems have been constructed to study adaptive change of habitat in a two-patch environment [74] as well as adaptive change of activity level (in behaviour, such as refuge use or habitat choice) [76]. The model in [76] also includes a

trade-off: activity of the prey increases its growth but also its risk of predation. Similarly, the predator growth rate increases with increased activity, but so does the predator death rate. Again, it was demonstrated that the adaptive behaviour has a stabilising effect on predator-prey population dynamics. This sometimes results in an equilibrium of predator-prey coexistence [76]. In addition, if both predator and prey adjust their activity levels, then there exists an upper bound (which is independent of the initial densities) for the amplitude of population density oscillations.

1.5 Models for population dynamics and adaptive change of traits

As opposed to an adaptive change in behaviour, such as prey switching in response to prey availability (which is an example of phenotypic plasticity [63]), adaptivity can be also understood as a change in traits as the result of evolution and seen as changes in the genome of a predator and/or prey [38]. There have been several investigations on the effect of evolutionary change of traits on predator-prey dynamics, and it has been suggested that evolution incorporated into a model for predator-prey interaction can either stabilise or destabilise equilibria (see [1] for a review). In addition, evolution can decrease or increase the amplitude of cycles of a predator-prey interaction [1]. Indeed, it has been clear since Darwin [21] that ecological differences drive evolution, which in turn influences ecological interactions. Hence, populations that are coupled, for example, through a predator-prey interaction have both a demographic and an evolutionary effect on each other [82].

Although this interplay has been generally considered as a slow process compared to ecological interactions [115], there have been several recent observations of evolution occurring and influencing ecological interactions on a time scale comparable to that of the ecological interactions (see [38, 49] for review). In particular, the evolutionary change of traits has been called "rapid" if it occurs on a time scale of about 1000 generations and can be observed in laboratory conditions [38]. These observations vary from mammals [100] to bacteria [10], and it has been reported that rapid evolutionary change can occur both in predator (e.g., in traits involving resource consumption [46] or in the ability to counteract prey defence mechanisms [50]) and prey (e.g., traits involving predator avoidance [61, 140]). In particular, rapid evolutionary change of traits has been observed in a plankton predator-prey system [37, 140], which is a good example system for studying the coupling between rapid evolution and predator-prey interaction for its short generation times and simple genetics [61].

Consequently, focusing only on ecological interaction without allowing properties of the interacting populations to undergo changes, which often come with a cost in the population density, does not give a complete picture of the dynamics of an ecosystem, let alone its ability to adapt to changing environmental conditions [62]. There are many ways in which a rapid evolutionary change of traits has been incorporated into a system of predator-prey interaction (see [38] for a review). When using a system of ordinary differential equations, ecological and evolutionary dynamics have been assumed to take place both on comparable and separate time scales. As an example of the former, the out-of-phase cycles between a predator (i.e., a small zooplankton) and prey (i.e., generically variable clonal lines of algae) populations observed in the experiments in [37, 140] have been reproduced with

a mathematical model with contemporary evolutionary and ecological dynamics. This model suggested that they emerge from prey evolution, especially when the trade-off between defence mechanism and the cost associated with it is flat (i.e., the defence mechanism is cheap) [62]. In an experiment with the same predator and an algal prey with no genetic variability, the predator and prey populations oscillate with a phase difference of a quarter of a cycle [140], which is predicted by classical predator-prey models such as the Lotka-Volterra system in (1.1). In addition, the level of variation in the adaptive trait value can act as a bifurcation parameter. That is, the extent of the difference in defence against predators that are present in the prey community determines what kind of dynamics (cycles or a steady state) are exhibited by the predator-prey system with evolution [8, 61].

However, the mathematical analysis of a system of differential equations that has comparable time scales of evolutionary and ecological dynamics and represents a specific experimental set-up provides challenges both for analysis (even with relatively simple nonlinearities) and for developing a general theory for coupling between ecology and evolution [61, 62]. Some approaches exploit the assumption of a separation of time scales between evolutionary and ecological interactions to reduce the dimension of the resulting system of equations. On the one hand, in the mathematical framework of *adaptive dynamics* [43], evolution is assumed to occur on a slower time scale than ecological interactions. On the other hand, *multiple time-scale dynamical systems* have been suggested as a general framework for gaining insight into evolutionary and ecological dynamics when these two processes occur on a comparable time scale by studying scenarios in which the evolutionary change occurs either on a slower [64] or on a faster [17] time scale than that of the ecological interactions.

The framework for studying rapid evolution and ecological dynamics using a *fast-slow dynamical system* was introduced in [17]. In this model, the population dynamics of a predator and a prey evolve on a slow time scale, whereas the evolution of a predator or prey trait occurs on a fast time scale. Thus, by considering a scenario in which the evolution of a species occurs much faster than the changes in population densities, one can retain analytical tractability and reduce the model dimension compared to a case in which there is no separation of time scales between the evolutionary and ecological interactions. As a result, one can predict the range of dynamics that a model with coupled ecological and evolutionary interactions exhibits, because these dynamics are determined by the shape of the predator functional response and the properties of trade-off curves incorporated in the model. Moreover, it was demonstrated that a fast-slow dynamical system as introduced in [17], can preserve the qualitative properties of dynamics exhibited by a model in which only one time scale is present [62]. Similar to a model with comparable time scales [62], a fast-slow dynamical system with rapid prey evolution reproduces out-of-phase predator-prey oscillations observed in laboratory experiments [140] that are not present in the analogous model without rapid evolution [17].

1.6 Outline of the rest of the thesis

The remainder of this thesis is organised as follows. In Chapter 2, we give some definitions of piecewise-smooth dynamical systems to introduce the tools and techniques that we will use later to analyse the piecewise-smooth 1 predator-2 prey

system of Chapter 3. In this piecewise-smooth system, a switching manifold divides the phase space into two smooth parts and gives the transition between them. In general, the right-hand side of a piecewise-smooth dynamical system (whose phase space can be divided into more than two smooth parts by more than one switching manifold) is not uniquely defined on the switching manifold. However, we show how a unique solution can be constructed using Filippov's convex method [29]. In addition, piecewise-smooth dynamical systems can exhibit a rich set of behaviours that do not arise in smooth dynamical systems. Such behaviour includes equilibria located on a switching manifold, dynamics governed by flow on a switching manifold, and discontinuity-induced bifurcations. We discuss these properties of piecewise-smooth dynamical systems in Chapter 2.

In Chapter 3, we derive a piecewise-smooth dynamical system for an optimally foraging predator and two prey in the presence of prey preference trade-off. We use the tools and techniques from Chapter 2 to investigate the 1 predator-2 prey system both analytically and numerically. First, we derive the flow on the switching boundary using Filippov's method and present analytical expressions for the equilibrium point on the switching boundary and for the points at which the two vector fields on the different sides of the boundary are tangent to the switching boundary between them. We then examine the dynamics numerically as we adjust the slope of the preference trade-off and discover a previously unknown bifurcation in piecewise-smooth systems. This (centre to two-part periodic orbit; "C2PO") bifurcation describes a transition between a centre located entirely on the switching boundary and a periodic orbit that evolves partly along the boundary and partly outside of it. As the distance to the bifurcation point increases, the periodic orbit experiences a period-doubling, which suggests a possible cascade to chaos. We also

carry out numerical computations as a first step towards formulating a normal-form map to describe this novel bifurcation. Finally, we compare simulations of our system with data on planktonic protozoa-algae dynamics collected from Lake Constance and conclude by discussing and commenting on the model assumptions and results.

In Chapter 4, we reformulate the 1 predator-2 prey piecewise-smooth dynamical system (from Chapter 3), which assumes a discontinuous switch in the predator's adaptive feeding behaviour, as a smooth dynamical system representing a gradual change in the trait that determines the predator's feeding mode. We first formulate the smooth system using hyperbolic tangent functions that allow us to turn the discontinuous switch in feeding behaviour of the piecewise-smooth model into a smooth prey-switching function. We then reformulate our second smooth analog of the piecewise-smooth system by considering a predator trait as a system variable. Hence, we develop a four-dimensional smooth dynamical system from a three-dimensional piecewise-smooth dynamical system. We use a similar approach to the ecological concept of *fitness-gradient dynamics*, which has been used previously to model evolutionary dynamics, and formulate an equation for the temporal evolution for the predator trait. This trait corresponds to a constant parameter that has different values on each side of the discontinuity in the piecewise-smooth system of Chapter 3. We derive analytical expressions and carry out linear stability analysis (numerically whenever analytical solutions are impossible or difficult to obtain) for the equilibria of the two smooth systems. Similarly to Chapter 3, we compare simulations of our two smooth systems with data on protozoa-algae dynamics collected from Lake Constance. In addition, we compare the two smooth systems with the piecewise-smooth system, and discuss the mathematical and eco-

logical findings and implications of the two different modelling approaches. Finally in Chapter 5, we summarise our findings and discuss future directions inspired by them.

Chapter 2

Tools and techniques

In this chapter, we discuss the tools that are used later in the analysis of our piecewise-smooth system (Chapter 3). This entails techniques that have been developed to account for the discontinuity—such as the definition of the sliding flow on the discontinuity boundary and tangencies between the vector fields and the boundary [23].

2.1 Piecewise-smooth dynamical systems

2.1.1 Introduction

The theory and methodology available for smooth dynamical systems provides a set of qualitative tools for understanding phenomena—such as bifurcations or chaotic behaviour—observed in dynamical systems. Some of these tools can be applied to piecewise-smooth dynamical systems as well, but discontinuous systems exhibit rich dynamics that require new mathematical tools [23].

A piecewise-smooth, continuous-time dynamical system—that is, a piecewise-smooth flow—is defined as follows [23]:

Definition 2.1 *A* **piecewise-smooth flow** *is given by a finite set of ordinary differential equations (ODEs)*

$$\dot{x} = f_i(x, \mu), \text{ if } x \in S_i\,, \tag{2.1}$$

where $\bigcup_i S_i = \mathcal{D} \subset \mathbb{R}^n$ *and each* S_i *has a nonempty interior. The intersection* $\Sigma_{ij} := \bar{S}_i \cap \bar{S}_j$ *is either an* $\mathbb{R}^{(n-1)}$*-dimensional manifold including the boundaries* ∂S_j *and* ∂S_i*, or is the empty set. Each vector field* f_i *is smooth in both the state* x *and the parameter* μ*, and it defines a smooth flow* $\phi_i(x,t)$ *within any open set* $U \supset S_i$*. In particular, each flow* ϕ_i *is well defined on both sides of the boundary* ∂S_j*.*

The boundary between the regions S_i and S_j is called a *discontinuity* or *switching boundary* (or a *discontinuity* or *switching set*) Σ_{ij}. Piecewise-smooth systems can be categorised by their *degree of smoothness*. The definition of the degree of smoothness [23] gives information on the behaviour of the piecewise-smooth ODE system as it crosses Σ_{ij}:

Definition 2.2 *The* **degree of smoothness** *at a point* x_0 *in a switching set* Σ_{ij} *of a piecewise-smooth ODE is the highest order* r *such that the Taylor series expansions of* $\phi_i(x_0,t)$ *and* $\phi_j(x_0,t)$ *with respect to* t*, evaluated at* $t = 0$*, agree up to terms of* $O(t^{r-1})$*. That is, the first non-zero partial derivative of the difference* $[\phi_i(x_0,t) - \phi_j(x_0,t)]\Big|_{t=0}$ *with respect to* t*, is of order* r*.*

For example, consider an ODE system with a single discontinuity boundary Σ_{12}

[23]:

$$\dot{x} = \begin{cases} f_1(x,\mu), & \text{if } x \in S_1\,, \\ f_2(x,\mu), & \text{if } x \in S_2\,, \end{cases} \tag{2.2}$$

where the quantities ϕ_1 and ϕ_2 are smooth flows defined, respectively, by f_1 and f_2:

$$\frac{\partial \phi_i}{\partial t}(x,t)\bigg|_{t=0} = f_i(x)\,, \tag{2.3}$$

and

$$\frac{\partial^2 \phi_i}{\partial^2 t}(x,t)\bigg|_{t=0} = \frac{\partial f_i}{\partial t}(x) = \frac{\partial f_i}{\partial \phi_i}(x)\frac{\partial \phi_i}{\partial t} = \frac{\partial f_i}{\partial x}(x) f_i(x) \equiv f_{i,x} f_i(x)\,. \tag{2.4}$$

Thus, according to Definition 2.2, if at a point $x \in \Sigma_{12}$, we have $f_1(x) = f_2(x)$ and $f_{1,x} \neq f_{2,x}$, then the system has a degree of smoothness of 2. Similarly, if at $x \in \Sigma_{12}$, we have $f_{1,x} = f_{2,x}$ but $f_{1,xx} \neq f_{2,xx}$, then the degree of smoothness is 3.

If $f_1(x) \neq f_2(x)$ at a point $x \in \Sigma_{12}$, then the first derivative of x has a discontinuity as Σ_{12} is crossed and the system has a degree of smoothness of 1. Piecewise-smooth systems that have a degree of smoothness equal to 1 are called *Filippov systems*. Because of the jump in the derivative, the points on the boundary can be attracted to, or repelled from, both sides at the same time, and these systems allow the possibility for the dynamics to evolve towards the switching manifold from both sides of the discontinuity. The evolution of the dynamics within Σ_{12} itself is called *sliding motion*, and we will define conditions for such motion in Section 2.1.2.1. To distinguish piecewise-smooth systems with a degree of smoothness of 2 or higher from Filippov systems, the former are often described as "continuous" piecewise-smooth systems. This terminology is used because the trajectories always cross the switching boundary without evolving along it in these

systems [23].

2.1.2 Filippov systems

2.1.2.1 Basic definitions

We now consider a piecewise-smooth system with degree of smoothness 1—that is, a Filippov system—that has a single boundary Σ written as the zero set of a smooth function h

$$\dot{x} = \begin{cases} f_-(x), & \text{if } h(x) < 0\,, \\ f_+(x), & \text{if } h(x) > 0\,. \end{cases} \tag{2.5}$$

As shown in Figure 2.1, the orientation of the vector fields f_+ and f_- determines whether the switching manifold is attracting or repelling. Three types of associated dynamics can occur near a switching manifold in a Filippov-type piecewise-smooth system. When the switching boundary is attracting from both sides of the discontinuity, the system is said to exhibit *sliding* (see Figure 2.1a). *Crossing* occurs when trajectories that start from one side of the discontinuity traverse the switching boundary without following the sliding field on the boundary (see Figure 2.1b). If both vector fields point outward from the discontinuity, then the region in the switching boundary is defined as a region in which *escaping* occurs (see Figure 2.1c).

The boundaries of sliding, crossing, and escaping are determined by computing the points at which there is a tangency between the vector fields f_- or f_+ and the discontinuity boundary $h = 0$ (see Figure 2.2). Determining the tangencies is crucial for studying the behaviour of a system near a switching boundary, and

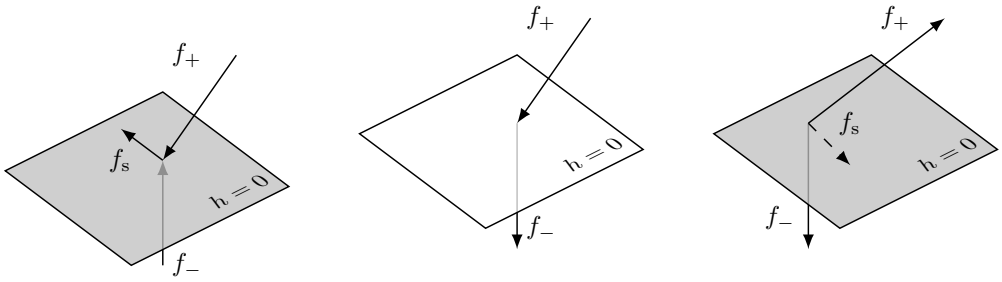

(a) sliding (b) crossing (c) escaping

Figure 2.1: The three possible types of dynamics in a piecewise-smooth system (2.5) close to the switching manifold $h = 0$: (a) sliding along the sliding vector field f_s, (b) crossing, and (c) escaping (i.e., unstable sliding). We have shaded the sliding and escaping regions.

it constitutes the first step for studying how dynamics in a piecewise-smooth dynamical system differ from those in a smooth dynamical system [16]. We give the analytical expression for the regions of crossing, sliding, and escaping in Section 2.1.2.2 and the sliding flow in (2.5) at $h = 0$ in Section 2.1.2.3.

There are three basic tangencies between a piecewise-smooth vector field and a switching boundary. In a *fold*, a vector field has a quadratic tangency with a switching boundary (see Figure 2.2a). In a *cusp*, the tangency is cubic (see Figure 2.2b). Finally, a *two-fold* occurs when two folds intersect, and there is a quadratic tangency between a switching manifold and each side of a vector field (see Figure 2.2c).

Studying the aforementioned tangencies in a piecewise-smooth system makes it possible to describe bifurcations that can occur when, for example, a limit cycle or an equilibrium point intersects a tangency point on a switching boundary. Such bifurcations are examples of *discontinuity-induced bifurcations* (DIBs) [23], which we discuss in Section 2.1.2.6. We compute analytical expressions for points at

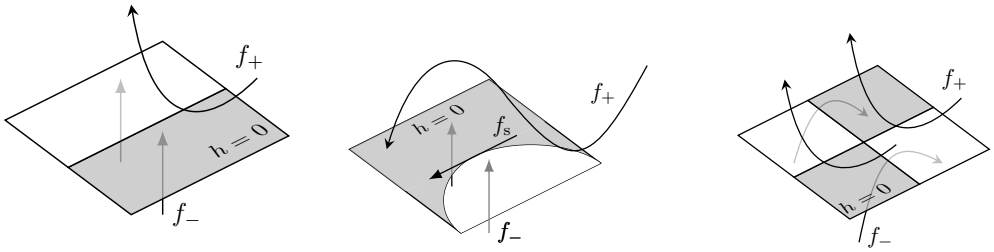

(a) a fold (b) a cusp (c) a two-fold

Figure 2.2: Three basic tangencies between a piecewise-smooth vector field and a switching manifold occur at (a) a fold (i.e., a quadratic tangency), (b) a cusp (i.e., a cubic tangency), and (c) a two-fold (i.e., an intersection of two folds). We have shaded the sliding and escaping regions.

which there is either a quadratic or a cubic tangency between one of the vector fields and the switching boundary in Section 2.1.2.5.

2.1.2.2 Regions of sliding, crossing, and escaping

We examine the system (2.5) near the discontinuity boundary $h(x) = 0$ and give the definition of a sliding region.

Definition 2.3 *The* **sliding region** *of the discontinuity set of a system of the form (2.5) with degree of smoothness* 1 *is given by that portion of the boundary of* $h(x)$ *for which*

$$\mathcal{L}_{f_+} h \mathcal{L}_{f_-} h < 0\,, \tag{2.6}$$

where $\mathcal{L}$ *denotes the Lie derivative along the flow* f *and is defined for* f_+ *as* $\mathcal{L}_{f_+} = f_+ \cdot \nabla = \dot{\mathbf{x}}\big|_{f_+} \cdot \frac{d}{d\mathbf{x}}$. *It is defined analogously for* f_- *as* $\mathcal{L}_{f_-} = f_- \cdot \nabla = \dot{\mathbf{x}}\big|_{f_-} \cdot \frac{d}{d\mathbf{x}}$.

Thus, the component of f_+ normal to h has the opposite sign to the component of f_- normal to h, and the boundary $h = 0$ is simultaneously attracting (or repelling)

from both sides. Therefore, when $\mathcal{L}_{f_+}h\mathcal{L}_{f_-}h > 0$, trajectories of (2.5) cross the switching boundary because the components of f_+ and f_- normal to $h = 0$ have the same sign. Thus, trajectories that start from one side of the boundary pass through $h = 0$ without evolving along it.

In stable sliding regions, the components of both f_+ and f_- that are normal to $h = 0$ point towards the switching manifold, and trajectories reach sliding motion in finite time. This occurs when

$$\mathcal{L}_{f_+}h < 0 < \mathcal{L}_{f_-}h\,. \tag{2.7}$$

Unstable sliding—that is, escaping—occurs because the components of both f_+ and f_- that are normal to $h = 0$ point away from $h = 0$. Trajectories that hit these regions are repelled from the switching manifold in finite time. Escaping motion is unattainable in simulations in forward time. In a system such as (2.5), escaping occurs when

$$\mathcal{L}_{f_+}h > 0 > \mathcal{L}_{f_-}h\,. \tag{2.8}$$

2.1.2.3 Sliding vector field

The solution to (2.5) at the discontinuity $h = 0$ can be expressed using *Filippov's differential inclusion* [29]. According to Filippov's method, the sliding flow f_s of (2.5) at $h = 0$ is determined by a linear convex combination of the two vector fields f_- and f_+ as follows:

$$f_s = (1 - \alpha(x))f_- + \alpha(x)f_+\,, \tag{2.9}$$

where

$$\alpha(x) = \frac{\mathcal{L}_{f_-} h}{\mathcal{L}_{f_-} h - \mathcal{L}_{f_+} h} \in [0, 1]\,. \tag{2.10}$$

The constant α defines the nonnegative constants of the combination (2.9) needed for the flow f_s to lie on the boundary Σ. If $\alpha = 0$, then the sliding flow f_s is given by f_-, so $h < 0$. Similarly, if $\alpha = 1$, then $f_s = f_+$, which implies that $h > 0$. Repelling sliding motion cannot be reached by following the system flow forward in time, whereas attracting sliding motion entails loss of information on initial conditions [23]. Filippov's method is a formulation to describe the evolution of flows written as in (2.5) when they undergo sliding motion on $h = 0$. We determine the divergence of the sliding vector field by calculating

$$\nabla \cdot f_s = \frac{\partial f_s^{(1)}}{\partial x_1} + \frac{\partial f_s^{(2)}}{\partial x_2} + \frac{\partial f_s^{(3)}}{\partial x_3}\,, \tag{2.11}$$

where $f_s^{(i)}$ ($i \in \{1, 2, 3\}$) denotes the ith component of the sliding flow (2.9).

2.1.2.4 Equilibrium points

Piecewise-smooth systems have a type of equilibrium that can lie on the boundary. In the case of Filippov systems, we give the following definition [23].

Definition 2.4 *A point $\tilde{x}$ is a* **pseudoequilibrium** *if it is an equilibrium of the sliding flow. In other words, for some scalar α,*

$$f_-(\tilde{x}) + \alpha(f_+ - f_-) = 0, \tag{2.12}$$

$$h(\tilde{x}) = 0\,. \tag{2.13}$$

If $\alpha = 0$, then the component of f_- normal to h is 0 and the sliding flow is determined only by f_- tangent to the discontinuity set Σ. If $\alpha = 1$, then the sliding flow is determined solely by f_+ tangent to Σ. At pseudoequilibrium, the sliding flow $f_s = 0$. Thus, $\alpha \in (0, 1)$. Usually, the pseudoequilibria are not equilibria of either f_- or f_+ [23].

2.1.2.5 Tangency points

At the boundary between the sliding and crossing regions, the vector fields f_- or f_+ become tangent to the switching manifold $h = 0$. At a fold, one vector field has a vanishing first Lie derivative and a non-vanishing second Lie derivative. That is, in the case of a fold (see Figure 2.2a) for f_+, we have

$$\mathcal{L}_{f_+} h = 0 \quad \text{and} \quad \mathcal{L}^2_{f_+} h = \mathcal{L}_{f_+}(\mathcal{L}_{f_+} h) \neq 0\,. \tag{2.14}$$

In addition, the gradient vectors of h and $\mathcal{L}_{f_+} h$ must be linearly independent of each other, and the other vector field satisfies $\mathcal{L}_{f_-} h \neq 0$ [16].[1]

At a cusp (see Figure 2.2b), a vector field has a cubic tangency to a boundary. For f_+, this occurs when

$$\mathcal{L}_{f_+} h = 0\,, \quad \mathcal{L}^2_{f_+} h = 0\,, \quad \text{and} \quad \mathcal{L}^3_{f_+} h \neq 0\,. \tag{2.15}$$

Thus, the sliding vector field has a quadratic tangency at the sliding boundary. The condition $\mathcal{L}_{f_-} h \neq 0$ must also hold. Additionally, the gradient vectors of h, the first Lie derivative $\mathcal{L}_{f_+} h$, and the second Lie derivative $\mathcal{L}^2_{f_+} h$ are required to

[1] Vice versa, in the case of a fold for f_-, we have $\mathcal{L}_{f_-} h = 0$, $\mathcal{L}^2_{f_-} h \neq 0$, and $\mathcal{L}_{f_+} h \neq 0$. The gradient vectors of h and $\mathcal{L}_{f_-} h$ must be linearly independent of each other [16].

be linearly independent [16].[2]

At a two-fold (see Figure 2.2c), there is a quadratic tangency between the sliding boundary and both f_+ and f_-. Therefore,

$$\mathcal{L}_{f_+}h = 0 \quad \text{and} \quad \mathcal{L}^2_{f_+}h = (\mathcal{L}_{f_+}h)^2 \neq 0\,, \tag{2.16}$$

$$\mathcal{L}_{f_-}h = 0 \quad \text{and} \quad \mathcal{L}^2_{f_-}h = (\mathcal{L}_{f_-}h)^2 \neq 0\,. \tag{2.17}$$

In addition, the gradient vectors of h, the first Lie derivative $\mathcal{L}_{f_+}h$, and $\mathcal{L}_{f_-}h$ are required to be linearly independent [16].

In Section 3.3.4, we will determine the points at which one of the vector fields of the 1 predator-2 prey piecewise-smooth system (3.4) has a quadratic or cubic tangency between the switching boundary. Although a two-fold can arise in three-dimensional piecewise-smooth dynamical systems, it does not occur in (3.4) because the crossing and sliding boundaries do not intersect on the switching manifold.

2.1.2.6 Discontinuity-induced bifurcations in Filippov systems

The tangencies between the vector fields and the discontinuity boundary are useful for determining which type of bifurcations involving a limit cycle can occur. In particular, in a system with three or more dimensions, such as the 1 predator-2 prey system (3.4) that we will introduce in Section 3.2, all generic one-parameter sliding bifurcations occur at either a fold, a cusp, or a two-fold (see Figure 2.2).

[2] At a cusp between f_- and the boundary between sliding and crossing regions, $\mathcal{L}_{f_-}h = 0$ and $\mathcal{L}^2_{f_-}h = 0$, and the conditions $\mathcal{L}^3_{f_-}h \neq 0$ and $\mathcal{L}_{f_+}h \neq 0$ must hold. In addition, the gradient vectors of h, the first Lie derivative $\mathcal{L}_{f_-}h$, and the second Lie derivative $\mathcal{L}^2_{f_-}h$ are required to be linearly independent [16].

Moreover, because the switching manifold $h = 0$ in (3.4) has *codimension* 1[3], all of its one-parameter sliding bifurcations can be categorised into 8 different cases (depending on the type of the tangency) [60].

In Filippov-type piecewise-smooth dynamical systems, there exists a classification for the principal codimension-1 discontinuity induced bifurcations that involve sliding. In these four bifurcations, a limit cycle of a Filippov system interacts with the boundary between sliding and crossing regions. If there is a cusp, then a trajectory that is situated entirely in the sliding region has a tangency with the boundary. That is, the sliding vector field has a quadratic tangency to the switching boundary (see f_s in Figure 2.2c). Perturbing the bifurcation parameter from the bifurcation point results in the sliding trajectory leaving the switching plane tangentially; because of the cubic tangency with the vector field, it returns to the sliding region. This is case (1) and it is called an *adding-sliding* bifurcation because a trajectory that was entirely a sliding trajectory becomes a trajectory that now includes both a non-sliding segment and a sliding segment [23]. A new sliding segment is thereby added to the trajectory.

In addition to the adding-sliding scenario, the limit cycle can interact with the boundary between sliding and crossing regions leading to the scenario of case (2): *crossing-sliding*, where a perturbation causes the trajectory that initially crossed the switching boundary to acquire a sliding segment and reach the attracting sliding region, or case (3): *grazing-sliding*, where a limit cycle that is initially located entirely in the region of one of the vector fields is perturbed into a trajectory that grazes the switching boundary, and thereby acquires a sliding segment, or case (4): *switching-sliding*, which is similar to crossing-sliding with the exception that

[3]That is, the difference between the dimension of the parameter space and the dimension of the bifurcation boundary is 1.

the sliding region is repelling. Thus, in switching-sliding, a trajectory that prior to the perturbation does not intersect the switching boundary, does intersect the boundary and undergoes sliding after the perturbation. The remaining four cases including a systematic classification of all 8 one-parameter sliding bifurcations at a smooth codimension-1 switching manifold of a n-dimensional system for $n \geq 3$ can be found in [60].

We will see in Chapter 3 that the 1 predator-2 prey piecewise-smooth system (3.4) exhibits an adding-sliding periodic orbit due to the presence of a cusp. We will study the periodic orbit in more detail through numerical simulations in Sections 3.4.3 and 3.4.5.

2.1.2.7 Poincaré maps

The study of existence and stability of closed orbits exhibited by a system of differential equations can be translated into a study of fixed points on an iterated map, such as the *Poincaré map*. A Poincaré map is a mapping from a *Poincaré section* Π, which is an $(N-1)$-dimensional surface of section that lies transverse to the flow arising from an N-dimensional vector field, to itself. Thus, for a three-dimensional vector field, the Poincaré map determines how a point on a plane—that is, a point on an intersection between the trajectory and the Poincaré section—changes when it returns to the plane after the first iteration of the Poincaré map. The Poincaré map P is a mapping from one intersection z_n on the Poincaré section to the next intersection z_{n+1} [121]:

$$z_{n+1} = P(z_n)\,. \tag{2.18}$$

A fixed point z^* of P satisfies $z^* = P(z^*)$. Furthermore, there exists a closed orbit that starts from z^* and returns to z^*. A Poincaré map can be used to prove the existence of a closed orbit. Additionally, one can determine the stability of a closed orbit by linearising the Poincaré map around the fixed point z^* and computing the characteristic multipliers [121].

Closed orbits exhibited by a piecewise-smooth dynamical system can be studied by first constructing a global "incorrect" Poincaré map around the closed orbit that does not take the discontinuity into account. One can then derive a non-smooth globally correct Poincaré map to describe the characteristics of the closed orbits by combining the first global map with a correction given by a *discontinuity map* [99]. The discontinuity map is a Poincaré map defined locally near where the interaction between the trajectory and the discontinuity boundary occurs. This technique has been used to describe the four principal sliding bifurcations mentioned in Section 2.1.2.6 [23]. We will use the same technique in Section 3.4.6, where we carry out numerical computations to formally describe the bifurcation in which the adding-sliding periodic orbit is created in the 1 predator-2 prey piecewise-smooth dynamical system (3.4).

2.1.2.8 Numerical simulations

Solving piecewise-smooth systems numerically requires a special numerical integration routine because most of the standard solvers assume that solutions are sufficiently smooth [23]. To simulate the 1 predator-2 prey piecewise-smooth system that we will introduce in this dissertation, we use the numerical method developed for Filippov systems and implemented in MATLAB [90] by Piiroinen

and Kuznetsov [101]. This kind of explicit *event-driven* scheme is appropriate in our case because we are considering fewer than 10 species and fewer than 10 discontinuity boundaries [23]. An event-driven scheme solves for the times at which an event (i.e., a trajectory reaches a discontinuity boundary or a vector field becomes tangent to the discontinuity boundary) occurs. The method introduced in [101] solves for trajectories within regions S_i [see Equation (2.1)] using MATLAB's standard numerical scheme (`ode45`, 4th–order Runge-Kutta method) and locates crossings of the discontinuity boundary and tangencies with MATLAB's built-in event-detection routines. After an event has been detected, the problem is re-initialised at the point of the event. Importantly, the method takes the attracting segments of the discontinuity boundary, where the dynamics of the system are governed by the sliding vector field f_s, into account [101].

In Chapter 3, we will derive a 1 predator-2 prey piecewise-smooth system and apply the tools and techniques we introduced in Section 2.1 to investigate our system both analytically and numerically.

Chapter 3

A piecewise-smooth 1 predator-2 prey model

In Chapter 2, we introduced general important concepts for piecewise-smooth dynamical systems, such as sliding flow, pseudoequilibrium, and tangencies. In this chapter, we use these ideas to analyse a 1 predator-2 prey piecewise-smooth system, which we construct, simulate numerically, and compare with data from observations. We present analytical expressions for the equilibrium point at the switching boundary and for the points at which the two vector fields on the different sides of the boundary are tangent to the switching boundary between them. We show that the 1 predator-2 prey system undergoes a novel adding-sliding-like (centre to two-part periodic orbit; "C2PO") bifurcation in which the prey ratio transitions from constant to time-dependent. We suggest prey switching in the presence of a preference trade-off as a possible mechanistic explanation for the observations of the preferred and alternative prey types of ciliates in Lake Constance in spring. Most of the contents of this chapter are based on a paper published in the *SIAM Journal on Applied Dynamical Systems* [102]. In Section 3.4.6 we discuss new ma-

terial on computations for a discontinuity mapping as a first step in constructing a normal form to describe the centre to two-part periodic orbit (C2PO) bifurcation exhibited by the piecewise-smooth 1 predator-2 prey model.

3.1 Introduction

The Lake Constance data set (see Section 1.2.2) refers to abundance of several plankton species, including ciliates (see Section 1.2.1) (i.e., eukaryotic single-celled organisms with animal-like behaviour—that is, a type of *protist*) that feed on small phytoplankton and constitute an important link between the bottom and higher levels of aquatic food webs [126]. Although the seasonal dynamics of ciliates and small phytoplankton follow the well-documented plankton seasonal succession [117] (see Section 1.3), ciliates and their algal prey populations also vary at shorter-than-seasonal temporal scales [126, 128] (see Section 1.2.2). In addition, ciliates have a prey preference and feed selectively, as different ciliate species benefit differently depending on the match between their feeding mode and the prey species that are abundant in the prey community [94] (see Section 1.2.2). Thus, it has been suggested that the driving forces for the sub-seasonal temporal variability seen in the Lake Constance data (see Figure 1.1 in Section 1.2.2) lie in predator-prey interactions between diverse predator and prey plankton communities rather than in nutrent limitation, particularly during periods of the year, such as in spring, in which environmental conditions are relatively stable [116, 128] (see Section 1.2.2).

The Lake Constance data set for ciliates and their algal prey exhibit coexistence of species in a shared environment. Such coexistence has been suggested to

arise from ecological trade-offs between traits [66]. Indeed, trait-based approaches consider traits and their distributions as system variables when constructing models for investigating the existence and persistence of co-occurring species [91] (see Section 1.3.2). In addition, prey switching has been suggested as a candidate mechanism for coexistence in communities with diverse prey [3] (see Section 1.4). Indeed, both ecological trade-offs between traits and adaptive feeding behaviour have been observed in plankton [83, 94].

Many investigations of prey switching have examined adaptive predator feeding behaviour as either a smooth or piecewise-smooth dynamical system (see Section 1.4.1). In this chapter, we focus on the latter approach and suppose that a predator behaves as an optimal forager and chooses a diet that maximises the predator's rate of energy intake [120]. Thus, following the ideas on Filippov systems for prey switching [70] (see Section 1.4.2), we apply optimal foraging theory to derive a novel piecewise-smooth dynamical system that models a predator that adaptively feeds on two prey species and takes into account a trade-off in prey preference. We make a pragmatic choice of using the Filippov convention instead of applying differential inclusions in our model [29]. We use the tools and techniques we introduced in Section 2.1 to examine the outcome of the population dynamics in this discontinuous 1 predator-2 prey system as we adjust the steepness of the linear preference trade-off. We thereby discover a previously unknown bifurcation in piecewise-smooth dynamical systems and provide a possible link between predator-prey dynamics and ecological trade-offs.

The rest of this chapter is organised as follows. In Section 3.2, we construct a piecewise-smooth dynamical system for an optimal forager and its preferred and alternative prey in the presence of a linear prey preference trade-off. In Section 3.3,

we investigate this 1 predator-2 prey system analytically and derive expressions for the sliding flow, pseudoequilibrium, and tangencies between the vector fields and the switching boundary. In Section 3.4, we simulate the system numerically to (1) examine its dynamics as we adjust the slope of the preference trade-off, (2) describe a novel bifurcation in piecewise-smooth dynamical systems, and (3) compare simulations of the system with data from Lake Constance. In Section 3.5, we discuss the model assumptions, results, and possible generalisations, before concluding in Section 3.6.

3.2 The model

In our framework, prey switching occurs because the predator can adjust the extent of consumption of its preferred prey. We assume that there is a trade-off in the prey preference, which effectively is a trade-off in how much energy the predator gains from eating the preferred prey instead of the alternative prey. An increase in specialisation towards the preferred prey comes at a cost of the predator population growth obtained from feeding on the alternative prey. For simplicity, we assume that the preference trade-off is linear:

$$q_2 = -a_q q_1 + b_q \,, \tag{3.1}$$

where $q_1 \geq 0$ is a nondimensional parameter that represents the extent of preference towards the preferred prey, $a_q > 0$ is the slope of the preference trade-off, $b_q \geq 0$ is the intercept of the preference trade-off, and $q_2 \geq 0$ is the extent of preference towards the alternative prey. Assuming a linear predator mortality and

a linear functional response between the predator growth and prey abundance (we discuss this assumption in Section 3.5), we define a fitness function that the predator maximises using the net per capita growth rate

$$R \equiv \frac{1}{z}\frac{dz}{dt} = eq_1\beta_1 p_1 + eq_2\beta_2 p_2 - m\,, \tag{3.2}$$

where z is the density of the predator population, p_1 is the density of the preferred prey, p_2 is the density of the alternative prey, $e > 0$ is the proportion of predation that goes into predator growth, β_1 and β_2 are the respective death rates of the preferred and alternative prey due to predation, and $m > 0$ is the predator per capita death rate per day.

We obtain the switching condition that describes when the predator chooses consumption with a large preference towards the preferred prey ($q_1 = q_{1_{\mathrm{L}}}$) or consumption with a small preference towards the preferred prey ($q_1 = q_{1_{\mathrm{S}}}$) to maximise fitness by substituting (3.1) into (3.2) and differentiating R with respect to q_1:

$$\frac{\partial R}{\partial q_1} = (\beta_1 p_1 - a_q \beta_2 p_2)\, e\,. \tag{3.3}$$

Thus, when $\frac{\partial R}{\partial q_1} > 0$, the largest feasible $q_{1_{\mathrm{L}}}$ maximises predator fitness; when $\frac{\partial R}{\partial q_1} < 0$, the smallest feasible $q_{1_{\mathrm{S}}}$ maximises predator fitness. For simplicity, we assume that $q_{1_{\mathrm{S}}} = 0$. This implies that the predator switches to the feeding mode of consuming only the alternative prey when predator fitness is maximised by having a small preference for consuming the preferred prey. We also assume (again for simplicity) that prey growth is exponential. This yields the following

piecewise-smooth 1 predator-2 prey model:

$$\dot{\mathbf{x}} = \begin{bmatrix} \dot{p_1} \\ \dot{p_2} \\ \dot{z} \end{bmatrix} = \left\{ \begin{array}{lll} f_+ = \begin{bmatrix} (r_1 - \beta_1 z)p_1 \\ r_2 p_2 \\ (eq_1\beta_1 p_1 - m)z \end{bmatrix}, & \text{if} & h = \beta_1 p_1 - a_q \beta_2 p_2 > 0 \\ f_- = \begin{bmatrix} r_1 p_1 \\ (r_2 - \beta_2 z)p_2 \\ (eq_2\beta_2 p_2 - m)z \end{bmatrix}, & \text{if} & h = \beta_1 p_1 - a_q \beta_2 p_2 < 0 \end{array} \right\}, \tag{3.4}$$

where $h = \beta_1 p_1 - a_q \beta_2 p_2$ determines the switching manifold $h = \beta_1 p_1 - a_q \beta_2 p_2 = 0$, and r_1 and r_2 (where $r_1 > r_2 > 0$) are the respective per capita growth rates of the preferred and alternative prey. The right-hand side of (3.4) cannot be determined uniquely for $h = 0$ by the criterion based on optimal foraging theory. For this part of the phase space, the flow at the discontinuity must be constructed from f_+ and f_-. We will specify (3.4) at the switching manifold $h = \beta_1 p_1 - a_q \beta_2 p_2 = 0$ in Equation (3.9) below.

In our numerical simulations in Section 3.4, we take $\beta_1 = \beta_2$. (For simplicity, we also take $\beta_1 = \beta_2 = 1$ in order to omit β_1 and β_2 in our analysis in Section 3.3.) Hence, we assume that the predator exhibits adaptive feeding behaviour by adjusting preference to, rather than attack rate on, the governing prey densities. We can use production-to-biomass ratio—where the biomass is the mass of all living and dead organic matter, and production represents the increase in biomass produced by phytoplankton organisms—calculated from measurements in Lake Constance as an index for phytoplankton growth. These data suggest that typical values for the phytoplankton per capita growth rate vary approximately from 0.2 per day to 0.6 per day during the course of a year. The values for r_1 (i.e., the

growth rate of the preferred prey), r_2 (i.e., the growth rate of the alternative prey), and m (i.e., the predator death rate) can be obtained from parameter fitting using approximate Bayesian computation (ABC) [129]. We discuss this method (that we use to fit the periodicity in the prey ratio predicted by the model to that exhibited in the Lake Constance data) in detail in Appendix B.

Because of the prey preference, the predator exerts more grazing pressure on the preferred prey than on the alternative prey. One can explain this advantage of experiencing lower predation pressure from above for the alternative prey by a difference in the use of limited nutrients. For example, the alternative prey might invest resources in building defence mechanisms such as a hard silicate cover, which is difficult for the predator to digest. As a result, the alternative prey has fewer resources left for population growth than the preferred prey (which does not have as good a defence against the predator). To compensate for the difference in preference, we assume that the growth rate of the preferred prey is larger than that of the alternative prey. In biology, this phenomenon is called the *evolutionary double bind*, and it refers to a situation in which resistance comes at a cost [41].

Our 1 predator-2 prey model assumes that the switch from the preferred prey to the alternative prey occurs instantaneously. It is reasonable to model prey switching via a piecewise-smooth dynamical system as long as predators are assumed to behave as optimal foragers. The discontinuity in (3.4) comes from using the principle of optimal foraging theory [120], which states that a predator chooses a diet that maximises its growth. Hence, to determine the optimal choice for consumption, we differentiate the mean energy intake rate with respect to the prey preference, which is the parameter that the predator can adjust. It is not clear whether in ecology there actually exist "discontinuous predators" (which switch

their feeding strategy instantaneously, as is the case in our model). To our knowledge, however, there is no evidence for any of the possible smooth approximations that one can choose to model prey switching. Therefore, we use an abrupt switch rather than a gradual switch and focus on a model with a discontinuity. We present two smooth analogs of the piecewise-smooth system (3.4) in Chapter 4, where we also comment on the differences and similarities between the models.

3.3 Analysis of the 1 predator-2 prey piecewise-smooth model

In this section, we examine how the ideas from piecewise-smooth dynamical systems that we introduced in Section 2.1 manifest in the model (3.4). In particular, we specify (3.4) at the switching manifold $h = p_1 - a_q p_2 = 0$ and compute analytical expressions for points at which there is a tangency between one of the vector fields in (3.4) and the switching boundary (see Figures 2.1 and 2.2).

3.3.1 Regions of sliding, crossing, and escaping

The piecewise-smooth 1 predator-2 prey system with Lotka-Volterra interaction terms in (3.4) contains a jump in the derivative of the population densities across the discontinuity boundary $h = 0$. This jump makes (3.4) a Filippov system, so its dynamics can interact with the switching boundary. The three types of such dynamics are sliding, crossing, and escaping (see Figure 2.1). The condition (2.7)

for sliding or escaping to occur in (3.4) is

$$\mathcal{L}_{f_+} h \mathcal{L}_{f_-} h = (a_q p_2)^2 \left[(r_1 - r_2)^2 - z^2 \right] < 0 \,. \tag{3.5}$$

Thus, either sliding or escaping occurs in (3.4) for $z^2 > (r_1 - r_2)^2$. When $z^2 < (r_1 - r_2)^2$, a solution of (3.4) crosses the switching boundary because the components of f_+ and f_- normal to $h = 0$ have the same sign. Therefore, trajectories that start from one side of the boundary pass through $h = 0$ without evolving along it.

In stable sliding regions, the components of both f_+ and f_- that are normal to $h = 0$ point towards the switching manifold, and trajectories reach sliding motion in finite time. This occurs in (3.4) when

$$\mathcal{L}_{f_+} h < 0 < \mathcal{L}_{f_-} h \implies -z < r_1 - r_2 < z \,. \tag{3.6}$$

Escaping (i.e., unstable sliding) occurs because the components of both f_+ and f_- that are normal to $h = 0$ point away from $h = 0$. Trajectories that hit these regions are repelled from the switching manifold in finite time. Escaping motion is unattainable in simulations in forward time. Escaping occurs in (3.4) when

$$\mathcal{L}_{f_+} h > 0 > \mathcal{L}_{f_-} h \implies -z > r_1 - r_2 > z \,. \tag{3.7}$$

However, escaping does not occur in (3.4) for physically meaningful quantities.

3.3.2 Sliding vector field

The solution to (3.4) at the discontinuity $h = 0$ can be expressed using Filippov's differential inclusion [29]. According to Filippov's method (see Section 2.10), the flow of (3.4) at $p_1 = a_q p_2$ is determined by a linear convex combination of the two vector fields f_- and f_+ as follows:

$$f_s = \left(1 - \frac{\mathcal{L}_{f_-} h}{\mathcal{L}_{f_-} h - \mathcal{L}_{f_+} h}\right) f_- + \frac{\mathcal{L}_{f_-} h}{\mathcal{L}_{f_-} h - \mathcal{L}_{f_+} h} f_+ \,. \tag{3.8}$$

Employing (3.8) and looking at $h = 0$, we thus see that the dynamics of (3.4) are governed by the sliding vector field

$$\begin{aligned} f_s &= \frac{1}{2} \begin{bmatrix} (r_1 + r_2 - z)p_1 \\ (r_1 + r_2 - z)p_2 \\ eq_1 p_1 (r_1 - r_2 + z) + eq_2 p_2 (r_2 - r_1 + z) - 2mz \end{bmatrix} \\ &= \frac{1}{2} \begin{bmatrix} (r_1 + r_2 - z)a_q p_2 \\ (r_1 + r_2 - z)p_2 \\ eq_1 a_q p_2 (r_1 - r_2 + z) + eq_2 p_2 (r_2 - r_1 + z) - 2mz \end{bmatrix} . \end{aligned} \tag{3.9}$$

The sliding vector field (3.9) is a linear convex combination of the two vector fields f_- and f_+ on each side of the switching manifold $h = p_1 - a_q p_2$. The following mechanisms drive the piecewise-smooth system in (3.4) to evolve according to the sliding vector field (3.9). The vector field f_- points towards the switching manifold for a sufficiently large predator population (for $z > r_1 - r_2$) because the predator prefers prey p_1 (which has an advantage in growth rate compared to the alternative prey), but it can also feed on the alternative prey p_2. When the predator

population is sufficiently small and the predator is feeding on the alternative prey (i.e., when $p_1 - a_q p_2 < 0$), the preferred prey population p_1 grows exponentially. As a result, the quantity $p_1 - a_q p_2$ increases as p_1 becomes more abundant, whereas the population p_2 decreases because of predation. Consequently, the predator switches to the preferred prey, which also contributes more to predator growth than the alternative prey.

If the predator population is still small (i.e., when $z < r_1 - r_2$) when the switch occurs, then the population of the preferred prey continues to grow after the switch. This, in turn, supports predator growth. At the same time, the population p_2 grows exponentially. However, because of the increasing number of predators that feed on p_1 and the increasing number of alternative prey p_2, the quantity $p_1 - a_q p_2$ eventually starts to decrease as predation catches up with the growth of p_1. At this point, f_+ starts to point towards the switching manifold. The vector field f_- also points towards the switching manifold because the population of the alternative prey p_2 (if it is being eaten by the predator) would decrease in the presence of a large predator population. Hence, at the switching manifold in the sliding region (i.e., when $z > r_1 - r_2$), the predator is feeding on both prey types because both f_- and f_+ point towards the switching manifold. In addition, trajectories that enter the switching manifold cannot leave it if the preference trade-off is sufficiently steep. We will discuss the reasons for this phenomenon in Sections 3.4.1 and 3.4.2. Consequently, on the switching manifold—for which the dynamics of the system are given by (3.9)—the predator feeds on both prey types and the ratio of the prey populations tends towards a_q.

The divergence of the sliding vector field is determined by

$$\nabla \cdot f_s = \frac{\partial f_s^{(1)}}{\partial p_1} + \frac{\partial f_s^{(2)}}{\partial p_2} + \frac{\partial f_s^{(3)}}{\partial z} = r_1 + r_2 - z + e(q_1 a_q + q_2)p_2 - 2m\,, \qquad (3.10)$$

where $f_s^{(i)}$ ($i \in \{1, 2, 3\}$) denotes the ith component of the sliding flow (3.9).

3.3.3 The equilibrium point

The sliding vector field (3.9) has an equilibrium point when $f_s(\tilde{p}_1, \tilde{p}_2, \tilde{z}) = 0$. For the system (3.4), there is a nontrivial pseudoequilibrium point at

$$\begin{aligned} \tilde{p}_1 &= \frac{a_q m(r_1 + r_2)}{e(q_1 a_q r_1 + q_2 r_2)}\,, \\ \tilde{p}_2 &= \frac{m(r_1 + r_2)}{e(q_1 a_q r_1 + q_2 r_2)}\,, \\ \tilde{z} &= r_1 + r_2\,. \end{aligned} \qquad (3.11)$$

By evaluating the Jacobian of f_s at $(\tilde{p}_1, \tilde{p}_2, \tilde{z})$, we find that its two eigenvalues are the complex conjugate pair $\lambda_{1,2}$, which satisfy the characteristic equation

$$\lambda_{1,2}^2 - \frac{m(r_2 - r_1)(q_1 a_q - q_2)}{2(q_1 a_q r_1 + q_2 r_2)}\lambda_{1,2} + \frac{m(r_1 + r_2)}{2} = 0\,. \qquad (3.12)$$

The eigenvalues $\lambda_{1,2}$ have negative real part when $a_q > q_2/q_1$, are imaginary when $a_q = q_2/q_1$, and have positive real part when $a_q < q_2/q_1$.

3.3.4 Tangency points

The boundaries of sliding, crossing, and escaping are points at which there is a tangency between the vector fields f_- or f_+ and the discontinuity boundary $h = 0$. The three basic tangencies between a piecewise-smooth vector field and a switching boundary are a fold, a cusp, and a two-fold (see Figure 2.2). Determining the tangencies is crucial for studying the behaviour of a system at a switching boundary, and it constitutes the first step for studying how dynamics in a piecewise-smooth dynamical system differ from that in a smooth dynamical system [16]. As we discuss in Section 2.1.2.5, the tangency conditions for a fold (a quadratic tangency between the vector field and the switching boundary) in (3.4) are

$$\mathcal{L}_{f_+} h = 0 \implies z = r_1 - r_2 \,, \tag{3.13}$$

and

$$\mathcal{L}_{f_-} h = 0 \implies z = r_2 - r_1 \,. \tag{3.14}$$

At a cusp there is a cubic tangency between the vector field and the switching boundary, and there is a quadratic tangency between the sliding vector field and the sliding or escaping boundary (see Section 2.1.2.5). For f_+ in the 1 predator-2 prey system (3.4), the quadratic tangency is given by

$$\mathcal{L}^2_{f_+} h = a_q p_2 \left[(r_1 - z)^2 - r_2^2 - z(e q_1 a_q p_2 - m) \right] \,. \tag{3.15}$$

Substituting $\mathcal{L}_{f_+} h = 0$ (i.e., $z = r_1 - r_2$) into (3.15) yields a cusp at

$$(p_1, p_2, z) = (m/(eq_1), m/(eq_1 a_q), r_1 - r_2) \,. \tag{3.16}$$

At (3.16), the sliding vector field (3.9) curves away from the discontinuity boundary $h = 0$. Similarly, the condition for a quadratic tangency for f_- is

$$\mathcal{L}_{f_-}^2 h = a_q p_2 \left[(r_2 - z)^2 - z(m - q_2 p_2) + r_1^2 \right] . \tag{3.17}$$

Substituting $\mathcal{L}_{f_-} h = 0$ (i.e., $z = r_2 - r_1$) into (3.17) yields a cusp at

$$(p_1, p_2, z) = (a_q m/(eq_2), m/(eq_2), r_2 - r_1) . \tag{3.18}$$

At (3.18), the sliding vector field (3.9) curves away from the discontinuity boundary $h = 0$. However, the cusp for f_- does not occur in (3.4) for physically meaningful quantities.

Studying the tangencies in a piecewise-smooth system makes it possible to determine bifurcations that can occur when, for example, a limit cycle or an equilibrium intersects a tangency point on the switching boundary. A bifurcation type can be attributed to the tangency [60] (see Section 2.1). For example, because of the presence of a cusp, the local flow near the tangency forces the trajectory of the periodic orbit to first leave the switching boundary tangentially and then to return to it in an adding-sliding bifurcation.

3.4 Numerical simulations

We now treat the slope a_q of the preference trade-off in (3.1) as a bifurcation parameter and study the 1 predator-2 prey system (3.4) numerically. We are interested in the dynamics of (3.4) as the complex conjugate pair of eigenvalues

of the pseudoequilibrium cross the imaginary axis. We will show that the system undergoes a novel bifurcation that is similar to the adding-sliding bifurcation (see Section 2.1.2.6).

The parameter a_q gives the slope of the tilted switching manifold, and it corresponds biologically to the slope of the assumed linear trade-off in the predator's preference for prey. A large a_q corresponds to a situation in which a small increase in the predator's desire to consume the preferred prey results in a large decrease in its desire for the alternative prey. When $a_q \to 0$, a small specialisation in consuming the preferred prey requires only a small decrease in how much energy the predator gains from eating the alternative prey. At $a_q = 0$, the preference trade-off no longer decreases (i.e., it is flat), which corresponds to a situation in which specialisation in one prey has no effect on the desire for consuming the alternative prey.

In Sections 3.4.1 – 3.4.3, we simulate (3.4) numerically in three different cases: (1) $a_q > q_2/q_1$, (2) $a_q = q_2/q_1$, and (3) $a_q < q_2/q_1$. These correspond, respectively, to (1) the complex conjugate pair $\lambda_{1,2}$ with negative real part, (2) the complex conjugate pair $\lambda_{1,2}$ with real part 0, and (3) the complex conjugate pair $\lambda_{1,2}$ with positive real part. To obtain our numerical solutions, we use the method developed in [101] (see Section 2.1.2.8) for simulating Filippov systems. From Section 3.4.3 onwards, we focus on the region in which the complex conjugate pair of the system (3.4) has positive real part and there exists a periodic orbit. In Section 3.4.5, we show the periodic orbit period-doubles as we decrease a_q further. In Section 3.4.6, we compute numerically a discontinuity map with the aim of obtaining an analytical description of the novel bifurcation in which the periodic orbit is born. Finally in Section 3.4.7, we compare the prey ratio of adding-sliding period-1 and

period-2 orbit exhibited by the model (3.4) with data on cryptophyte (i.e., the preferred prey type of ciliate-predators) and diatom prey (the alternative prey type of ciliate-predators) collected from Lake Constance.

3.4.1 The pseudoequilibrium point

From our analytical results, we know that the pseudoequilibrium has a complex conjugate pair of eigenvalues with negative real part when $a_q > q_2/q_1$. In addition, the divergence of the sliding vector field (3.10) evaluated at the pseudoequilibrium (3.11) is negative. Thus, the pseudoequilibrium behaves as a sink when $a_q > q_2/q_1$. Accordingly, numerical simulations of (3.4) in this parameter regime have trajectories that converge to the pseudoequilibrium in (3.11). See Figure 3.1 for an example trajectory.

3.4.2 Sliding centres

At $a_q = q_2/q_1$, the complex conjugate pair of eigenvalues $\lambda_{1,2}$ have a real part equal to 0, and the divergence of the sliding vector field evaluated at the pseudoequilibrium is also 0. Because the pseudoequilibrium is neither attracting nor repelling in the linearised dynamics, every entirely sliding orbit is a periodic orbit that surrounds the pseudoequilibrium (see Figure 3.2). Thus, the amplitude of a periodic orbit depends on the point at which a trajectory intersects the switching surface. In addition to these sliding periodic orbits, there exist periodic orbits that cross the boundary between sliding and crossing regions (but which initially are not entirely sliding) and converge slowly (with dimensional simulation times on

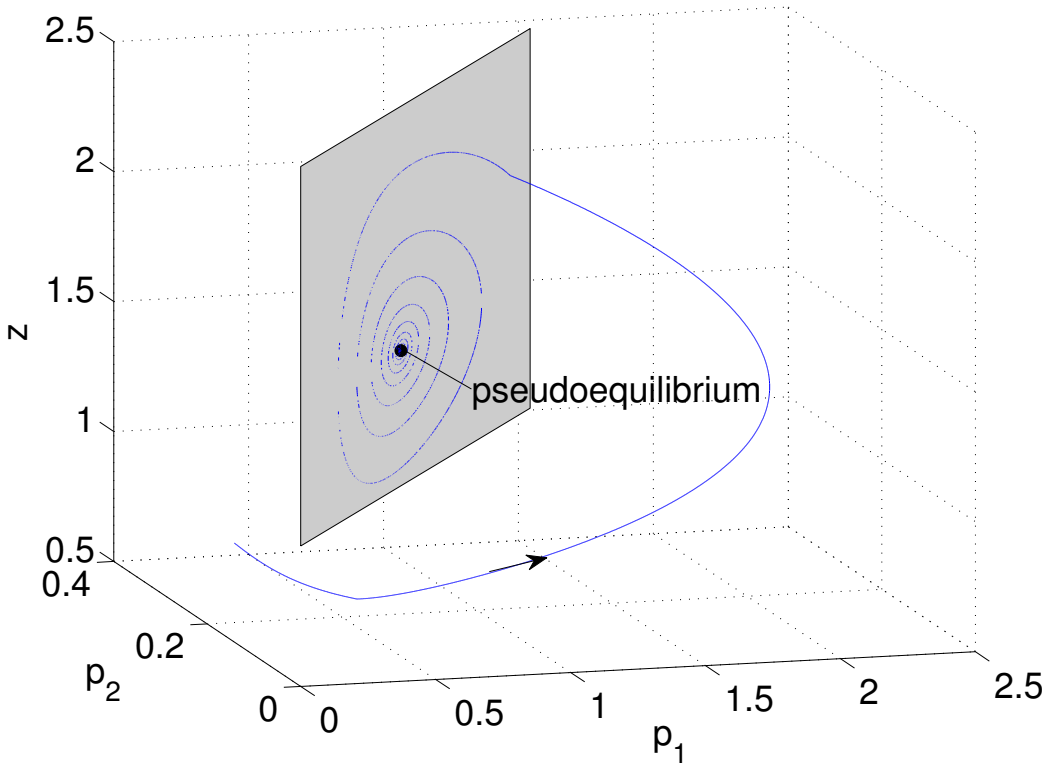

Figure 3.1: Example trajectory of the 1 predator-2 prey model (3.4) for parameter values $a_q = 4$, $q_1 = 1$, $q_2 = 0.5$, $r_1 = 1.3$, $r_2 = 0.26$, $e = 0.25$, $m = 0.14$, and $\beta_1 = \beta_2 = 1$. The system converges to the pseudoequilibrium (black circle) given by (3.11). The predator's diet is composed of both prey types when the system dynamics evolves on the switching boundary $h = 0$ (shaded) according to the sliding vector field (3.9).

the order of 10^3 days or larger) to an entirely sliding periodic orbit that is tangent to the sliding-crossing boundary (see Figure 3.2).

At the bifurcation point $a_q = q_2/q_1$, the dynamics of equation (3.4) on the switching manifold are governed by the two-dimensional sliding vector field (3.9). This system is effectively the Lotka-Volterra predator-prey system in Equation (1.1). Therefore, we can find a first integral of the sliding vector field on the

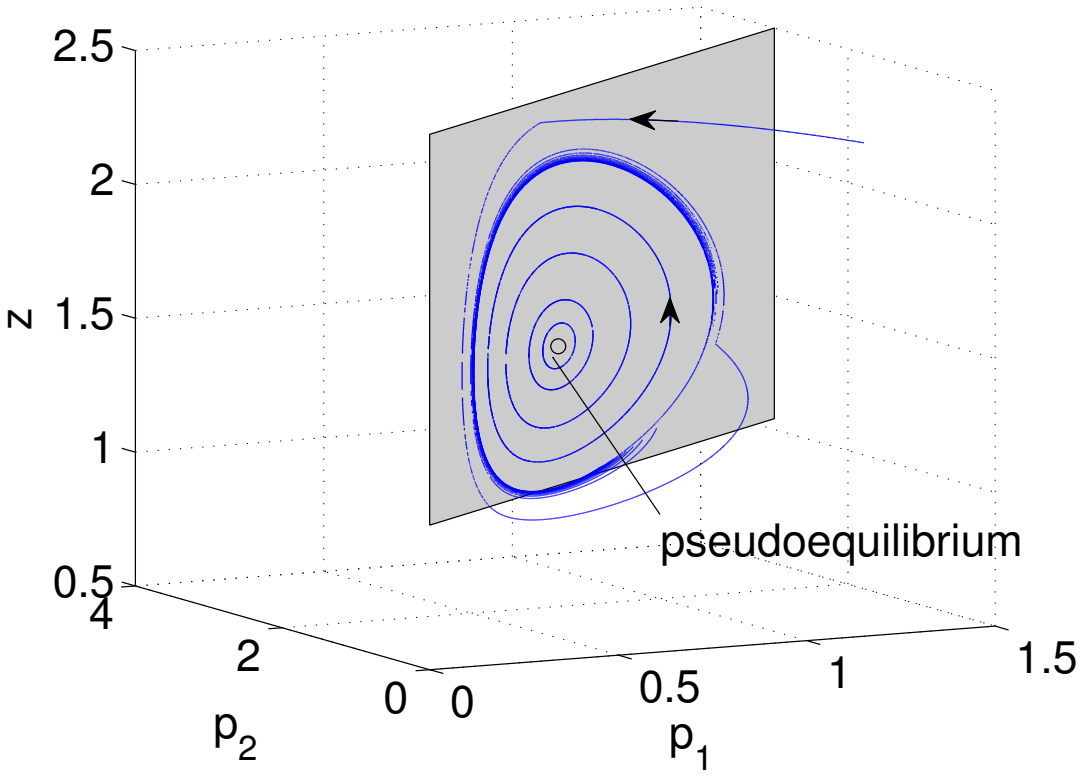

Figure 3.2: Example trajectory of (3.4) for parameter values $a_q = 0.5$, $q_1 = 1$, $q_2 = 0.5$, $r_1 = 1.3$, $r_2 = 0.26$, $e = 0.25$, $m = 0.14$, and $\beta_1 = \beta_2 = 1$. The pseudoequilibrium (black circle) is surrounded by periodic orbits that evolve on the switching manifold $h = 0$ in the stable sliding region (shaded). Periodic orbits that reach the boundary between sliding and crossing eventually converge to the periodic orbit that is tangent to the sliding boundary (blue trajectory).

switching manifold to show that the sliding vector field on the switching manifold is a centre. First, we introduce the following change of coordinates:

$$\begin{aligned} u_1 &= p_1 - a_q p_2 \,, \\ u_2 &= a_q p_1 + p_2 \,, \\ u_3 &= z \,. \end{aligned} \tag{3.19}$$

The switching manifold $h = p_1 - a_q p_2 = 0$ of the original system in (3.4) thereby becomes $u_1 = 0$. In the new coordinates (u_1, u_2, u_3) in (3.19), the sliding vector field (3.9) becomes

$$\begin{aligned}
\dot{u_1} &= \dot{p_1} - a_q \dot{p_2} = f_s^{(1)} - a_q f_s^{(2)} = 0\,, \\
\dot{u_2} &= a_q \dot{p_1} + \dot{p_2} = a_q f_s^{(1)} + f_s^{(2)} = (a_q^2 + 1) p_2 (r_1 + r_2 - z)\,, \\
\dot{u_3} &= \dot{z} = f_s^{(3)} = e p_2 (r_1 - r_2)(q_1 a_q - q_2) + z(e p_2 (q_1 a_q + q_2) - 2m)\,,
\end{aligned} \tag{3.20}$$

where $f_s^{(i)}$ $(i = 1, 2, 3)$ is the ith component of the sliding flow in (3.9). We obtain $p_2 = u_2/(1 + a_q^2)$ and $z = u_3$ from (3.19) and substitute them into (3.20) at the bifurcation point $a_q = q_2/q_1$ to yield a two-dimensional sliding flow on the switching manifold $u_1 = 0$:

$$\begin{aligned}
\dot{u_2} = u_2(a - u_3) \rightarrow \frac{\dot{u_2}}{u_2} &= a - u_3\,, \\
\dot{u_3} = u_3(b u_2 - c) \rightarrow \frac{\dot{u_3}}{u_3} &= b u_2 - c\,,
\end{aligned} \tag{3.21}$$

where $a = r_1 + r_2$, $b = \frac{2eq_2}{1+(q_2/q_1)^2}$, and $c = 2m$. We let $\xi = \log u_2$ and $\eta = \log u_3$ to obtain

$$\begin{pmatrix} \dot{\xi} \\ \dot{\eta} \end{pmatrix} = \begin{pmatrix} 0 & -1 \\ b & 0 \end{pmatrix} \begin{pmatrix} e^{\xi} - \frac{c}{b} \\ e^{\eta} - a \end{pmatrix}\,, \tag{3.22}$$

which has a centre at $(\xi, \eta) = (\log c/b, \log a)$ with eigenvalues $\lambda_{1,2} = \pm i\sqrt{ac}$. We can now eliminate time from (3.22) by dividing $\dot{\xi}$ by $\dot{\eta}$:

$$\frac{d\xi}{d\eta} = \frac{\dot{\xi}}{\dot{\eta}} = \frac{a - e^{\eta}}{b e^{\xi} - c}\,. \tag{3.23}$$

We then separate variables to obtain

$$(be^{\xi} - c)d\xi = (a - e^{\eta})d\eta\,, \tag{3.24}$$

which we integrate to get

$$be^{\xi} - c\xi = a\eta - e^{\eta} + C\,, \tag{3.25}$$

where C is an arbitrary constant of integration. We carry out a Taylor expansion of both sides of (3.25) around the fixed point $(\xi, \eta) = (\log c/b, \log a)$. Defining $\triangle\xi = \xi - \log c/b$ and $\triangle\eta = \eta - \log a$, the expansion becomes

$$c - c\log\frac{c}{b} + \frac{c}{2}\triangle\xi^2 + \mathcal{O}(\triangle\xi^3) = a\log a - a + C - \frac{a}{2}\triangle\eta^2 + \mathcal{O}(\triangle\eta^3)\,. \tag{3.26}$$

Finally, by rearranging and discarding the higher-order terms, we can express the sliding centres shown in Figure 3.2 as circles that satisfy

$$\frac{c}{2}\triangle\xi^2 + \frac{a}{2}\triangle\eta^2 = c(\log\frac{c}{b} - 1) + a(\log a - 1) + C\,. \tag{3.27}$$

The largest sliding centre in Figure 3.2 grazes the boundary between crossing and sliding at $r_1 - r_2$. Furthermore, the pseudoequilibrium in the u_1-u_2-u_3-system (3.20) is located at $r_1 + r_2$ on the u_3- (or z-) axis. Thereby, we can calculate a lower and an upper bound for the predator oscillations at the bifurcation point $a_q = q_2/q_1$. The piecewise-smooth system (3.4) predicts the predator population oscillates between a minimum of $r_1 - r_2$ and a maximum of $r_1 + 3r_2$.

These analytically obtained upper and lower bounds are mirrored in the Lake Constance data over the period 1979–1999 better for the abundance of the unselec-

tive ciliate predator than that of the selective predator species (see Figure 3.3). For the unselective predator, we simulate a sliding centre exhibited by the piecewise-smooth system (3.4) with prey growth rates $r_1 = 1.3$ and $r_2 = 0.26$ obtained from parameter fitting (see Appendix B). As concerns the unselective (i.e., filter feeder) ciliate, there is some agreement between the data and the model prediction in early May (see Figure 3.3a). If we choose prey growth rates $r_1 = 4$ and $r_2 = 0.5$, the data and the upper and lower bounds predicted by the model (3.4) are closest in mid May for the selective (i.e., interception feeder) ciliate predator (see Figure 3.3b). However, we note that in the data comparison for the unselective predator species in Figure 3.3b, $r_1 = 4$ is greater than what we obtain from our parameter fitting (see Appendix B).

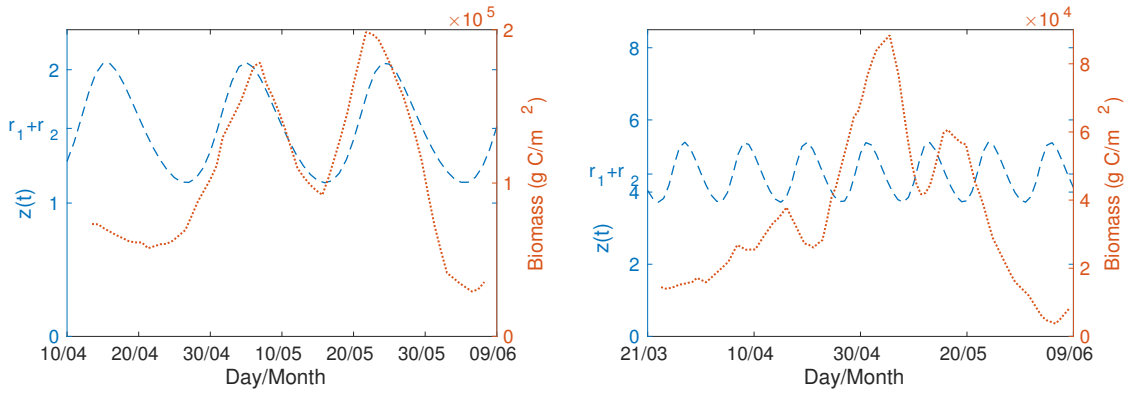

(a) (b)

Figure 3.3: (Dashed curves) Predator abundance $z(t)$ for simulations of (3.4) [for parameter values $e = 0.25$ $m = 0.14$ $a_q = 0.5$ $\beta_1 = \beta_2 = 1$, (a) $r_1 = 1.3$, $r_2 = 0.26$, and (b) $r_1 = 4$, and $r_2 = 0.5$] and (points) mean data calculated for the (a) unselective and (b) selective predator species in spring in Lake Constance over the period of 1979–1999. The unselective predator group is composed of data for *Rimostrombidum lacustris*. The selective predator group is composed of data for *Balanion planctonicum*.

3.4.3 Adding-sliding periodic orbit

For $a_q < q_2/q_1$, the pseudoequilibrium (3.11) of the sliding flow is repelling because the complex conjugate pair of eigenvalues $\lambda_{1,2}$ have negative real part. The sliding vector field (3.9) behaves as a source (because $\nabla \cdot f_s\big|_{(\tilde{p_1},\tilde{p_2},\tilde{z})} > 0$). There is also a periodic orbit. From our analytical calculations in Section 3.3.4, we know that the vector field f_+ has a cubic tangency with the switching boundary at the cusp at $(p_1, p_2, z) = (m/(eq_1), m/(eq_1a_q), r_1 - r_2)$. Because of the cusp, the local flow near the tangency forces the trajectory of the periodic orbit to first leave the switching boundary tangentially and then to return to it. In doing this, the periodic orbit acquires a non-sliding segment before returning to the switching manifold $h = 0$ (see Figure 3.4).

One can detect adding-sliding periodic orbits using the sliding condition, as there are two separate pieces of sliding trajectories when $p_1/(a_qp_2) = 1$. Between the sliding pieces, there is a non-sliding segment when $p_1/(a_qp_2) > 1$. Using numerical simulations of (3.4), we examine how the amplitude of the adding-sliding periodic orbit measured from the pseudoequilibrium $(\tilde{p}_1, \tilde{p}_2, \tilde{z})$ in (3.11) scales with the distance to the bifurcation point $a_{q_{\text{crit}}} = q_2/q_1$. For $a_{q_{\text{crit}}} - a_q < 0.1$, we record the amplitude as the difference in the maximum and minimum values of $H - \tilde{H}$, $G - \tilde{G}$, and $z - \tilde{z}$, where

$$H = p_1 - a_qp_2\,, \quad \tilde{H} = \tilde{p_1} - a_q\tilde{p_2}\,, \quad G = a_qp_1 + p_2\,, \quad \tilde{G} = a_q\tilde{p_1} + \tilde{p_2}\,.$$

Based on visual inspection, the scaling near $a_{q_{\text{crit}}}$ appears to be linear (see Figure 3.5). For comparison, a linear scaling relation is known to arise for the "generalised Hopf bifurcation" for piecewise-smooth dynamical systems discussed

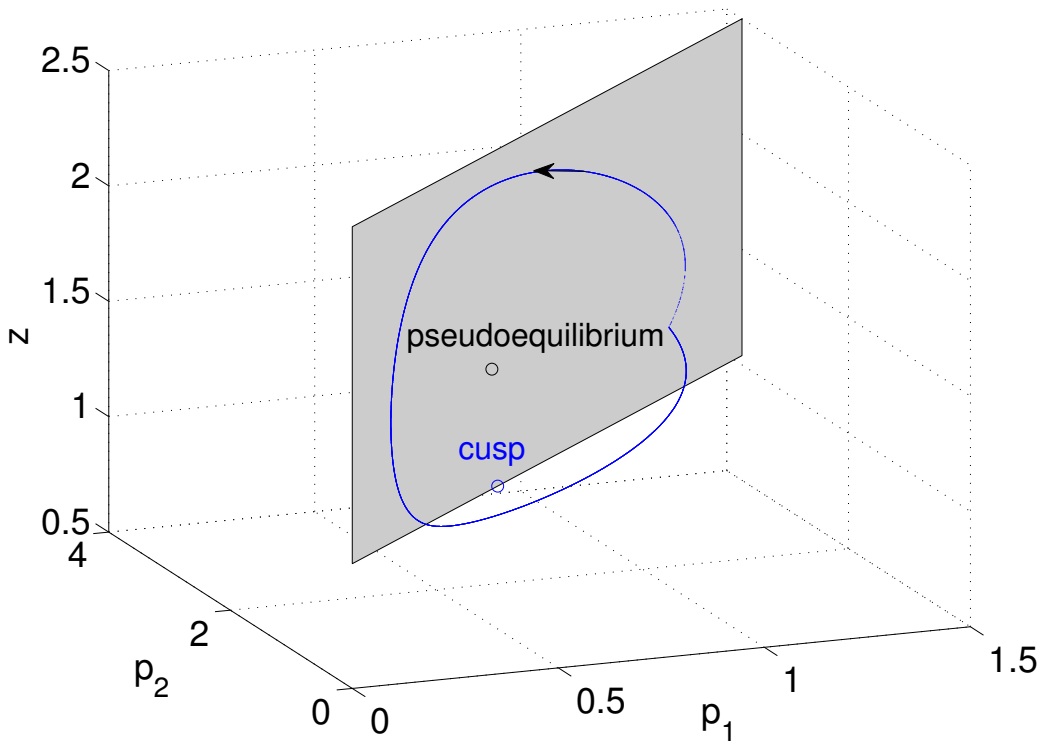

Figure 3.4: Example trajectory of (3.4) for $a_q = 0.4$, $q_1 = 1$, $q_2 = 0.5$, $r_1 = 1.3$, $r_2 = 0.26$, $e = 0.25$, $m = 0.14$, and $\beta_1 = \beta_2 = 1$. The system has a periodic orbit that leaves the switching manifold (the stable sliding region is shaded) and returns to it because of a cubic tangency between f_+ and the switching manifold. Most of the time, the predator feeds on both prey types because the system's dynamics evolves on the switching boundary according to the sliding vector field (3.9). With these parameter values, the adding-sliding periodic orbit of (3.4) has a period of approximately 20 days. In a single cycle, the alternative prey is not being predated and $p_1/(a_q p_2) > 1$ for approximately 5.5 days.

in [114]. In this context, such a generalised Hopf bifurcation refers to a periodic orbit that is born when an equilibrium point of a planar, piecewise-smooth continuous system crosses the switching boundary. Recall that "continuous" is used to describe piecewise-smooth systems with a degree of smoothness of 2 or higher (see Definition 2.2) in which the trajectories always cross the switching boundary

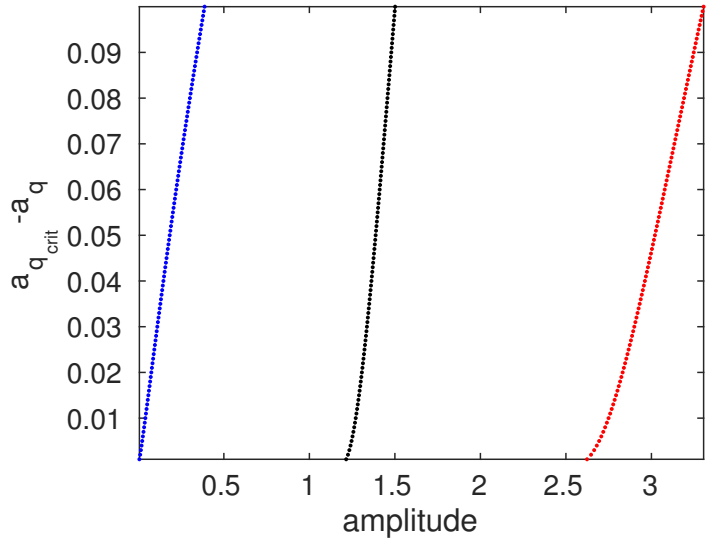

Figure 3.5: Amplitude of $H - \tilde{H}$ (blue), $G - \tilde{G}$ (red), and $z - \tilde{z}$ (black) of (3.4) [for parameter values $q_1 = 1$, $q_2 = 0.5$, $r_1 = 1.3$, $r_2 = 0.26$, $e = 0.25$, $m = 0.14$, and $\beta_1 = \beta_2 = 1$] versus the distance $a_{q_{\text{crit}}} - a_q < 0.1$ from the bifurcation point $a_{q_{\text{crit}}} = q_2/q_1$. We calculate a least-squares fit of a straight line to the amplitudes (calculated as the difference in the maximum and minimum values) and the equations for these lines are $(H - \tilde{H})$ $y = 0.26x$ ($R^2 \approx 0.99$); $(G - \tilde{G})$ $y = 0.16x - 0.43$ ($R^2 \approx 0.99$); and $(z - \tilde{z})$ $y = 0.38x - 0.47$ ($R^2 \approx 0.98$).

without evolving along it [23]. In the generalised Hopf bifurcation, a complex conjugate pair of eigenvalues of a piecewise-linear system (which is obtained by linearising a piecewise-smooth system) have a negative real part on one side of the switching boundary, a zero real part on the switching boundary, and a positive real part on the other side of the switching boundary [114]. In a similar bifurcation in three-dimensional piecewise linear systems—namely, in the focus-centre-limit cycle bifurcation—the amplitude of the limit cycle scales as $d^{2/3}$, where d is the distance from the bifurcation point [34].

The bifurcation in (3.4), in which an adding-sliding periodic orbit arises from a centre, has not (to our knowledge) been studied previously. Because a centre

transitions to such a two-part periodic orbit, we call this a *centre to two-part periodic orbit ("C2PO") bifurcation.* In the C2PO bifurcation, adding-sliding periodic orbits are born via a two-event sequence. First, there is a bifurcation reminiscent of the standard Hopf bifurcation from smooth dynamical systems. This arises via the behaviour of the eigenvalues of the sliding vector field f_s, as the pseudoequilibrium changes from attracting to repelling and a periodic orbit appears. Second, as the distance to the bifurcation point increases, the periodic orbit grows and an adding-sliding bifurcation ensues [23].

The C2PO bifurcation satisfies all four of the non-degeneracy conditions for an adding-sliding bifurcation [23] (see Appendix A). Indeed, the C2PO bifurcation resembles the standard adding-sliding bifurcation, in which a periodic orbit with a sliding segment and a non-sliding segment is born from an entirely sliding periodic orbit, but the way in which the periodic orbit is born is not quite the same. In contrast to the standard adding-sliding bifurcation, the C2PO bifurcation includes a family of entirely sliding centres (which we have proven are closed curves in Section 3.4.2) at the bifurcation point. The standard adding-sliding bifurcation has only one entirely sliding periodic orbit that grows to encompass a non-sliding segment as the distance from the bifurcation point increases [23].

3.4.4 Mechanism for the C2PO bifurcation

Using the change of coordinates we introduced in (3.19), we can write the sliding vector field in the u_2-u_3-plane as

$$\begin{aligned} \dot{u_2} &= u_2(r_1 + r_2 - u_3)\,, \\ \dot{u_3} &= e\frac{u_2}{1+a_q^2}(r_1 - r_2)(q_1 a_q - q_2) + u_3(e\frac{u_2}{1+a_q^2}(q_1 a_q + q_2) - 2m)\,. \end{aligned} \tag{3.28}$$

The system in (3.28) has a u_2-nullcline determined by $u_3 = r_1 + r_2$, and a u_3-nullcline determined by

$$u_3 = \frac{\frac{u_2}{1+a_q^2}e(r_1 - r_2)(q_1 a_q - q_2)}{2m - \frac{u_2}{1+a_q^2}e(q_1 a_q + q_2)}\,. \tag{3.29}$$

The pseudoequilibrium lies at the intersection of the nullclines and is given in the u_2-u_3-system by

$$\begin{aligned} \tilde{u}_2 &= \frac{2m(r_1 + r_2)(1 + a_q^2)}{e[(r_1 - r_2)(q_1 - a_q q_2) + (r_1 + r_2)(q_1 a_q + q_2)]}\,, \\ \tilde{u}_3 &= r_1 + r_2\,. \end{aligned} \tag{3.30}$$

By studying the nullclines of the two-dimensional u_2-u_3-system, we find the following mechanism for the C2PO bifurcation. For $a_q < a_{q_{\text{crit}}} = q_2/q_1$, the cusp (for f_+ in the system (3.4)) $(u_2, u_3) = (\frac{m}{eq_1 a_q}(1 + a_q^2), r_1 - r_2)$ lies at the intersection of the boundary between crossing and sliding regions (i.e., $u_3 = r_1 - r_2$) and one branch of the hyperbola determined by the u_3-nullcline in (3.29) (see Figure 3.6a). At the bifurcation point $a_q = a_{q_{\text{crit}}} = q_2/q_1$, both the pseudoequilibrium and the cusp move and become located on the same line (see Figure 3.6c). This happens at the

same time as the eigenvalues of the pseudoequilibrium cross the imaginary axis in the C2PO bifurcation. When $a_q > a_{q_{\text{crit}}} = q_2/q_1$, the pseudoequilibrium and the cusp are no longer aligned on the same line (see Figure 3.6b). Thus, the C2PO bifurcation involves two co-occurring events: (1) the eigenvalues of the pseudoequilibrium cross the imaginary axis and (2) the cusp for f_+ becomes aligned with the pseudoequilibrium.

3.4.5 Period-doubling

We compute a bifurcation diagram for (3.4) by determining the local maxima of the quantity $p_1/(a_q p_2) > 1$ when $a_q \to 0$ and $b_q \to q_2$. The period-1 adding-sliding periodic orbit that emerges when $a_q < q_2/q_1$ period-doubles as we decrease a_q from the bifurcation point. As we illustrate in Figure 3.7 (see Figure 3.8 for example trajectories and sliding segments of a period-2, period-4, and chaotic orbit), this suggests that there is a cascade to chaos as $a_q \to 0$. From a biological perspective, $a_q \to 0$ corresponds to the situation in which there is little decrease in the preference towards the alternative prey if the predator has an increase in specialisation towards the preferred prey.

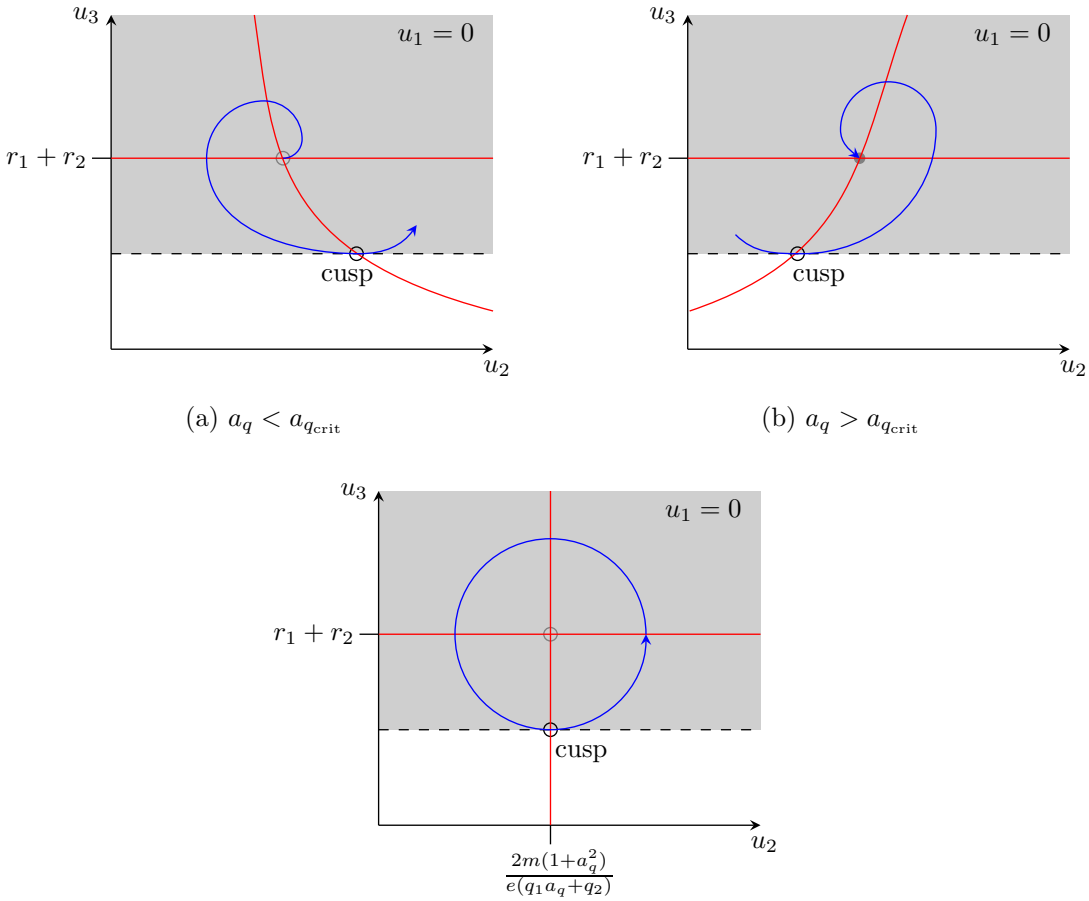

(a) $a_q < a_{q_{\text{crit}}}$

(b) $a_q > a_{q_{\text{crit}}}$

(c) $a_q = a_{q_{\text{crit}}}$

Figure 3.6: The mechanism for the C2PO bifurcation in (3.4) represented on the u_2-u_3-plane of the u_1-u_2-u_3-system (3.20). (a) When $a_q < a_{q_{\text{crit}}} = q_2/q_1$, the pseudoequilibrium is repelling (open grey circle). The cusp (open black circle) is located at the intersection of the boundary between sliding and crossing (dashed line) and the u_3-nullcline (red curve). (c) At the bifurcation point $a_q = q_2/q_1$, the cusp moves to be aligned on the same line (i.e., the u_3-nullcline) with the pseudoequilibrium. (b) When $a_q > q_2/q_1$, the cusp is located on the left branch of the u_3-nullcline and to the left of the attracting pseudoequilibrium (filled grey circle). The u_2- and u_3-nullclines are given in red and an example trajectory is in blue. We have shaded the sliding region.

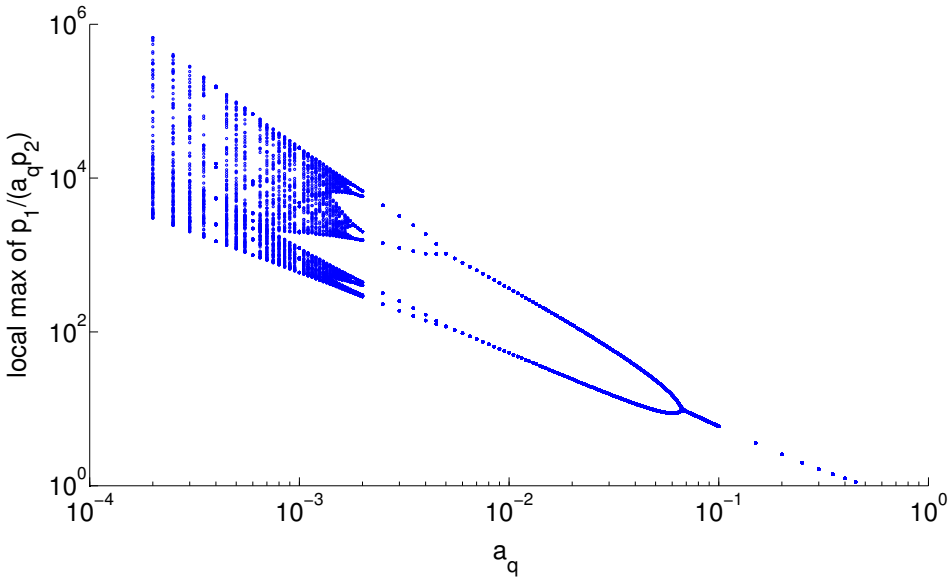

Figure 3.7: Local maxima of $p_1/(a_q p_2) > 1$ as $a_q \to 0$ for (3.4) with parameter values $r_1 = 1.3$, $r_2 = 0.26$, $e = 0.25$, $m = 0.14$, $\beta_1 = \beta_2 = 1$, and dimensional simulation time of 8000 days. We discarded the first 4000 days as a transient.

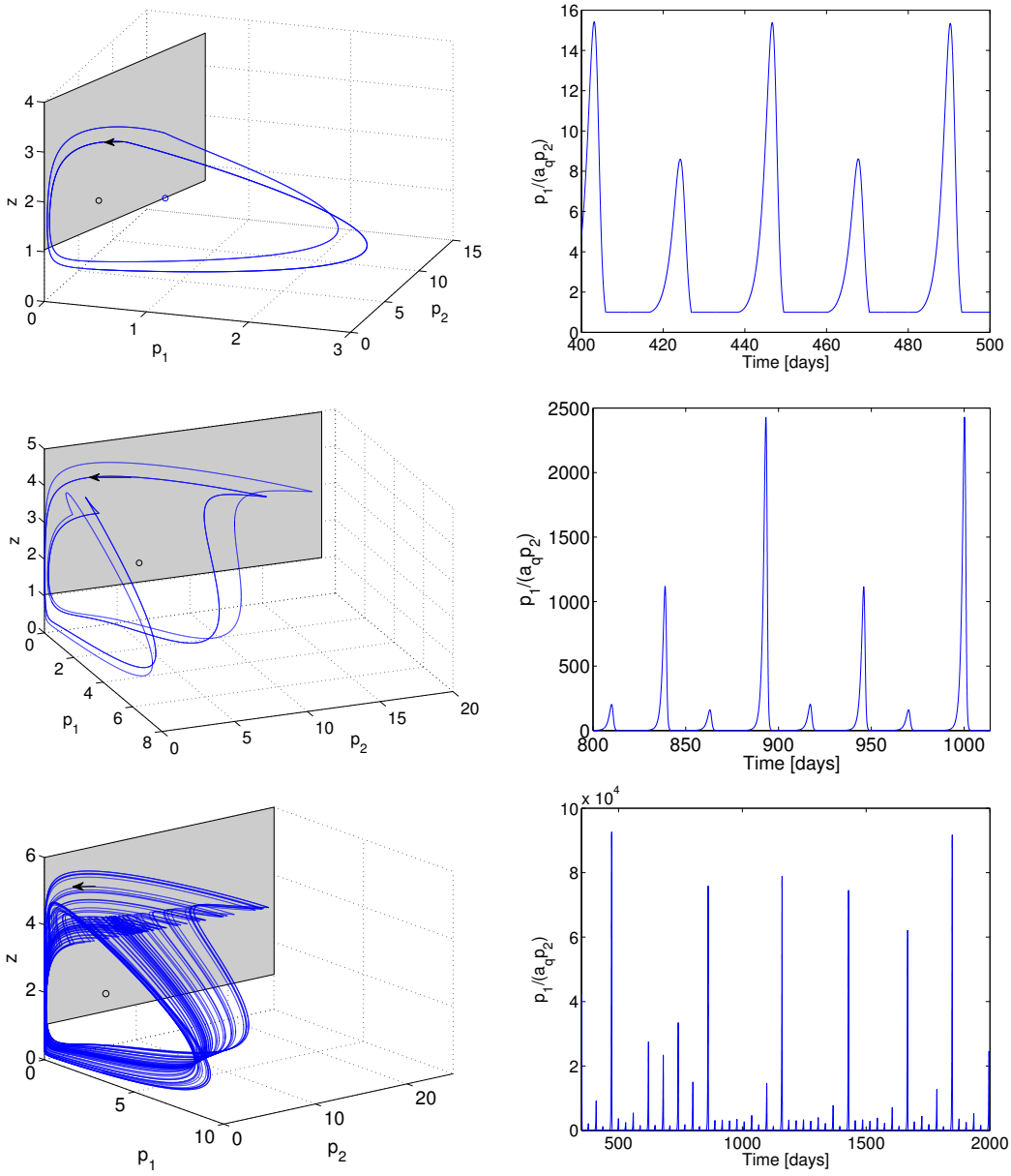

Figure 3.8: (Left) Example trajectories and (right) scaled prey ratio $p_1/(a_q p_2)$ of (3.4) with (top) $a_q = 0.06$, (middle) $a_q = 0.0035$, and (bottom) $a_q = 0.0005$ for the parameter values $q_1 = 1$, $q_2 = 0.5$, $r_1 = 1.3$, $r_2 = 0.26$, $e = 0.25$, $m = 0.14$, and $\beta_1 = \beta_2 = 1$.

The following mechanisms drive the piecewise-smooth system in (3.4) to exhibit the cascades seen in Figures 3.7 and 3.8. When $a_q = 0$, we write the system in (3.4) as

$$\dot{\mathbf{x}} = \begin{bmatrix} \dot{p_1} \\ \dot{p_2} \\ \dot{z} \end{bmatrix} = \left\{ \begin{array}{lll} f_+ = \begin{bmatrix} (r_1 - \beta_1 z)p_1 \\ r_2 p_2 \\ (eq_1\beta_1 p_1 - m)z \end{bmatrix}, & \text{if} & h = \beta_1 p_1 > 0 \\ f_- = \begin{bmatrix} r_1 p_1 \\ (r_2 - \beta_2 z)p_2 \\ (eq_2\beta_2 p_2 - m)z \end{bmatrix}, & \text{if} & h = \beta_1 p_1 < 0 \end{array} \right\}. \tag{3.31}$$

However, we note that the system (3.31) never crosses the boundary $\beta_1 p_1 = 0$ from f_+ to f_- for physically meaningful values. Effectively, when $a_q = 0$, the 1 predator-2 prey model in (3.4) is a Lotka-Volterra predator-prey system for z and p_1, while the alternative prey p_2 can grow exponentially. The system in (3.31) exhibits stable sliding for $z > r_1$. At $p_1 = 0$, the dynamics of (3.31) are governed by the sliding vector field

$$f_s = \frac{1}{2} \begin{bmatrix} 0 \\ (r_1 + r_2 - z)p_2 \\ z(eq_2 p_2 - m) - r_1 eq_2 p_2 \end{bmatrix}. \tag{3.32}$$

The two-dimensional sliding flow (3.32) has an equilibrium point at $(\tilde{p}_1, \tilde{p}_2, \tilde{z}) = (0, m(r_1 + r_2)/(r_2 eq_2), r_1 + r_2)$ with eigenvalues

$$\lambda_{1,2} = \frac{\frac{r_1 m}{r_2} \pm \sqrt{\left(\frac{r_1 m}{r_2}\right)^2 - 4(r_1 + r_2)m}}{2}.$$

For small (nonzero) a_q, the predator population is sufficiently small and the predator feeds on the alternative prey (i.e., when $p_1 - a_q p_2 < 0$), the preferred prey population p_1 grows exponentially. However, the quantity $p_1 - a_q p_2$ increases quickly after an increase in p_1 population, because the population p_2 decreases due to predation. As a result, the predator switches to feed on the preferred prey, and the alternative prey population p_2 starts to grow exponentially. Therefore, for small (nonzero) a_q, the trajectories follow a limit cycle in the z-p_1-phase plane which allows p_2 to reach a large population size. This phenomenon is seen as large peaks in the prey ratio $p_1/(a_q p_2)$ in the bottom right panel of Figure 3.8. Eventually, p_1 is predated by z and the trajectories reach the sliding region. In the case of $a_q = 0$, when a trajectory hits the sliding region $z > r_1$, the predator population either increases or decreases, depending on whether the point at which the switching boundary is reached is located to the left or to the right from a branch of the z-nullcline $z = r_1 e q_2 p_2/(e q_2 p_2 - m)$.

3.4.6 Numerical computations for calculating a normal form for the "C2PO" bifurcation

Because bifurcation diagrams from dynamical systems that represent processes in several different applications may look similar, it is necessary to classify (at least near the bifurcation points) all possible bifurcations in a formal way. Thus, one of the central aims of bifurcation theory is to assign each bifurcation a *normal form*, and impose *defining* and *non-degeneracy conditions*, to describe and distinguish a certain type of bifurcation from others. A normal form serves as an example system for a certain type of bifurcation. In smooth dynamical systems, the calculation

of a normal form involves using smooth and invertible parameter and coordinate changes (and time-reparametrisations) to transform the dynamical system to its simplest parameter-dependent form. The normal form is derived under the defining and non-degeneracy conditions that are the equality and inequality conditions, respectively, that specify a certain type of bifurcation [47, 72].

In the case of smooth dynamical systems, there is theory for several different kinds of bifurcations [72]. In Filippov-type piecewise-smooth dynamical systems, there exists a classification for the principal *codimension-1*[1] discontinuity-induced bifurcations that involve sliding (see Section 2.1.2.6). In these four cases—which we recall are (1) adding-sliding, (2) crossing-sliding, (3) grazing-sliding, and (4) switching-sliding—a limit cycle of a Filippov system interacts with the boundary between sliding and crossing regions.

The aforementioned four sliding bifurcations can be described analytically with *normal-form maps* [23]. The calculations of these maps include a local "discontinuity map" [99] that is defined near the point at which the trajectory of a piecewise-smooth system interacts with the discontinuity boundary. The discontinuity map is needed to correct for the extra passage acquired in the bifurcation. For example, in the general adding-sliding bifurcation, this extra passage is the non-sliding segment added to the trajectory when an entirely sliding periodic orbit is perturbed and leaves the switching manifold before landing back on it. In the classification of the sliding bifurcations, one is interested in a sliding bifurcation of a limit cycle and thereby in obtaining a global Poincaré map (see Section 2.1.2.7) for the piecewise-smooth vector field that exhibits a periodic orbit. Because such a Poincaré map is constructed as a composition of several Poincaré maps, of which one is the

[1]That is, the difference between the dimension of the parameter space and the dimension of the bifurcation boundary is 1.

name	Poincaré section	maps from	maps to	location
P_N	Π	z_n	z_{n+1}	see Figure 3.9 (left)
P_{12}	Π_1	z_1	$\hat{z}_2$	see Figure 3.9 (right)
P_{DM}	-	$\hat{z}_2$	$\hat{z}_3$	see Figure 3.9 (right)
P_{21}	Π_2	$\hat{z}_3$	z_4	see Figure 3.9 (right)

Table 3.1: A summary of the maps that we compute in this section. We compute the global map P_N by following a trajectory of (3.4) when $a_q < q_2/q_1$ [see Figure 3.9 (left)]. We compute P_{12} and P_{21} by following the sliding flow (3.9) across the boundary between sliding and crossing regions (see dashed lines in Figure 3.9), and we compute P_{DM} from the calculations for P_N, P_{12}, and P_{21}.

discontinuity map, the resulting global Poincaré map is also discontinuous [23].

The C2PO bifurcation satisfies all of the defining and non-degeneracy conditions of the adding-sliding bifurcation (see Appendix A). Thus, it will be possible to take advantage of the calculations [23] for the adding-sliding bifurcation in computing a normal-form map for the C2PO bifurcation. Therefore, the first step for such a computation is to find a discontinuity map P_{DM} that corrects for the extra passage acquired as the periodic orbit undergoes adding-sliding. In the case of the C2PO bifurcation, such a discontinuity map can be computed numerically using Poincaré sections.

We compute P_{DM} for the C2PO bifurcation as a combination of three maps: A global map P_N that takes into account, and two maps P_{12} and P_{21} that ignore, the cusp between f_+ and the switching boundary $h = 0$ [see Equation (3.16)]. For the corresponding Poincaré sections and points that P_N, P_{12}, P_{DM}, and P_{21} map, see Figure 3.9 and Table 3.1.

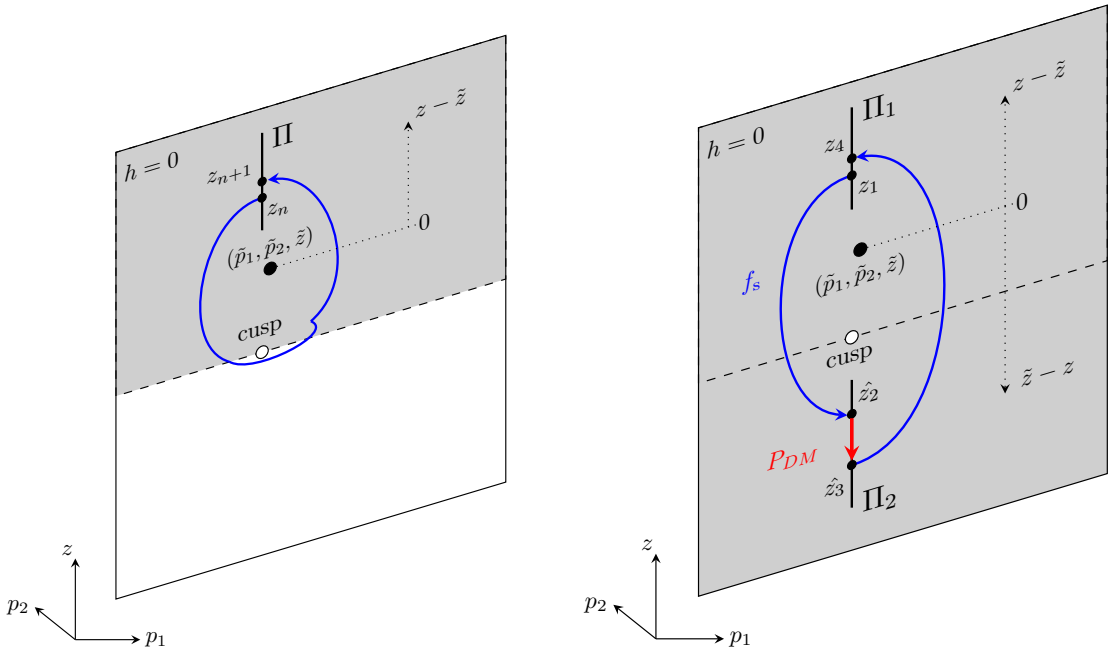

Figure 3.9: Location of the Poincaré sections (left) Π and (right) Π_1 and Π_2. The sliding region is shaded. (Left) The dashed line marks the boundary between the sliding and crossing regions, and the location of the pseudoequilibrium is marked with a black circle. (Right) The sliding region is extended beyond the boundary between the sliding and crossing regions (marked with the dashed line). This boundary is ignored and only sliding flow is considered in order to find the correction map P_{DM} (red). The location of the (unstable) pseudoequilibrium is marked with a black circle.

3.4.6.1 Calculation of the global map P_N

We calculate P_N with a Poincaré section Π located at the cusp given by Equation (3.16) (see Figure 3.9 (left) for the location of Π shown in the case of $a_q < q_2/q_1$). Thus, for a point z_{n+1} on Π

$$z_{n+1} = P_N(z_n)\,. \tag{3.33}$$

As expected from our numerical simulations in Section 3.4, there exists a periodic orbit for $a_q < a_{q_{\text{crit}}} = q_2/q_1$. Hence, P_N has a fixed point [see Figure 3.10 (top)] and intersects with the line $z_{n+1} = z_n$. At the bifurcation point $a_q = a_{q_{\text{crit}}} = q_2/q_1$, there is a family of centres, of which the largest has a radius of about 0.6 [see Figure 3.10 (bottom left)]. For $a_q > a_{q_{\text{crit}}} > q_2/q_1$, there exists an attracting pseudoequilibrium [see Figure 3.10 (bottom right)].

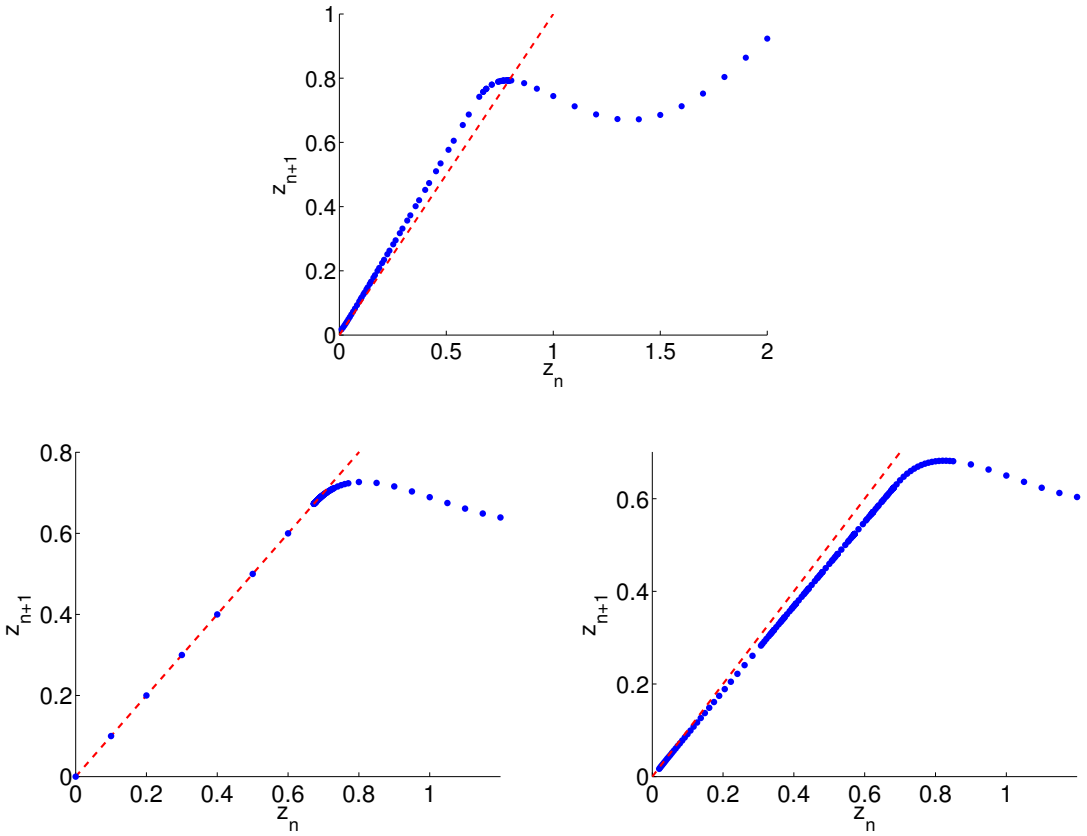

Figure 3.10: Numerical computations of P_N in (3.33) for (top) $a_q = 0.4 < a_{q_{\text{crit}}}$, (bottom left) $a_q = 0.5 = a_{q_{\text{crit}}}$, and (bottom right) $a_q = 0.6 > a_{q_{\text{crit}}}$. The initial distance (i.e., from point z_n) to the pseudoequilibrium is given on the horizontal axis. The vertical axis is the distance to the pseudoequilibrium after one iteration of the map (i.e., z_{n+1}). The red line is $z_{n+1} = z_n$.

3.4.6.2 Calculations of the local maps P_{12}, P_{21}, and P_{DM}

In order to find the discontinuity map P_{DM} [see Figure 3.9 (right)], we are only interested in a_q values near the bifurcation where the 1 predator-2 prey system (3.4) exhibits an adding-sliding periodic orbit (i.e., $a_q = 0.4 < q_2/q_1$). In addition, we are only interested in centres that are greater than the largest entirely sliding centre at the bifurcation when $a_q = q_2/q_1$ (see the blue trajectory that reaches the boundary between sliding and crossing, and slowly converges to the periodic orbit that is tangent to the sliding boundary in Figure 3.2).

For the calculation of P_{DM} from numerical simulations, we introduce the following matrix operation to represent a general mapping P from a point z_n to z_{n+1}

$$z_{n+1} = Pz_n = \begin{pmatrix} z_{n+1}^1 \\ z_{n+1}^2 \\ \vdots \\ z_{n+1}^N \end{pmatrix} = \begin{pmatrix} P^{1,1} & 0 & \cdots & 0 \\ 0 & P^{2,2} & \cdots & 0 \\ \vdots & \vdots & \ddots & \vdots \\ 0 & 0 & \cdots & P^{NN} \end{pmatrix} \begin{pmatrix} z_n^1 \\ z_n^2 \\ \vdots \\ z_n^N \end{pmatrix}. \tag{3.34}$$

Because P is diagonal, we can compute its entries from $P^{i,i} = \frac{z_{n+1}^i}{z_n^i}$.

We use a similar approach that is presented in [23] to derive the discontinuity maps for the four principal sliding bifurcations. Thus, we calculate the maps P_{12} and P_{21} that ignore the cusp (and the boundary between sliding and crossing regions) by following the sliding flow f_s (3.9) of the 1 predator-2 prey system (3.4). The locations of the Poincaré sections Π_1 and Π_2 for these maps are sketched in Figure 3.9 (right). Therefore, if we start from a point z_1 on Π_1, and follow a trajectory of the sliding flow (3.9) that reaches, and goes across, the boundary

between sliding and crossing [i.e., the dashed line in Figure 3.9 (right)], we reach $\hat{z}_2$ on Π_2. For $\hat{z}_2$, we have

$$\hat{z}_2 = P_{12}(z_1)\,. \tag{3.35}$$

Similarly, we can follow a trajectory of the sliding flow (3.9) from a point $\hat{z}_3$ on Π_2 that reaches, and goes across, the boundary between sliding and crossing before reaching z_4 located on Π_1. For z_4, we have

$$z_4 = P_{21}(\hat{z}_3)\,. \tag{3.36}$$

Thereby, the unknown discontinuity map P_{DM}, which is the correction needed for the non-sliding segment in the adding-sliding periodic orbit, relates the two points $\hat{z}_2$ and $\hat{z}_3$ on Π_2 by

$$\hat{z}_3 = P_{DM}(\hat{z}_2)\,. \tag{3.37}$$

Using Equations (3.35)–(3.37), we can write the returning point z_4 on Π_1 [see Figure 3.9 (right)] as a combination of three maps:

$$z_4 = P_{21} \circ P_{DM} \circ P_{12}(z_1)\,. \tag{3.38}$$

In addition, from our earlier computations for P_N in (3.33), we know that $z_4 = P_N(z_1)$. Thus, we substitute (3.36) to (3.38) to give

$$P_N(z_1) = P_{21}(P_{DM}(P_{12}(z_1)))\,. \tag{3.39}$$

Finally, we obtain

$$P_{DM} = [P_{21}]^{-1}(P_N(z_1))\,. \tag{3.40}$$

Considering each map in the matrix form that we gave in (3.34), and using the equations above, we show a numerical computation of P_{DM} in Figure 3.11.

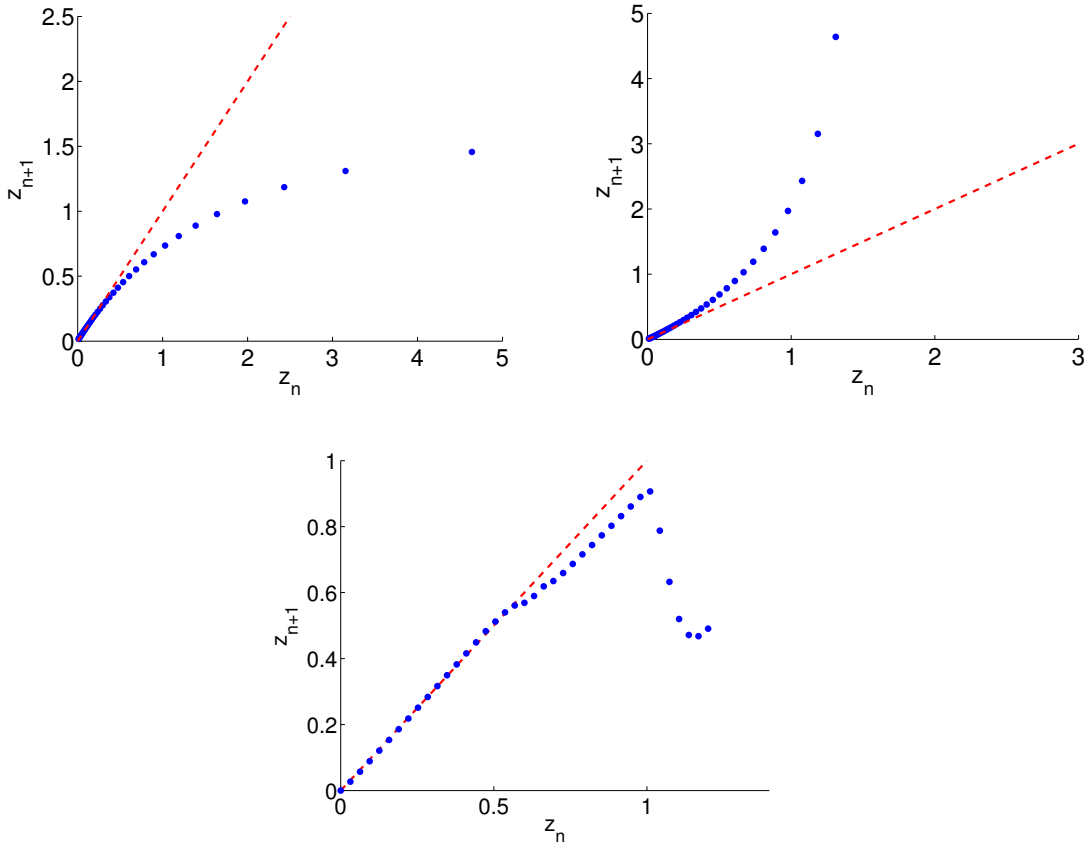

Figure 3.11: Numerical computations of (top left) P_{12}, (top right) P_{21}, and (bottom) P_{DM}. The initial distance (i.e., from point z_n) to the pseudoequilibrium is given on the horizontal axis. The vertical axis is the distance to the pseudoequilibrium after one iteration of the map (i.e., z_{n+1}). The red line is $z_{n+1} = z_n$.

The numerical computations for the discontinuity map P_{DM} are a necessary step in the derivation of a globally correct Poincaré map for the C2PO bifurcation. Above, we obtained a numerical description of the discontinuity map P_{DM} that is determined locally near the point where the interaction between the trajectory and the boundary between sliding and crossing occurs. Using numerical computations

similar to above combined with Taylor series expansions, we can derive an "incorrect" map (for the whole period) that is determined in the region where there is no interaction between the trajectories and the boundary between sliding and crossing. By combining these computations with the computations above, we can derive a (non-smooth) globally correct Poincaré map to describe the characteristics of closed orbits exhibited by the 1 predator-2 prey system in (3.4). Finally, by taking advantage of the calculations in [23] for the adding-sliding bifurcation, we can compute a normal-form map for the C2PO bifurcation.

3.4.7 Comparison of 1 predator-2 prey model simulations and planktonic protozoa-algae data

In this section, we compare the prey ratio of adding-sliding period-1 and period-2 orbits from the 1 predator-2 prey model (3.4) with data on cryptophyte and diatom prey collected from Lake Constance in spring (see Section 1.2.2). We choose to compare the scaled prey ratio $p_1/(a_q p_2)$ predicted by the model with the scaled prey ratio calculated from the data because $p_1/(a_q p_2) = 1$ indicates when the dynamics of the 1 predator-2 prey system (3.4) are governed by the sliding vector field (3.9) at the switching boundary.

Previous studies of the Lake Constance data set suggest that ciliates are the most abundant herbivorous zooplankton group in spring, whereas cryptophytes and diatoms are the dominant species groups in the phytoplankton community [126]. Our motivation to compare the data and our prey-switching model is the prey preference among ciliate species that actively select against diatom prey when offered a mixed diet of both cryptophytes and diatom prey [94]. We restrict the

time window of comparison to spring, as it has been suggested that predator-prey feeding interactions are an important factor in explaining the ciliate-algal dynamics in Lake Constance in that season [128]. Moreover, it is also believed that in the spring such interactions have larger relative importance than environmental conditions [116].

We use six different cryptophyte species as the group of preferred prey and three different diatoms species to represent the ciliates' alternative prey. We include data for phytoplankton whose cell size is sufficiently small compared to the size of ciliate predators and which dominate the algal community in Lake Constance in spring [126]. For both species groups, we use linear interpolation to obtain intermediate biomass values for each day of the year from approximately bi-weekly measurements. We then calculate the mean of the 20 interpolated yearly data between 1979 and 1999. These data exhibit an increasing trend. We remove the trend by subtracting a least-squares fit of a straight line from the data. In Figure 3.12, we compare these data with the prey ratio that we obtain from simulations of Equation (3.4). Although the model does not capture the increasing trend, it successfully reproduces the periodic pattern early in the growing season when one can argue that predator-prey interactions govern the protist-algae dynamics more than physical driving forces in water masses that are rich in nutrients [116].

3.5 Discussion

We have combined adaptive predator behaviour and ecological trade-offs to model the dynamics of a predator that feeds on a preferred and alternative prey as a

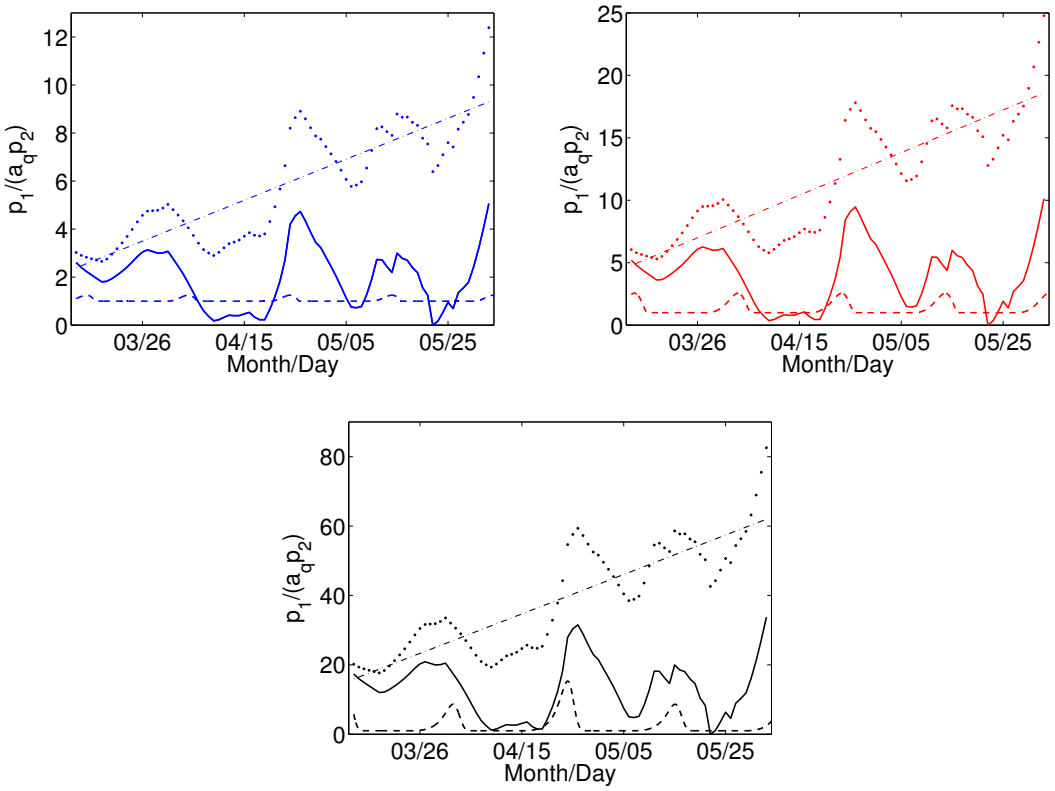

Figure 3.12: (Dashed curves) Scaled prey ratio $p_1/(a_q p_2)$ for simulations of (3.4) [for parameter values $r_1 = 1.3$, $r_2 = 0.26$, $e = 0.25$, $m = 0.14$, and $\beta_1 = \beta_2 = 1$]; (points) mean data calculated for the scaled prey ratio $p_1/(a_q p_2)$ in spring in Lake Constance over the period 1979–1999; and (solid curves) processed data. The prey ratios are scaled by (top left) $a_q = 0.4$, (top right) $a_q = 0.2$, and (bottom) $a_q = 0.06$. For each panel, we obtain the processed data by subtracting a least-squares fit of a straight line (dash-dotted lines) to the means of the data. The equations for these lines are (top left) $y = 0.08x + 2.49$, where the norm of the residuals is 10.97; (top right) $y = 0.17x + 4.77$, where the norm of the residuals is 21.94; and (bottom) $y = 0.57x + 15.91$, where the norm of the residuals is 73.12. We then rescale the detrended data to have a minimum of 0. The preferred prey p_1 is composed of data for *Cryptomonas ovata*, *Cryptomonas marssonii*, *Cryptomonas reflexa*, *Cryptomonas erosa*, *Rhodomonas lens*, and *Rhodomonas minuta*. The alternative prey group p_2 is composed of data for small and medium-size *Chlamydomonas* spp. and *Stephanodiscus parvus*.

piecewise-smooth dynamical system. The model in Equation (3.4) describes a predator that can adaptively change its diet depending on the abundances of its

preferred and alternative prey. We assumed a linear trade-off in prey preference and analysed the dynamics of the system as we adjusted the slope of the trade-off. To compensate for the preference, we assumed that the preferred prey has a larger growth rate than the alternative prey.

The model predicts a steady state for the predator and prey populations as long as the trade-off in prey preference is sufficiently steep. In other words, a steady state occurs when a small increase in specialisation towards the preferred prey would result in a large decrease in how much energy the predator could gain from the alternative prey. As we decrease the slope of the preference trade-off, a periodic orbit appears and period-doubles as the slope approaches 0. After the bifurcation, the population densities oscillate and the prey ratio is no longer constant. From a biological perspective, a mild trade-off suggests that a small increase in the energy gained from the preferred prey would come at a small cost in the energy gained from the alternative prey. We considered a linear preference trade-off as a first step towards studying the effect of such a trade-off in a predator-prey interaction in which prey switching occurs. Although several studies and observations support the existence of trade-offs [66, 83], it is not clear what kind of functional form they take. A previous model for population dynamics and prey switching studied a convex (i.e., concave down) trade-off between the attack rate and the degree of specialisation exhibited by a predator [3]. Concave relationships have been formulated for the consumption of, and the energy obtained from, two prey species in an approach in which these functions are plotted in the same picture in order to solve the problem of optimal diet [106]. To develop a more complete understanding of the effects of a preference trade-off on population dynamics, it would be useful to consider generalisations of the model with nonlinear trade-off

functions. From a mathematical perspective, a nonlinear trade-off could lead to a more complex switching boundary, which in turn could lead to different types of bifurcation scenarios than in the current model.

We chose to use exponential prey growth to simplify analytical calculations. An important generalisation is to consider logistic prey growth, as nutrient limitation is one of the most important nonliving factors that can drive the temporal pattern of phytoplankton growth [117]. However, it has been suggested that the importance of nutrient limitation is less pronounced than protist grazing at the beginning of a growth season [116] for water masses that are rich in nutrients. Although considering logistic prey growth increases the number of parameters in the model (in addition to making analytical calculations significantly more challenging), it has two key advantages: (1) it would expand the suitable time window for comparing simulations with data in water masses that are rich in nutrients; and (2) its less restrictive assumptions yield a model that is also reasonable in principle for water masses with low nutrient levels [116]. In addition, such a generalisation would result in a Filippov system with more than one steady state to interact with the switching manifold and thereby create different dynamical behaviour than in the current model with unlimited prey growth.

The 1 predator-2 prey system (3.4) describes a feeding interaction in which there is a known predator preference and in which there is active selection against an alternative prey. This model reproduces the periodicity in the scaled prey ratio during the early growing season in Lake Constance, during which predator-prey interaction has been suggested as an important driving factor for ciliate-algae dynamics. However, it does not capture the increasing trend in the data. We speculate that a generalisation of the model that allows the prey growth to increase

slowly in time might make it possible to also capture the increasing trend. We motivate the time-dependent prey growth rate by the fact that the phytoplankton production-to-biomass ratio calculated for Lake Constance exhibits a linear increase in the prey growth in spring and a decrease in the autumn [39]. Scaling the prey ratio by the time since the start of the spring would then allow us to test whether growth is slowly increasing over the length of the growing season. However, we recall that Lake Constance (that in its natural state would be a lake with a low level of productivity) was categorised as a lake with an intermediate level of productivity when the data were collected [128] (see Section 1.2.2). Nowadays, Lake Constance is again categorised as a lake with a low level of productivity [36]. Thus, it is possible that the increasing trend in the prey ratio reflects not only a change in nutrient availability from early to mid growing season but also a change in the lake's level of productivity.

The model exhibits a novel (so-called "C2PO") bifurcation, in which the dynamics transitions at the bifurcation point between convergence to a pseudoequilibrium and periodic adding-sliding oscillations through a centre. This emergence of adding-sliding orbits differs from the way in which they usually emerge in piecewise-smooth dynamical systems [23]. The standard mechanism entails the birth of an adding-sliding periodic orbit following a bifurcation in which the eigenvalues of the pseudoequilibrium cross the imaginary axis, so that the pseudoequilibrium changes from attracting to repelling and an entirely sliding periodic orbit is born. As the amplitude of the periodic orbit (which lies entirely on the switching boundary) grows, the sliding periodic orbit eventually becomes tangent to the boundary between sliding and crossing. Finally, this periodic orbit becomes a trajectory that has a sliding segment separated by a non-sliding segment [23].

We observed numerically that the amplitude scaling of the adding-sliding periodic orbit that emerges from the C2PO bifurcation appears to be linear in the distance from the bifurcation, which is also the case for the generalised Hopf bifurcation in piecewise-smooth dynamical systems [114]. The C2PO bifurcation resembles the focus-centre-limit cycle bifurcation in three-dimensional piecewise linear systems [34]. However, the difference in amplitude scaling in the C2PO and focus-centre-limit cycle bifurcation suggests that different normal forms characterise these bifurcations [72]. In addition, the C2PO bifurcation satisfies all of the defining and non-degeneracy conditions of the standard adding-sliding bifurcation [23]. Thus, by following the derivation of a normal-form map for a sliding bifurcation [23], we started the construction of a normal form for the C2PO bifurcation by computing numerically the discontinuity map that is defined near the point at which the trajectory of a piecewise-smooth system interacts with the discontinuity boundary.

3.6 Conclusions

In this chapter, we combined two ecological concepts—prey switching and trade-offs—and used the framework of piecewise-smooth dynamical systems to develop a model of one predator that feeds on a preferred and an alternative prey. We derived analytical expressions for the pseudoequilibrium, its eigenvalues, and the points for tangencies between the two vector fields and the switching boundary. We then confirmed our analytical results using numerical simulations, and we discovered a novel bifurcation in which an adding-sliding periodic orbit is born from a centre.

Based on numerical simulations close to the bifurcation point, the amplitude of the adding-sliding periodic orbit seems to scale linearly with the distance from the bifurcation point. In addition, we carried out numerical computations for constructing a normal-form map to describe the centre to two-part periodic orbit ("C2PO") bifurcation.

Although we have motivated our investigation primarily from a biological perspective, it is also important to stress the utility of our model for development of new theoretical understanding in piecewise-smooth dynamical systems. The biological and mathematical motivations complement each other very well, and investigating the condition for sliding corresponds to studying a scaled prey ratio, and this in turn offers a possible link between ecological trade-offs and population dynamics. Hence, the model offers an encouraging example of how combining theoretical and practical perspectives can give new insights both for the development of theory of piecewise-smooth dynamical systems as well as for the development of models of population dynamics with predictive power.

In this chapter, we have interpreted adaptation as flexible feeding behaviour of a predator that has two feeding modes for consuming its preferred and alternative prey. In addition, we have assumed that the switch in the predator's feeding behaviour is discontinuous. Therefore, in the next chapter, we will relax this assumption and consider a gradual change in the predator's feeding mode. Thus, we will construct a smooth dynamical-system analog of (3.4) in two different ways to enable a comparison of piecewise-smooth and smooth dynamical systems, and to give insight into modelling an abrupt or a gradual change in feeding behaviour and population dynamics.

Chapter 4

Two smooth analogs of the piecewise-smooth 1 predator-2 prey dynamical system

In Chapter 3, we constructed and studied the dynamical behaviour of a 1 predator-2 prey piecewise-smooth system based on the assumption of an optimal forager adaptively switching between two prey. In the piecewise-smooth system, the change in the predator's diet choice is discontinuous. In this chapter, we aim to relax this assumption of a discontinuous switch and construct a 1 predator-2 prey system that allows a gradual change in the predator's adaptive feeding behaviour. We do this in two different ways. First, we write a smooth analog for the system in (3.4) by using hyperbolic tangent functions. Second, we obtain another smooth analog of (3.4) by considering the desire to consume the preferred prey—a parameter that changes abruptly across the discontinuity in the piecewise-smooth system—as a variable that changes along with the population dynamics. By carrying out stability analyses for the two smooth systems, simulating them in

a biologically relevant parameter regime, and comparing model predictions with data from Lake Constance, we gain insight into not only the differences between the adaptive feeding behaviour of unselective (i.e., "filter feeders") and selective (i.e., "interception feeders") ciliate predators, but also different *regularisations* of a piecewise-smooth dynamical system.

4.1 Introduction

Traditionally, the parameters that represent ecologically important traits of predator and prey species in models of population dynamics are taken to be fixed quantities (see Section 1.1.1). However, as we discussed in Section 1.1.2, there has been an increasing number of both theoretical and empirical studies that report the effects of phenotypic change in prey and/or predator species on predator-prey population dynamics. It has become evident that evolutionary and ecological dynamics should not be considered separately in cases in which it is possible for evolutionary change of traits to occur on a time scale comparable to that of the ecological interactions [38]. Recent studies have demonstrated that rapid adaptation of traits affects ecological interactions and can be observed especially in organisms with short lifespans, such as species in plankton communities [8, 61].

In Chapter 3, we considered an optimal forager that can adaptively change its diet in response to the abundances of its preferred and alternative prey. The assumption of an optimal forager results in an abrupt change of diet and a discontinuity between the two vector fields. However, it is unclear whether there exist such "discontinuous predators". However, no evidence has been reported

(to our knowledge) for any of the possible smooth approximations that one can choose to model prey switching. Therefore, in this chapter, we aim to relax the assumption of a discontinuous switch and consider a 1 predator-2 prey system that includes a gradual change in the predator's adaptive feeding behaviour. Thus, by reformulating the 1 predator-2 prey piecewise-smooth dynamical system as a three-dimensional smooth dynamical system with hyperbolic tangent functions, and as a four-dimensional smooth dynamical system, we construct two novel (to our knowledge) models for a predator and its two prey that accounts for adaptive feeding and an ecological trade-off in prey preference.

4.2 Smooth analog I of the piecewise-smooth 1 predator-2 prey dynamical system

A smooth analog of the piecewise-smooth 1 predator-2 prey system (3.4) can be written using hyperbolic tangent functions as follows:

$$\begin{aligned}
\dot{p_1} &= (r_1 - \beta_1 z)p_1 \left(\frac{1+\tanh(k(\beta_1 p_1 - a_q\beta_2 p_2))}{2}\right) + r_1 p_1 \left(\frac{1-\tanh(k(\beta_1 p_1 - a_q\beta_2 p_2))}{2}\right) \\
&\equiv f(p_1, p_2, z)\,, \\
\dot{p_2} &= r_2 p_2 \left(\frac{1+\tanh(k(\beta_1 p_1 - a_q\beta_2 p_2))}{2}\right) + (r_2 - \beta_2 z)p_2 \left(\frac{1-\tanh(k(\beta_1 p_1 - a_q\beta_2 p_2))}{2}\right) \\
&\equiv g(p_1, p_2, z)\,, \qquad (4.1) \\
\dot{z} &= (eq_1\beta_1 p_1 - m)z \left(\frac{1+\tanh(k(\beta_1 p_1 - a_q\beta_2 p_2))}{2}\right) \\
&+ (eq_2\beta_2 p_2 - m)z \left(\frac{1-\tanh(k(\beta_1 p_1 - a_q\beta_2 p_2))}{2}\right) \equiv h(p_1, p_2, z)
\end{aligned}$$

where k determines the steepness in the transition of the predator's feeding behaviour. To follow the assumptions that we made in the construction of the piecewise-smooth system and thereby to facilitate the future comparison between the piecewise-smooth and smooth system I, we take $\beta_1 = \beta_2 = 1$, as in Chapter 3, in order to omit β_1 and β_2 in our analysis.

4.2.1 Linear stability analysis of the smooth system I

At a steady state, $f(p_1, p_2, a) = g(p_1, p_2, z) = h(p_1, p_2, z) = 0$. This yields

$$\begin{aligned} f &= p_1 \left(r_1 - z \left(\frac{1 + \tanh(k(p_1 - a_q p_2))}{2} \right) \right) = 0 \\ &\Rightarrow z \left(\frac{1 + \tanh(k(p_1 - a_q p_2))}{2} \right) = r_1, \qquad (4.2) \\ g &= p_2 \left(r_2 - z \left(\frac{1 - \tanh(k(p_1 - a_q p_2))}{2} \right) \right) = 0 \\ &\Rightarrow z \left(\frac{1 - \tanh(k(p_1 - a_q p_2))}{2} \right) = r_2 \,. \qquad (4.3) \end{aligned}$$

Summing (4.3) and (4.2) and setting (4.3) equal to (4.2) yields the following equations for a steady state solution $(\tilde{p}_1, \tilde{p}_2, \tilde{z})$:

$$\begin{aligned} \tilde{z} &= r_1 + r_2 \\ (eq_1\tilde{p}_1 - m)r_1 + (eq_2\tilde{p}_2 - m)r_2 &= 0 \qquad (4.4) \\ \tanh(k(\tilde{p}_1 - a_q\tilde{p}_2)) &= \frac{r_1 - r_2}{r_1 + r_2} \,, \end{aligned}$$

which can be solved numerically. The Jacobian of the system (4.1) is

$$\begin{bmatrix} r_1 - \frac{z}{2}B\left(1 + p_1 kC\right) & \frac{zp_1 ka_q}{2}BC & \frac{-p_1}{2}B \\ \frac{zp_2 k}{2}BC & r_2 - \frac{z}{2}C\left(1 + p_2 ka_q B\right) & \frac{-p_2}{2}C \\ \frac{eq_1 z}{2}B\left(1 + p_1 kC\right) - \frac{eq_2 p_2 zk}{2}BC & \frac{eq_2 z}{2}C\left(1 + p_2 ka_q B\right) - \frac{eq_1 p_1 zka_q}{2}BC & \frac{eq_1 p_1}{2}B + \frac{eq_2 p_2}{2}C - m \end{bmatrix}, \tag{4.5}$$

where

$$\begin{aligned} A &= \tanh\left(k\left(p_1 - a_q p_2\right)\right), \\ B &= 1 + A, \\ C &= 1 - A. \end{aligned} \tag{4.6}$$

At $a_q = p_1/p_2$, $\tanh(k(p_1 - a_q p_2)) = 0$ and for any k the system (4.1) is given by

$$\begin{aligned} \dot{p_1} &= p_1\left(r_1 - \frac{z}{2}\right), \\ \dot{p_2} &= p_2\left(r_2 - \frac{z}{2}\right), \\ \dot{z} &= z\left(\frac{eq_1 p_1 + eq_2 p_2}{2} - m\right), \end{aligned} \tag{4.7}$$

which has three equilibria. There is a saddle at $(p_1, p_2, z) = (0, 0, 0)$. The eigenvalues of this saddle are $\lambda_1 = r_1$, $\lambda_2 = r_1$, and $\lambda_3 = -m$. There is an unstable focus-node (that exists for $a_q = 0$) at $(p_1, p_2, z) = (0, 2m/eq_2, r_2)$, and the eigenvalues are $\lambda_1 = r_1 - r_2/2$ and $\lambda_{2,3} = r_2/4 \pm 1/2\sqrt{r_2(r_2/4 - 2m)}$. Finally, there is another saddle (that exists for $a_q = \infty$) at $(p_1, p_2, z) = (2m/eq_1, 0, r_1)$. The eigenvalues of this saddle are $\lambda_1 = r_2 - r_1/2$ and $\lambda_{2,3} = r_1/4 \pm 1/2\sqrt{r_1(r_1/4 - 2m)}$.

When $a_q < p_1/p_2$ and $k \to \infty$, then $\tanh(k(p_1 - a_q p_2)) \to 1$. In addition, the

system (4.1) reduces to

$$\begin{aligned} \dot{p_1} &= (r_1 - z)p_1 \,, \\ \dot{p_2} &= r_2 p_2 \,, \\ \dot{z} &= (eq_1 p_1 - m)z \,. \end{aligned} \tag{4.8}$$

This has a nonhyperbolic equilibrium at $(\tilde{p}_1, \tilde{p}_2, \tilde{z}) = (m/eq_1, 0, r_1)$ with one real eigenvalue $\lambda_1 = r_2$, a pair of pure-imaginary eigenvalues $\lambda_{2,3} = \pm i\sqrt{mr_1}$, and an unstable equilibrium at $(\tilde{p}_1, \tilde{p}_2, \tilde{z}) = (0, 0, 0)$. The eigenvalues of the unstable equilibrium are $\lambda_1 = r_1$, $\lambda_2 = r_2$, and $\lambda_3 = -m$. If $a_q > p_1/p_2$ and $k \to \infty$, then $\tanh(k(\tilde{p}_1 - a_q\tilde{p}_2)) \to -1$ and the system (4.1) can be written as

$$\begin{aligned} \dot{p_1} &= r_1 p_1 \,, \\ \dot{p_2} &= (r_2 - z)p_2 \,, \\ \dot{z} &= (eq_2 p_2 - m)z \,. \end{aligned} \tag{4.9}$$

This has a nonhyperbolic equilibrium at $(\tilde{p}_1, \tilde{p}_2, \tilde{z}) = (0, m/eq_2, r_2)$, where the real eigenvalue is $\lambda_1 = r_1$ and the pair of purely imaginary eigenvalues is $\lambda_{2,3} = \pm\sqrt{mr_2}$, and an unstable equilibrium at $(\tilde{p}_1, \tilde{p}_2, \tilde{z}) = (0, 0, 0)$ with eigenvalues $\lambda_1 = r_1$, $\lambda_2 = r_2$, and $\lambda_3 = -m$. We summarize our findings of the linear stability analysis above in Table 4.1.

	state		$\tilde{p}_1$	$\tilde{p}_2$	$\tilde{z}$
I	trivial	$\circ$	0	0	0
II	p_1 extinct		0	$eq_2\tilde{p_2} = \frac{2m}{1-\tanh(k(-a_q\tilde{p}_2))}$	$\frac{2r_2}{1-\tanh(k(-a_q\tilde{p}_2))}$
	$k \to \infty$	$\star$	0	$m/(eq_2)$	r_2
III	p_2 extinct		$eq_1\tilde{p_1} = \frac{2m}{1+\tanh(k(\tilde{p}_1))}$	0	$\frac{2r_1}{1+\tanh(k(\tilde{p}_1))}$
	$k \to \infty$	$\star$	$m/(eq_1)$	0	r_1
VI	coexistence[1]		$\frac{a_q m(r_1+r_2)+\frac{eq_2r_2\operatorname{arctanh}\left(\frac{r_1-r_2}{r_1+r_2}\right)}{k}}{e(q_1a_qr_1+q_2r_2)}$	$\frac{m(r_1+r_2)-\frac{eq_1r_1\operatorname{arctanh}\left(\frac{r_1-r_2}{r_1+r_2}\right)}{k}}{e(q_1a_qr_1+q_2r_2)}$	r_1+r_2
	$k \to \infty$[2]		$\frac{a_q m(r_1+r_2)}{e(q_1a_qr_1+q_2r_2)}$	$\frac{m(r_1+r_2)}{e(q_1a_qr_1+q_2r_2)}$	r_1+r_2

[1] see Figure 4.1c in Section 4.2.2
[2] • if $a_q > q_2/q_1$

Table 4.1: Summary of the linear stability analysis for the smooth system I in Equation (4.1). We indicate an unstable steady state with an open circle, a non-hyperbolic equilibrium point with a star, and a stable steady state with a filled circle.

4.2.2 Numerical computations for the equilibrium point of the smooth system I

We now vary the slope a_q of the preference trade-off and the steepness of the prey switching k and study the steady state solution of the smooth system I in (4.4) numerically. With parameter values $(r_1, r_2, q_1, q_2, m, e) = (1.3, 0.26, 1, 0.5, 0.14, 0.25)$, the three eigenvalues of the steady state (4.4) have all a negative real part when both a_q and k are small (i.e., $k \lessapprox 3$) (see Figure 4.1c). We choose these parameter values from our parameter fitting of the piecewise-smooth model (see Appendix B) and they are the same as the values we use to simulate the piecewise-smooth system in Chapter 3. For larger a_q values (i.e., $a_q > 0.5$), the steady state is stable when k is large (i.e., $k \gtrapprox 70$). When a_q is small, the unstable steady state solution for the preferred prey $\tilde{p}_1$ is at its minimum, except for a very small k, when $\tilde{p}_1$

reaches its maximum concentration at a stable equilibrium (see Figure 4.1a). The steady-state concentration of the alternative prey $\tilde{p}_2$ reaches its maximum values when a_q is small, except for a very small k, when $\tilde{p}_2$ is at its minimum values (see Figure 4.1b). This behaviour of the steady state in (4.4) suggests that $k \to 0$ is a singular limit of the smooth system I in (4.1).

4.2.3 Comparison of the smooth analog I model simulations and planktonic protozoa-algae data

We now compare the predator abundance from the smooth system I model (4.1) with data on ciliate predators collected from Lake Constance in spring (see Section 1.2.2). We choose to compare the predator abundances predicted by the model with the data from years 1991 and 1998 because during these years the spring bloom lasted for several weeks and ciliate biomasses exhibit recurring patterns of increases followed by declines (see Section 1.2.2).

Similarly to Chapter 3, our motivation to compare the data and our prey-switching model is the prey preference among ciliate species that actively select against diatom prey when offered a mixed diet of both cryptophytes and diatom prey [94]. In addition, ciliate predators can be categorised roughly in terms of being more or less selective [136] (see Section 1.2.2). As well as in Chapter 3, we restrict the time window of comparison to spring in the case of the smooth system I, as it has been suggested that predator-prey feeding interactions are an important factor in explaining the ciliate-algal dynamics in Lake Constance in that season [128]. It is also believed that in the spring such interactions have larger relative importance than environmental conditions [116].

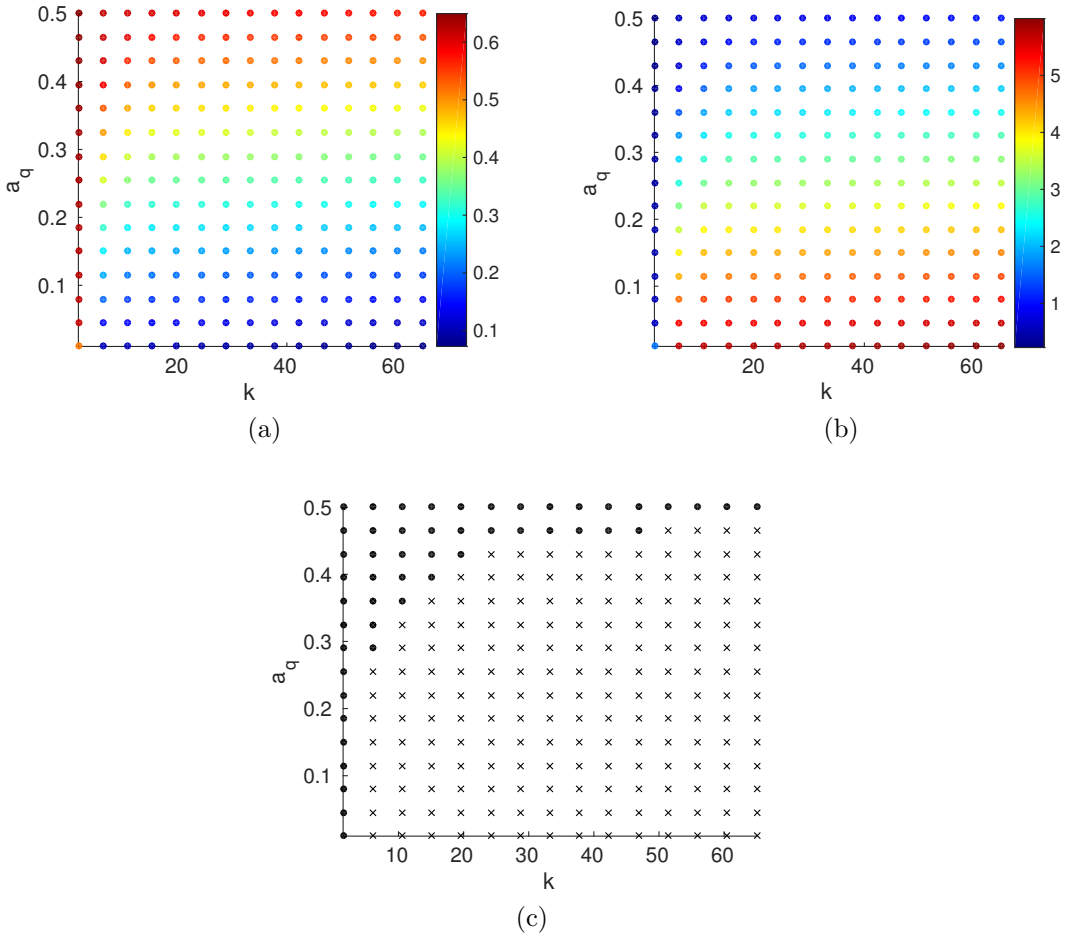

Figure 4.1: Numerical computations for the population density at equilibrium in (4.4) [for parameter values $e = 0.25$, $\beta_1 = \beta_2 = 1$, $r_1 = 1.3$, $r_2 = 0.26$, and $m = 0.14$] of the (a) preferred prey $\tilde{p}_1$ and (b) alternative prey $\tilde{p}_2$ at the indicated values of the slope of the preference trade-off a_q (vertical axis) and steepness of the predator switching k (horizontal axis). We indicate the value of the prey density at equilibrium in colour and compute numerically the steady-state solution of the smooth system I in (4.4) using MATLAB's `solve` function. To study the stability of these equilibria, we compute the eigenvalues of the Jacobian in (4.5) and indicate in panel (c) a stable steady state (4.4) with a filled circle (i.e., all the three eigenvalues of the Jacobian have a negative real part) and an unstable steady state with a cross (i.e., at least one of the three eigenvalues of the Jacobian has a positive real part).

We use two different predator species. For the predator that is more selective, we include data for *Balanion planctonicum* that hunt as interception feeders. By

contrast, for the predator that is less selective, we consider data for *Rimostrombidum lacustris* that sieve suspended food particles and are thus ciliate filter feeders (see Section 1.2.2). For both species abundances, we first normalise the approximately bi-weekly measurements by L_2-norm (see Appendix B). In Figures 4.2 and 4.4, we compare these data with the normalised predator abundance that we obtain from simulations of Equation (4.1).

In 1991, the model successfully reproduces the first increase in the selective predator abundance early in the growing season, and predicts an oscillatory pattern later during spring when one can argue that predator-prey interactions govern the protist-algae dynamics more than physical driving forces in water masses that are rich in nutrients [116] (see Figure 4.2, left). In addition, the parameter fitting suggests that the best fit between the model prediction and data is found in a parameter regime where the steepness of the switching function k of the selective predator species is large (see Figure 4.3, left). In the case of the unselective predator species, there is good agreement between the peak abundances predicted by the model and seen in the data (see Figure 4.2, right). The target distribution for the steepness of the prey switching suggests that a good fit between the data and the model prediction is found with both small and large k values (see Figure 4.3, right). However, the predator oscillations predicted by the model are not solely determined by k but depend also on the slope of the preference trade-off a_q. Indeed, the probability density estimate for a_q in the case of the unselective predator species in 1991 is concentrated on larger a_q values than in the case of the selective predator species (see Appendix B).

In 1998, the model successfully reproduces the peak abundances in the selective predator species in spring (see Figure 4.4, left). In addition, our parameter fitting

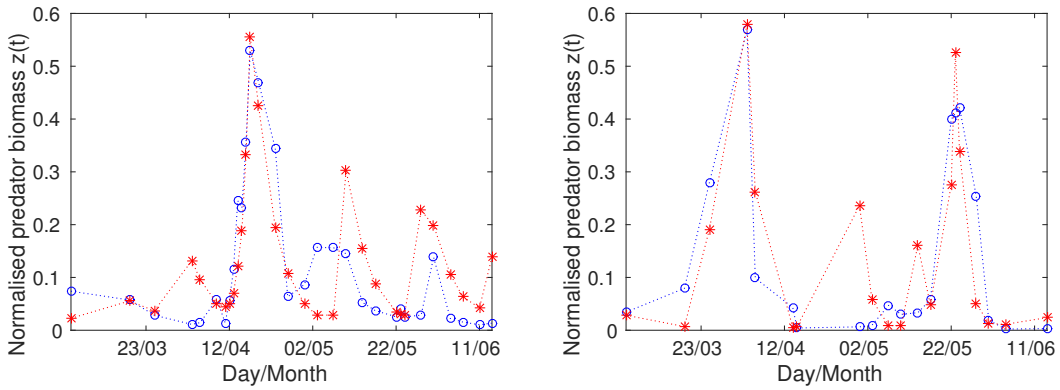

Figure 4.2: (Asterisks) Normalised predator abundance $z(t)$ for simulations of (4.1) [for parameter values $e = 0.25$, $\beta_1 = \beta_2 = 1$, (left) $r_1 = 1.06$, $r_2 = 0.30$, $m = 0.20$, $a_q = 0.03$, $k = 84$, and (right) $r_1 = 1.25$, $r_2 = 0.79$, $m = 0.47$ $a_q = 0.13$, $k = 27$] and (circles) normalised data calculated for (left) the selective and (right) unselective predator groups in spring in Lake Constance in 1991. We normalise the data and the model simulation using L_2-norm (see Appendix B). The unselective predator group is composed of data for *Rimostrombidum lacustris*. The selective predator group is composed of data for *Balanion planctonicum*.

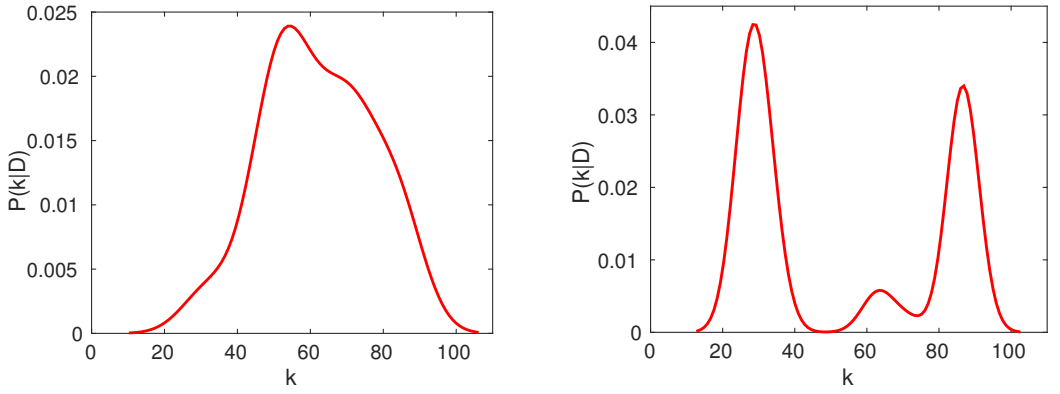

Figure 4.3: Smooth probability density estimate at the most strict tolerance level calculated using MATLAB's `ksdensity` function for the steepness of the prey switching k of the (left) selective and (right) unselective predator species in the 1 predator-2 prey smooth model (4.1) [for parameter values $e = 0.25$ and $\beta_1 = \beta_2 = 1$] using the ABC SMC method [129] (steps 1–7). We show here only the target distribution of k, for probability denstity estimates at intermediate tolerance levels, and for other parameters, see Appendix B.

suggests that adaptive feeding of a selective predator would be best represented with a steep switching function (i.e., with a large k value of the tanh function in Equation (4.1)) (see Figure 4.5, left). Similarly to year 1991, the probability density estimate for k in the case of the unselective predator is more stretched than in the case of the selective predator (see Figure 4.5, right). Furthermore, the model successfully reproduces the oscillatory pattern in the unselective predator species in 1998, when the feeding behaviour of a unselective predator is represented with a shallow switching function in the model in (4.1) (see Figure 4.4, right). For more details of the parameter fitting, and for the distributions of k at intermediate steps of the parameter fitting, see Appendix B.

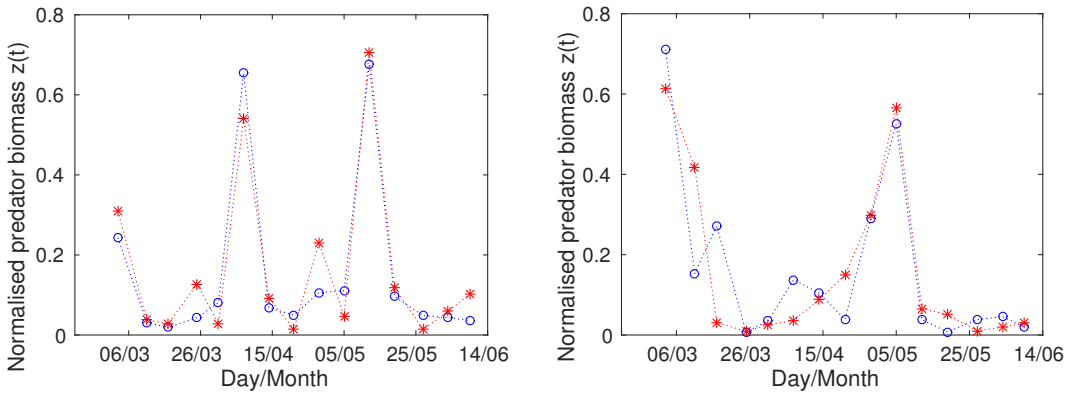

Figure 4.4: (Asterisks) Normalised predator abundance $z(t)$ for simulations of (4.1) [for parameter values $e = 0.25$, $\beta_1 = \beta_2 = 1$, (left) $r_1 = 1.07$, $r_2 = 0.58$, $m = 0.27$, $a_q = 0.08$, $k = 43$, and (right) $r_1 = 1.75$, $r_2 = 0.71$, $m = 0.86$ $a_q = 0.06$, $k = 32$] and (circles) normalised data calculated for (left) the selective and (right) unselective predator groups in spring in Lake Constance in 1998. We normalise the data and the model simulation using L_2-norm (see Appendix B). The unselective predator group is composed of data for *Rimostrombidum lacustris*. The selective predator group is composed of data for *Balanion planctonicum*.

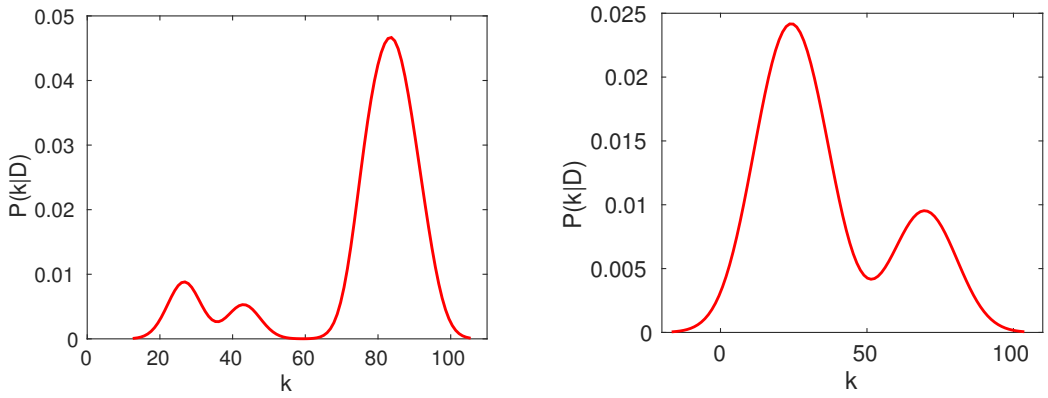

Figure 4.5: Smooth probability density estimate at the most strict tolerance level calculated using MATLAB's `ksdensity` function for the steepness of the prey switching k of the (left) selective and (right) unselective predator species in the 1 predator-2 prey smooth model (4.1) [for parameter values $e = 0.25$ and $\beta_1 = \beta_2 = 1$] using the ABC SMC method [129] (steps 1–7). We show here only the target distribution of k, for probability denstity estimates at intermediate tolerance levels, and for other parameters, see Appendix B.

4.3 Smooth analog II of the piecewise-smooth 1 predator-2 prey dynamical system

We begin the reformulation of the piecewise-smooth system (3.4) as a four-dimensional smooth system by first constructing the equation for the temporal evolution of a predator population (z) and its preferred and alternative prey populations (p_1 and p_2, respectively). We then define an expression for the temporal evolution of the predator's desire to consume the preferred prey (q) that undergoes rapid evolution (or phenotypic plasticity).

4.3.1 Ecological dynamics

In our reformulation of the 1 predator-2 prey piecewise-smooth system as a smooth system with predator trait evolution, we assume that the predator's desire q to consume the preferred prey is bounded between its smallest and largest feasible values (q_S and q_L, respectively). We make this assumption to obtain a smooth system that is as similar to the piecewise-smooth system (3.4) as possible. Thus, we require that the extreme when q is at its maximum ($q = q_L$), corresponds to the case in which the predator fitness is maximised with a large preference towards the preferred prey ($q_1 = q_{1_L}$) in the piecewise-smooth 1 predator-2 prey system (3.4). Similarly, we require that the extreme when q is at its minimum ($q = q_S$) corresponds to the case in which the predator fitness is maximised with a small preference towards the preferred prey ($q_1 = q_{1_S}$) in the piecewise-smooth 1 predator-2 prey system (3.4). For simplicity—and to ensure similarity to the piecewise-smooth system (3.4)—we consider exponential prey growth and linear functional response between the predator growth and prey abundance. This yields the following system of differential equations for the population dynamics of the 1 predator-2 prey smooth system II:

$$\begin{aligned}
\frac{\mathrm{d}p_1}{\mathrm{d}t} &= r_1 p_1 - (q - q_S)\beta_1 p_1 z\,, \\
\frac{\mathrm{d}p_2}{\mathrm{d}t} &= r_2 p_2 - (q_L - q)\beta_2 p_2 z\,, \\
\frac{\mathrm{d}z}{\mathrm{d}t} &= e(q - q_S)\beta_1 p_1 z + e(q_L - q)q_2\beta_2 p_2 z - mz\,,
\end{aligned} \tag{4.10}$$

where r_1 and r_2 (with $r_1 > r_2 > 0$) are the respective per capita growth rates of the preferred and alternative prey, β_1 and β_2 are the respective death rates of

the preferred and alternative prey due to predation, $e > 0$ is the proportion of predation that goes into predator growth, $q_2 \geq 0$ is nondimensional parameter that represents the extent of preference towards the alternative prey, and $m > 0$ is the predator per capita death rate per day. We will construct the equation for the temporal evolution of q in Section 4.3.2.

To follow the assumptions that we made in the construction of the piecewise-smooth system and thereby to facilitate the future comparison between the piecewise-smooth and smooth system II, we take $\beta_1 = \beta_2 = 1$, as in Chapter 3, in order to omit β_1 and β_2 in our analysis in Section 4.3.4. Hence, we assume that the predator exhibits adaptive feeding behaviour by adjusting its preference toward—rather than its attack rate on—the governing prey densities. Similarly, to compensate for the difference in prey preference, we assume that the growth rate of the preferred prey is greater than that of the alternative prey. In addition, we assume that a small preference towards the preferred prey amounts to a feeding mode of consuming only the alternative prey ($q_S = 0$) and that a large preference towards the preferred prey amounts to a feeding mode of consuming only the preferred prey ($q_L = 1$). These assumptions simplify the system (4.10) representing the population dynamics of the smooth 1 predator-2 prey system II to

$$\begin{aligned} \frac{\mathrm{d}p_1}{\mathrm{d}t} &= r_1 p_1 - q p_1 z\,, \\ \frac{\mathrm{d}p_2}{\mathrm{d}t} &= r_2 p_2 - (1-q) p_2 z\,, \\ \frac{\mathrm{d}z}{\mathrm{d}t} &= eq p_1 z + e(1-q) q_2 p_2 z - m z\,. \end{aligned} \tag{4.11}$$

4.3.2 Evolutionary dynamics

In reformulating the three-dimensional piecewise-smooth dynamical system (3.4) as a four-dimensional smooth system (4.13), we describe the rate of change of the predator's desire to consume the preferred prey by a bounding function that limits the predator trait between its smallest ($q_S = 0$) and largest ($q_L = 1$) feasible value. Futhermore, for the similarity between the four-dimensional smooth dynamical system II and the three-dimensional piecewise-smooth system, we will determine that the rate of change of the mean trait value is proportional to the quantity $p_1 - a_q p_2$, which we derived as the condition for prey switching using optimal foraging theory in Chapter 3. Thus, the temporal evolution of the predator trait takes the following form:

$$\frac{\mathrm{d}q}{\mathrm{d}t} = q(1-q)\left(p_1 - a_q p_2\right) . \tag{4.12}$$

where a_q (similarly to Chapter 3) is the slope of the prey preference trade-off.

4.3.3 Coupled ecological and evolutionary dynamics

By combining the ecological dynamics in (4.11) with the evolutionary dynamics in (4.12), we obtain the following smooth 1 predator-2 prey system II with predator

evolution:

$$\begin{aligned}
\frac{\mathrm{d}p_1}{\mathrm{d}t} &= \dot{p_1} = g_1(p_1, p_2, z, q) = r_1 p_1 - q p_1 z\,, \\
\frac{\mathrm{d}p_2}{\mathrm{d}t} &= \dot{p_2} = g_2(p_1, p_2, z, q) = r_2 p_2 - (1-q) p_2 z\,, \\
\frac{\mathrm{d}z}{\mathrm{d}t} &= \dot{z} = g_3(p_1, p_2, z, q) = eq p_1 z + e(1-q) q_2 p_2 z - m z\,, \\
\frac{\mathrm{d}q}{\mathrm{d}t} &= \dot{q} = f(p_1, p_2, q) = q(1-q)(p_1 - a_q p_2)\,.
\end{aligned} \tag{4.13}$$

When $p_1 > a_q p_2$ in the piecewise-smooth system (3.4), the predator feeds only on the preferred prey and the dynamics of the piecewise-smooth 1 predator-2 prey system (3.4) are governed by f_+. Because of our similar assumptions for smooth analog II, the system in (4.13) reduces to f_+ in (3.4) when $q = 1$. Likewise, the vector field of the smooth system II (4.13) corresponds to f_- of the piecewise-smooth system in (3.4) when $q = 0$, and the predator's diet is composed solely of the alternative prey type.

4.3.4 Linear stability analysis of the smooth system II

The system in (4.13) has an equilibrium point when $g_1(\tilde{p_1}, \tilde{p_2}, \tilde{z}, \tilde{q})$, $g_2(\tilde{p_1}, \tilde{p_2}, \tilde{z}, \tilde{q})$, $g_3(\tilde{p_1}, \tilde{p_2}, \tilde{z}, \tilde{q})$, and $f(\tilde{p_1}, \tilde{p_2}, \tilde{z}, \tilde{q})$ are zero. The smooth model II in (4.13) has four equilibria (see Table 4.2). We note that the predator and prey densities at the steady state IV are equivalent to those at the equilibrium point (when $q_1 = 1$) of the piecewise-smooth 1 predator-2 prey model (3.4) we analysed in Section 3.3.3. We analyse the linear stability of these four equilibria by calculating the

state	$\tilde{p}_1$	$\tilde{p}_2$	$\tilde{z}$	$\tilde{q}$
I	0	0	0	arbitrary
II	0	$m/(eq_2)$	r_2	0
III	m/e	0	r_1	1
IV	$\frac{a_q m(r_1+r_2)}{e(r_1 a_q+r_2 q_2)}$	$\frac{m(r_1+r_2)}{e(r_1 a_q+r_2 q_2)}$	r_1+r_2	$\frac{r_1}{r_1+r_2}$

Table 4.2: Four equilibria of the smooth system II in Equation (4.13).

eigenvalues of the Jacobian of the system in (4.13) evaluated at the equilibria:

$$J = \left.\begin{pmatrix} \frac{\partial g_1}{\partial p_1} & \frac{\partial g_1}{\partial p_2} & \frac{\partial g_1}{\partial z} & \frac{\partial g_1}{\partial q} \\ \frac{\partial g_2}{\partial p_1} & \frac{\partial g_2}{\partial p_2} & \frac{\partial g_2}{\partial z} & \frac{\partial g_2}{\partial q} \\ \frac{\partial g_3}{\partial p_1} & \frac{\partial g_3}{\partial p_2} & \frac{\partial g_3}{\partial z} & \frac{\partial g_3}{\partial q} \\ \frac{\partial f}{\partial p_1} & \frac{\partial f}{\partial p_2} & \frac{\partial f}{\partial z} & \frac{\partial f}{\partial q} \end{pmatrix}\right|_{(\tilde{p}_1,\tilde{p}_2,\tilde{z},\tilde{q})} \tag{4.14}$$

$$= \begin{pmatrix} r_1-\tilde{q}\tilde{z} & 0 & -\tilde{q}\tilde{p}_1 & -\tilde{p}_1\tilde{z} \\ 0 & r_2-(1-\tilde{q})\tilde{z} & -(1-\tilde{q})\tilde{p}_2 & \tilde{p}_2\tilde{z} \\ e\tilde{q}\tilde{z} & e(1-\tilde{q})q_2\tilde{z} & e\tilde{q}\tilde{p}_1+e(1-\tilde{q})q_2\tilde{p}_2-m & e\tilde{p}_1\tilde{z}-eq_2\tilde{p}_2\tilde{z} \\ \tilde{q}(1-\tilde{q}) & -a_q\tilde{q}(1-\tilde{q}) & 0 & (1-2\tilde{q})(\tilde{p}_1-a_q\tilde{p}_2) \end{pmatrix}.$$

We present our findings of the linear stability analysis in Table 4.3.

Steady state I is the trivial steady state of the system. Biologically, steady state II corresponds to a situation where only the alternative prey and predator are present. Steady state III represents a situation in which the population of the alternative prey is zero.

Steady state IV is the most interesting state biologically because at state IV, all three population densities are nonzero. At the steady state IV, which is equivalent to the pseudoequilibrium of the piecewise-smooth system (3.4) with $\tilde{q} = r_1/(r_1 +$

r_2), the Jacobian becomes

$$J = \begin{pmatrix} 0 & 0 & \frac{-r_1 a_q m}{e(r_1 a_q + r_2 q_2)} & \frac{-a_q m (r_1+r_2)^2}{e(r_1 a_q + r_2 q_2)} \\ 0 & 0 & \frac{-r_2 m}{e(r_1 a_q + r_2 q_2)} & \frac{m(r_1+r_2)^2}{e(r_1 a_q + r_2 q_2)} \\ er_1 & er_2 q_2 & 0 & \frac{e(a_q - q_2) m (r_1+r_2)^2}{e(r_1 a_q + r_2 q_2)} \\ \frac{r_1 r_2}{(r_1+r_2)^2} & \frac{-a_q r_1 r_2}{(r_1+r_2)^2} & 0 & 0 \end{pmatrix}. \tag{4.15}$$

When $a_q = q_2$, the four eigenvalues of the state IV satisfy the characteristic equation

$$\lambda_{1,2,3,4}^4 + \frac{m[2r_1 r_2 + e(r_1^2 + r_2^2)]}{e(r_1 + r_2)} \lambda_{1,2,3,4}^2 + \frac{m^2 r_1 r_2}{e} = 0\,. \tag{4.16}$$

Instead of analysing Equation (4.16) directly, we write $u = \lambda^2$, and study the following equation:

$$u^2 + \frac{m[2r_1 r_2 + e(r_1^2 + r_2^2)]}{e(r_1 + r_2)} u + \frac{m^2 r_1 r_2}{e} = 0\,. \tag{4.17}$$

Similarly to Chapter 3, we are interested only in physically meaningful parameter values (i.e., r_1, r_2, q_2, m, e, $a_q > 0$). Therefore, the intercept of the Equation (4.17) is located on the positive vertical axis and Equation (4.17) reaches its minimum when u_i is less than zero, $i = 1, 2$. Thus, the two solutions u_1 and u_2 to Equation (4.17) are both real and less than zero. As a result, the four eigenvalues $\lambda_{1,2,3,4}$ that satisfy Equation (4.16) consist of two complex conjugate pairs with zero real part, $\lambda_{1,2} = \pm\sqrt{u_1}i$ and $\lambda_{3,4} = \pm\sqrt{u_2}i$, where u_1 and u_2 satisfy Equation (4.17). Furthermore, the steady state IV is nonhyperbolic when $a_q = q_2$.

For $a_q \neq q_2$ (and $r_1 \neq r_2$), the eigenvalues of the state IV satisfy the following

state	description	λ_1	λ_2	λ_3	λ_4
I	trivial	r_1	r_2	$-m$	0
II	p_1 extinct	r_1	$\sqrt{m/(eq_2)}i$	$-\sqrt{m/(eq_2)}i$	$-a_q m/(eq_2)$
III	p_2 extinct	$\sqrt{mr_1}i$	r_2	$-\sqrt{mr_1}i$	$-m/e$
IV	coexistence				
	$a_q = q_2$	$\sqrt{u_1}i$	$-\sqrt{u_1}i$	$\sqrt{u_2}i$	$-\sqrt{u_2}i$,
		where u_i, $i = 1, 2$ satisfies Equation (4.17)			
	$a_q \neq q_2$	see Equation (4.18)			

Table 4.3: Summary of the linear stability analysis for the smooth system II in Equation (4.13) that we calculate in this section.

characteristic equation

$$\lambda_{1,2,3,4}^4 + \left[a_q r_1 r_2 m + \frac{me(a_q r_1^2 + q_2 r_1^2) + a_q r_1 r_2 m}{e(a_q r_1 + q_2 r_2)}\right] \lambda_{1,2,3,4}^2 + \frac{a_q r_1 r_2 m^2 (a_q - q_2)(r_1 - r_2)}{e(a_q r_1 + q_2 r_2)} \lambda_{1,2,3,4} + \frac{2 a_q r_1 r_2 m^2 (r_1 + r_2)}{e(a_q r_1 + q_2 r_2)} = 0\,. \tag{4.18}$$

Solving Equation (4.18) numerically, we find that the real parts of the eigenvalues of the steady state IV cross the imaginary axis at $a_q = q_2$ from opposite directions, and in pairs of two eigenvalues. In other words, in the neighbourhood of $a_q \neq q_2$, the real part of two of the eigenvalues has a negative sign, while the real part of the other two eigenvalues has a positive sign.

4.3.5 Comparison of the smooth analog II model simulations and planktonic protozoa-algae data

In this section, we compare the predator abundance from the smooth system II model (4.13) with data on ciliate predators collected from Lake Constance in spring (see Section 1.2.2). Similarly to the parameter fitting of the smooth model I in

Section (4.2.3), we choose to compare predator abundance predicted by the model with the data from years 1991 and 1998, when the spring bloom lasted for several weeks and ciliate biomasses exhibit recurring patterns of increases followed by declines (see Section 1.2.2).

Similarly to Chapter 3, and to the smooth system II in Section 4.2.3, our motivation to compare the data and our third prey-switching model is the prey preference among ciliate species that actively select against diatom prey when offered a mixed diet of both cryptophytes and diatom prey [94]. In contrast to our procedure for the smooth system II, we combine the total predator abundance from the two different predator species. Thus, the diversity of the predator group is represented through the dynamics of the mean predator trait q in our smooth model II (4.13). We combine the data for the total predator abundance from data for the selective predator *Balanion planctonicum* that hunt as interception feeders, and unselective predator *Rimostrombidum lacustris* that hunt as filter feeders (see Section 1.2.2). Similarly to the data comparison in Section 4.2.3, we first normalise the total predator abundance composed of the approximately bi-weekly measurements by L_2-norm (see Appendix B). However, in contrast to the parameter fitting we carry out for the data comparison in Section 4.2.3, in the parameter fitting for the smooth system II, we fix the prey growth rates based on the results we obtained in the parameter fitting for the smooth system I. In data comparison of the smooth system II model (4.13), we fit the total predator mortality rate m and the perturbance ν from the nonhyperbolic steady state IV when $a_q = q_2$ (for more details of the parameter fitting, see Appendix B). In Figures 4.6 and 4.8, we compare normalised Lake Constance data with the total predator abundance (i.e., $z(t)$) and the predator trait dynamics (i.e., $q(t)$) that we

obtain from simulations of the smooth system II model (4.13).

In year 1991, the model reproduces the large increases in the total predator abundance in spring, when one can argue that predator-prey interactions govern the protist-algae dynamics more than physical driving forces in water masses that are rich in nutrients [116] (see Figure 4.6). As a result, the model prediction for the predator trait dynamics suggests that during peak abundances, the predator population is feeding mostly on the predferred prey (i.e., q is near 1) (see Figure 4.7, top). Importantly, the peaks in the scaled prey ratio $p_1/(a_q p_2)$ are associated with q near 1 which is similar to the model prediction of our 1 predator-2 prey piecewise-smooth system (3.4) in Chapter 3 (see Figure 4.7, bottom). When the scaled prey ratio is low, the model predicts that the predator's diet choice has a quick transition from a mixed diet (i.e., $q \in (0, 1)$) to the alternative prey (i.e, $q = 0$) (see Figure 4.7, bottom).

In year 1998, the smooth model II (4.13) successfully reproduces the timings of the peak abundances in the total predator abundance in spring, when we again assume that predator-prey interactions govern the protist-algae dynamics more than physical driving forces in water masses that are rich in nutrients [116] (see Figure 4.8). When we fit the model to data from year 1998, the predator trait dynamics show less pronounced switching than in the model prediction for year 1991, when the predators' diet was mostly composed of either the preferred or the alternative prey. The model predicts that during high predator abundance, either of the unselective or the selective predator, the total predator population is feeding on the preferred prey (i.e., $q = 1$) (see Figure 4.9, top). Based on visual inspection, the model predicts that the predator population has a mixed diet (i.e., $q \in (0, 1)$) for longer periods of time than in year 1991. Similarly to year 1991, and to the

mean data for years 1979–1999 we use in the data comparison of the piecewise-smooth model (3.4) in Chapter 3, there is a periodicity in the calculated scaled prey ratio. However, for year 1998, a large scaled prey ratio is not necessarily associated with $q = 1$ (see Figure 4.9, bottom).

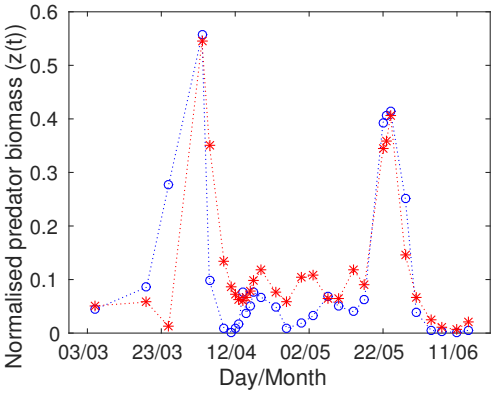

Figure 4.6: (Asterisks) Normalised total predator abundance $z(t)$ for simulations of (4.13) (for parameter values $e = 0.25$, $\beta_1 = \beta_2 = 1$, $r_1 = 1$, $r_2 = 0.4$, $a_q, q_2 = 0.5$, $m = 0.26$, and $\nu = 4.8$, and initial values $[p_1(0), p_2(0), z(0), q(0)] = [a_q m(r_1 + r_2)/[e(r_1 a_q + r_2 q_2)], m(r_1 + r_2)/[e(r_1 a_q + r_2 q_2)], \nu(r_1 + r_2), r_1/(r_1 + r_2)]$) and (circles) normalised data calculated for the total predator abundance in spring in Lake Constance in 1991. We normalise the data and the model simulation using L_2-norm (see Appendix B). The total predator adunbance is composed of data for the unselective predator *Rimostrombidum lacustris* and the selective predator *Balanion planctonicum*.

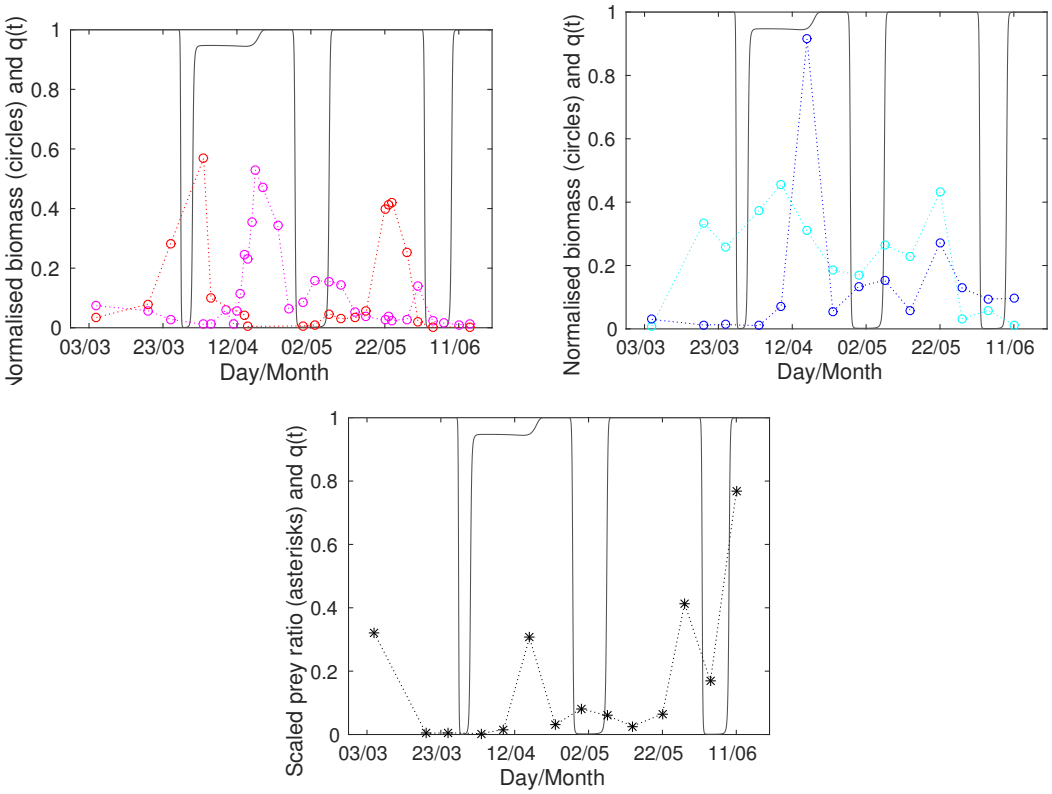

Figure 4.7: (Grey curve) Predator trait dynamics $q(t)$ from simulations of (4.13) (for parameter values $e = 0.25$, $\beta_1 = \beta_2 = 1$, $r_1 = 1$, $r_2 = 0.4$, $a_q, q_2 = 0.5$, $m = 0.26$, and $\nu = 4.8$, and initial values $[p_1(0), p_2(0), z(0), q(0)] = [a_q m(r_1 + r_2)/[e(r_1 a_q + r_2 q_2)], m(r_1 + r_2)/[e(r_1 a_q + r_2 q_2)], \nu(r_1 + r_2), r_1/(r_1 + r_2)]$). (Circles) Normalised data calculated for the (blue) preferred prey, (cyan) alternative prey, (red) unselective predator, and (magenta) selective predator group in spring in Lake Constance in 1991. (Asterisks) Normalised prey data calculated for the scaled prey ratio $p_1/(a_q p_2)$ in Lake Constance in spring 1991. We normalise the data and the model simulation using L_2-norm (see Appendix B). The preferred prey p_1 is composed of data for *Cryptomonas ovata*, *Cryptomonas marssonii*, *Cryptomonas reflexa*, *Cryptomonas erosa*, *Rhodomonas lens*, and *Rhodomonas minuta*. The alternative prey group p_2 is composed of data for small and medium-size *Chlamydomonas* spp. and *Stephanodiscus parvus*. The unselective predator group is composed of data for *Rimostrombidum lacustris*. The selective predator group is composed of data for *Balanion planctonicum*.

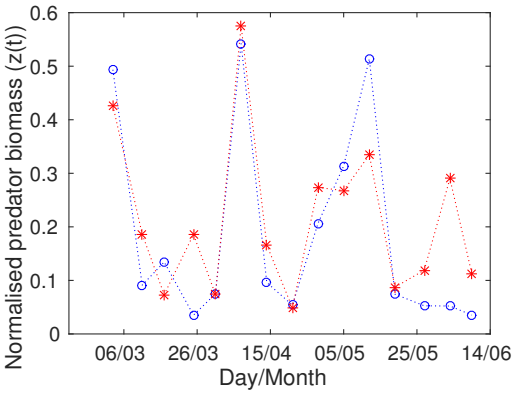

Figure 4.8: (Asterisks) Normalised total predator abundance $z(t)$ for simulations of (4.13) (for parameter values $e = 0.25$, $\beta_1 = \beta_2 = 1$, $r_1 = 1$, $r_2 = 0.4$, $a_q, q_2 = 0.5$, $m = 0.19$, and $\nu = 3.0$, and initial values $[p_1(0), p_2(0), z(0), q(0)] = [a_q m(r_1 + r_2)/[e(r_1 a_q + r_2 q_2)], m(r_1 + r_2)/[e(r_1 a_q + r_2 q_2)], \nu(r_1 + r_2), r_1/(r_1 + r_2)]$). (Circles) Normalised data calculated for the total predator abundance in spring in Lake Constance in 1998. We normalise the data and the model simulation using L_2-norm (see Appendix B). The total predator adunbance is composed of data for the unselective predator *Rimostrombidum lacustris* and the selective predator *Balanion planctonicum*.

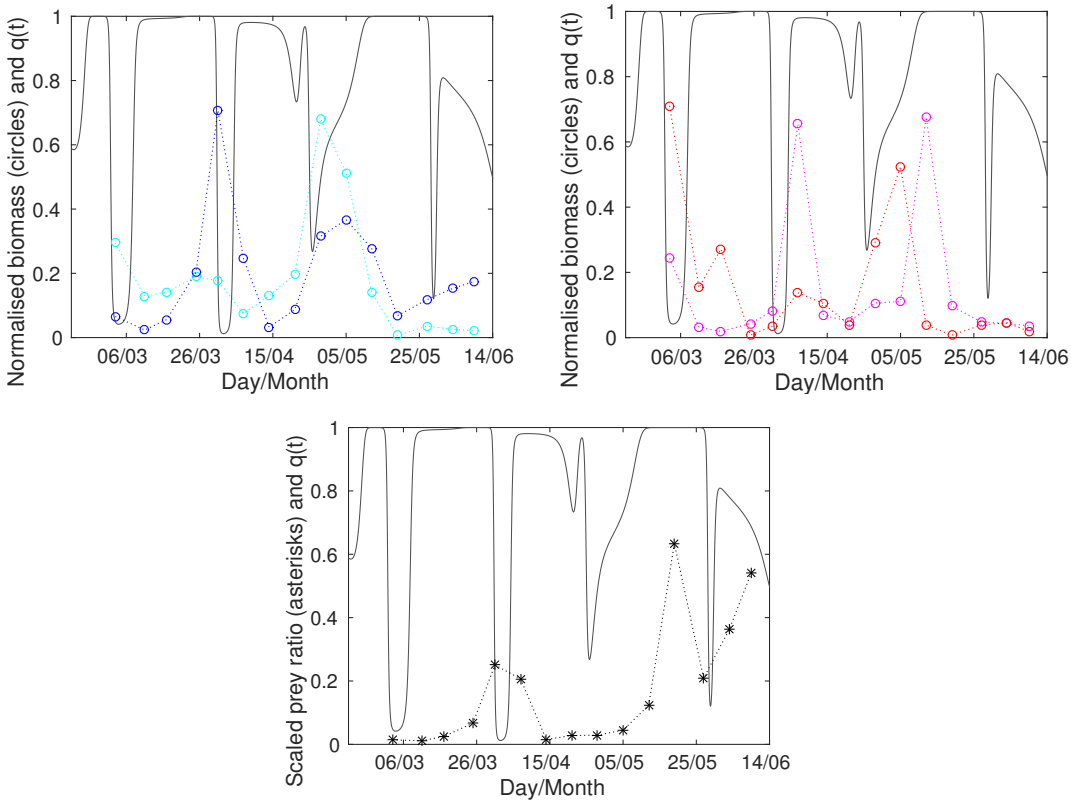

Figure 4.9: (Grey curve) Predator trait dynamics $q(t)$ from simulations of (4.13) (for parameter values $e = 0.25$, $\beta_1 = \beta_2 = 1$, $r_1 = 1$, $r_2 = 0.4$, $a_q, q_2 = 0.5$, $m = 0.19$, and $\nu = 3.0$, and initial values $[p_1(0), p_2(0), z(0), q(0)] = [a_q m(r_1 + r_2)/[e(r_1 a_q + r_2 q_2)], m(r_1 + r_2)/[e(r_1 a_q + r_2 q_2)], \nu(r_1 + r_2), r_1/(r_1 + r_2)]$). (Circles) Normalised data calculated for the (blue) preferred prey, (cyan) alternative prey, (red) unselective predator, and (magenta) selective predator group in spring in Lake Constance in 1991. (Asterisks) Normalised prey data calculated for the scaled prey ratio $p_1/(a_q p_2)$ in Lake Constance in spring 1998. We normalise the data and the model simulation using L_2-norm (see Appendix B). The preferred prey p_1 is composed of data for *Cryptomonas ovata*, *Cryptomonas marssonii*, *Cryptomonas reflexa*, *Cryptomonas erosa*, *Rhodomonas lens*, and *Rhodomonas minuta*. The alternative prey group p_2 is composed of data for small and medium-size *Chlamydomonas* spp. and *Stephanodiscus parvus*. The unselective predator group is composed of data for *Rimostrombidum lacustris*. The selective predator group is composed of data for *Balanion planctonicum*.

state	description	smooth I	smooth II	piecewise-smooth
I	trivial	○	⋆	○
II	p_1 extinct	⋆[1]	⋆	⋆
III	p_2 extinct	⋆[1]	⋆	⋆
IV	coexistence	●[2]	○,⋆[3]	●[4]

[1] as $k \to \infty$
[2] stable if $a_q > a_q^*(k)$ (see Figure 4.1c) where $a_q^*(k) \to q_2/q_1$ as $k \to \infty$
[3] centre if $a_q = q_2$
[4] stable if $a_q > q_2/q_1$

Table 4.4: Summary of the linear stability analysis for the smooth system I in Equation (4.1), smooth system II in Equation (4.13), and piecewise-smooth system in Equation (3.4). We indicate an unstable steady state with an open circle, a nonhyperbolic equilibrium point with a star, and a stable steady state with a filled circle. The densities of the two prey and predator populations at the coexistence state IV [i.e., $(p_1, p_2, z) = (\tilde{p}_1, \tilde{p}_2, \tilde{z})$] in the smooth system II (see state IV in Table 4.2) are equivalent to the population densitites at the pseudoequilibrium of the piecewise-smooth system [see Equation (3.11)]. In the smooth system I, the population densities at the coexistence equilibrium point (that lies on the switching plane $p_1 = a_q p_2$ as $k \to \infty$) are $(p_1, p_2, z) = (\tilde{p}_1 + \delta_{p_1}, \tilde{p}_2 - \delta_{p_2}, \tilde{z})$[1](see Figures 4.1a and 4.1b) where δ_{p_1},$\delta_{p_2} \to 0$ as the slope of the hyperbolic tangent $k \to \infty$.

4.4 Discussion

Numerical simulations demonstrate that the piecewise-smooth system (3.4) and its smooth analog I (4.1) produce similar behaviour as long as the steepness of the hyperbolic tangent k is sufficiently large. In particular, both systems settle to a steady state for $a_q > q_2/q_1$ and to a periodic orbit for $a_q < q_2/q_1$. However, when the steepness of the transition in the hyperbolic tangent k is small, then the smooth system I (4.1) predicts that the predator and the two prey also coexist at steady state levels (instead of oscillating) when $a_q < q_2/q_1$ (see Table 4.4).

[1] $\delta_{p_1} = \frac{e^2(q_1 a_q r_1 + q_2 r_2) q_2 r_2 \operatorname{arctanh}\left(\frac{r_1 - r_2}{r_1 + r_2}\right)}{k}$, $\delta_{p_2} = \frac{e^2(q_1 a_q r_1 + q_2 r_2) q_1 r_1 \operatorname{arctanh}\left(\frac{r_1 - r_2}{r_1 + r_2}\right)}{k}$

The smooth dynamical systems I (4.1) and II (4.13) allow one to use standard theory to determine the stability of an equilibrium using linear stability analysis and to study bifurcations. In the case of the smooth system I (4.1), the analytical expressions for the eigenvalues are complicated, so the bifurcation analysis is difficult to carry out with analytical calculations. However, it can be done numerically (see Figure 4.1c). In addition, the smooth system I (4.1) requires one to use an extra parameter k which has an influence on the system's qualitative behaviour. Moreover, for very large k, the system becomes stiff and hence more challenging to be solved computationally.

The smooth system II (4.13) has the same number of parameters as the piecewise-smooth system (3.4) but adds a new dimension (i.e., the predator trait q) to the system. As a result, the steady state IV of the smooth system II (4.13) [that corresponds to the prey and predator abundances at the pseudoequilibrium of the piecewise-smooth system (3.4)] can be found analytically. In the piecewise-smooth system the pseudoequilibrium is stable if $a_q > q_2/q_1$. In the smooth system II the corresponding equilibrium is a centre for $a_q = q_2$ and unstable otherwise (see Table 4.4). However, the analytical expression for the 4 eigenvalues is more complicated than the expression for the 3 eigenvalues of the piecewise-smooth system (3.4). This complexifies bifurcation analysis.

The theory for piecewise-smooth dynamical systems is not as well established as that for smooth dynamical systems. Furthermore, standard methods used for solving ODEs numerically are not applicable to piecewise-smooth systems and the theory for the analysis of the numerical simulations in piecewise-smooth systems is not complete [23]. However, the equilibrium in the piecewise-smooth system (3.4) can be determined explicitly, and there exists an analytical expression for the flow

at the discontinuity boundary (i.e., $h = p_1 - a_q p_2 = 0$). In addition to the definition for the flow at the boundary, the theory available for piecewise-smooth systems identifies the bifurcation that we observed as a type of adding-sliding bifurcation. This result helps to facilitate understanding of the behaviour of the system (3.4) close to the boundary. Moreover, this understanding can be used when analysing the zooplankton-phytoplankton dynamics predicted by the model.

Assuming a linear trade-off between the prey preferences, in the case of the 1 predator-2 prey piecewise-smooth system (3.4), the ratio between the preferred and alternative prey type is constant before the bifurcation and time-varying after the bifurcation. Furthermore, the slope of the trade-off is directly included in the modelling and present in the expression for the switching boundary. Taking a piecewise-smooth approach entails following the condition for sliding given in terms of the prey ratio (i.e., the system (3.4) is sliding when $p_1/(a_q p_2) = 1$). This is different from previous work [128], which studied the actual value, rather than the ratio, of prey population densities predicted by the model. Using a piecewise-smooth model, the analytical calculations can be as tedious as in smooth systems, but there is one fewer model parameter, or model dimension, as there is no need to define the "slope" of the tanh function, or the dynamics of the predator trait. This is our advantage especially when more species are included, and the analytical calculations are not complexified by hyperbolic tangent functions or high dimensionality of the system.

With a smooth dynamical system approach, we can relax the assumption of "discontinuous" predator of the piecewise-smooth system (3.4). Furthermore, using tanh functions to smooth the piecewise-smooth system (3.4), we can use data to determine the steepness in the transition in the predator's feeding behaviour for

a particular predator type. Indeed, our parameter fitting to the Lake Constance data suggests that a more selective predator species would be better modelled with a steeper tanh function than a less selective predator species. If we regularise the piecewise-smooth system (3.4) by considering a predator trait as a variable, we add an extra dimension to the system and obtain a model prediction for predator trait dynamics with the smooth analog II model (4.13). As future work, this model prediction could be tested against results from controlled laboratory experiments where the genetic diversity of the predator species can be manipulated and recorded. Such trait dynamics cannot be obtained from either the piecewise-smooth system (3.4) or the smooth analog I model (4.1). Our smooth model II predicts that a large scaled prey ratio occurs when the predator is feeding only on the preferred prey. This phenomenon agrees with the results we obtained with the piecewise-smooth model in Chapter 3.

The predator trait dynamics predicted by the smooth system II (4.13) could be further compared with data collected from the field or from controlled experiments with genetically diverse prey and/or predator populations. From an ecological perspective, the piecewise-smooth 1 predator-2 prey system (3.4) models the effects of the predator's adaptive change of diet in response to prey abundance; this is an example of phenotypic plasticity [63]. The smooth system II (4.13) describes the population dynamics of a predator and its two prey in the presence of rapid evolution in prey preference. These two mechanisms (i.e., phenotypic plasticity and rapid evolution) both cause rapid adaptation and affect the population dynamics [112, 139]. Although it is not clear how these different mechanisms affect the population dynamics, it has been suggested that models that account for phenotypic plasticity exhibit a stable equilibrium more often than models accounting

for rapid evolution [139]. It has been hypothesized that this can arise from a faster response time of plastic genotypes than that of nonplastic genotypes to fluctuating environmental conditions [139]. Indeed, the piecewise-smooth system (3.4) converges to a steady state when the ecological trade-off is steep enough, but we have not observed convergence to a steady state in the smooth system II (4.13).

4.5 Conclusions

To relax the assumption of a discontinuous switch in predator feeding behaviour that we made for the piecewise-smooth 1 predator-2 prey model (3.4), and to be able to compare a piecewise-smooth system with two associated smooth system, we constructed smooth models using (I) tanh functions and (II) considering the predator trait as a system variable. While using tanh function is a textbook approach for regularising piecewise-smooth systems [16], considering a predator trait as a system variable is an appropriate framework for studying the underlying mechanisms and effects of a rapid adaptive change of a predator on the predator-2 prey dynamics, when one assumes that the speed of evolution is comparable to that of ecological interactions. Rapid evolution has been observed in several organisms, including plankton [37,38,140]. Because plankton have short lifespans, they make a good example system for studying the coupling between ecological and evolutionary dynamics.

We constructed both the smooth systems I and II, (4.1) and (4.13), respectively, so that they reduce to the vector fields of the piecewise-smooth dynamical system (3.4) at the extremes where $q = 1$ or $q = 0$. We constructed the predator evolution

in (4.13) by assuming that the change of the predator trait is similar to *fitness gradient* dynamics [79]. However, for the smooth system II, instead of calculating the fitness gradient from the equation for the predator population, we determine the gradient to be equivalent to the switching condition in the piecewise-smooth system (3.4). We then investigated analytically and numerically the equilibria and eigenvalues of the two smooth systems using linear stability analysis. Finally, we compared both smooth systems to the Lake Constance data, and to the piecewise-smooth model (3.4).

Chapter 5

Conclusions and future directions

5.1 Models for adaptive feeding in plankton

In order to develop reliable predictions about the state of ecosystems under changing environmental conditions, the ability of organisms to adapt should not be ignored in models for population dynamics. Models for population dynamics represented with smooth differential equations evolving on the same time scale include a long-established theory for the analysis of the resulting systems of equations. However, as it is not yet clear in what mathematical form phenomena like prey switching or rapid evolution should be represented, alternative approaches, such as piecewise-smooth dynamical systems, offer promising directions for investigation (see Chapter 1). In addition, the novelty of this approach makes it possible to ask both ecological and mathematical questions about the models.

For example, in Chapter 3, we used the piecewise-smooth framework to construct a model for a 1 predator-2 prey interaction with unlimited prey growth and a tilted switching manifold between the two sides of discontinuous vector fields

(see Section 3.2). The model (3.4) hypothesises prey switching in the presence of an ecological trade-off in prey preference as a possible mechanistic explanation for recurring patterns of increases followed by declines in ciliate and phytoplankton biomasses that are exhibited in the Lake Constance data (see Section 1.2.2). In addition, we discovered that the model (3.4) undergoes a novel adding-sliding-like bifurcation (see Section 3.4). We summarise these findings in Section 5.1.1. In Chapter 4, we relaxed the simplified approach of a discontinous prey switching in the piecewise-smooth system by regularising it using (I) tanh function and (II) adding a new dimension for the predator trait into the system. While model I hypothesises prey switching is the steeper the more selective the predator species is, with model II we gain extra insight into the predator trait dynamics that could be further validated with data on genetic diversity of an adaptive feeding predator species. Thus, although the motivation of the models comes primarily from a mathematical perspective, such modelling investigations have utility for the development of new biological understanding of the coupling between ecology and evolution.

5.1.1 Piecewise-smooth 1 predator-2 prey model

Using the principle of optimal foraging theory, we combined two ecological concepts—prey switching and trade-off—in the framework of piecewise-smooth dynamical systems to develop a model of one predator that feeds on a preferred and an alternative prey (see Chapter 3). We derived analytical expressions for the pseudoequilibrium, its eigenvalues, and the points for tangencies between the two vector fields and the switching boundary. We confirmed our analytical re-

sults using numerical simulations. We also discovered a novel bifurcation, which we named the "Centre to two-part Periodic Orbit" (C2PO) bifurcation, in which an adding-sliding periodic orbit is born from a centre. At the bifurcation point, there is a family of entirely sliding centres which we proved are closed curves. Based on numerical simulations close to the bifurcation point, the amplitude of the adding-sliding periodic orbit seems to scale linearly with the distance from the bifurcation point. We also carried out numerical computations to facilitate the future development of a normal-form map to describe the C2PO bifurcation.

We compared the results of our simulations with data on freshwater plankton (see Section 1.2). Plankton are an important and suitable model system for not only theoretical ecology but also for complex systems more generally. Similar to many other organisms, adaptive feeding and ecological trade-offs have been observed in plankton. There has been a lot of work on models of plankton dynamics using dynamical systems (see Section 1.3) that have been successful in offering various explanations for observations of plankton dynamics, such as triggering mechanisms of plankton blooms, and reproducing patterns seen in the data, such as relatively constant total prey biomass in contrast to highly variable individual prey species' biomasses. By comparing our simulations of the adding-sliding periodic orbit with data, we reproduced the coexistence of species and suggested prey switching in the presence of a prey preference trade-off as a possible mechanistic explanation for cycles in the observed prey ratio during spring. The periodic orbit exists in the parameter range in which there is a mild trade-off in the prey preference—that is, a predator with a small increase in the energy gained from the preferred prey would exhibit only a small decrease in the energy gained from the alternative prey. We used plankton as our example organism because of their

suitability and importance, but similar prey-switching models can also be formulated for any other 1 predator-2 prey interaction in which it is viable to use models based on low-dimensional differential equations (i.e., large population size, well-mixed environment, and the use of community-integrated parameters).

There are several future directions for this work. As concerns the derivation of the model, optimal foraging theory combines the predator's decision—that is, the choice of habitat or prey—with the predator's attempt to maximise a variable related to its fitness (such as the mean energy intake rate). This decision is made within certain constraints which can be set, for example, by the area the predator can search or exploit [120]. Additionally, optimal foraging theory assumes that the predator has available complete information on prey densities, which is a strong assumption and should be relaxed. One such approach would be to incorporate stochasticity in the prey densities observed by the predator, which can be implemented as noise included in the switching condition. Earlier work on a Filippov-type piecewise-smooth system (i.e., a relay control system) indicates that noise has an important effect on the periodicity and amplitude of the periodic orbits with sliding segments [113]. Hence, considering noise in a predator's information on prey densities would increase understanding of population dynamics between two prey and a "noisy" optimal forager as well as of stochastic Filippov systems more generally.

In Section 3.5, we discussed several generalisations of our piecewise-smooth model (3.4)—such as limited prey growth and nonlinear trade-offs. These generalisations would expand the suitable time window for comparing simulations with data (i.e., from early growing season to mid and late growing season) and help to develop a better understanding of the effect of ecological trade-offs on

population dynamics. In addition, these generalisations (and other ecologically motivated generalisations, such as prey competition, saturating predator response or two functionally different predator species) have a potential utility for *unfolding* the C2PO bifurcation—that is, providing a family of vector fields whose local flows contain all possible small perturbations of the flow generated by (3.4) [48]. Thus, an unfolding of (3.4) would provide a dynamical system that exhibits a C2PO bifurcation as well as all other possible bifurcations of the pseudoequilibrium (3.11) [96]. Although the C2PO bifurcation satisfies the conditions that define a nondegenerate adding-sliding bifurcation, a variation of the equations that reduces the C2PO bifurcation to the standard adding-sliding bifurcation would (1) be helpful for the development of the normal-form map to describe the C2PO bifurcation (and its comparison with the normal-form map of the standard adding-sliding bifurcation) and (2) increase understanding of the relationship between the C2PO bifurcation and other bifurcations in more detail. In addition to the standard adding-sliding bifurcation, these include a similar bifurcation to the C2PO bifurcation in piecewise-linear systems [34] and piecewise-continuous systems [114].

As a step towards studying models of adaptive predator behaviour and ecological trade-offs, we started from the simplest case (i.e., a system with one predator and two prey). In our model, functional diversity is present only in the prey community and it arises as the difference in prey growth rates. Accordingly, we chose species from a large data set to consider representative prey groups. Thus, these choices leave predator diversity for future work. As we discussed in Section 1.2.2, ciliates are known to have different modes of predator behaviour, and they can be categorised roughly in terms of their selectivity. One can represent such diversity in a predator community using different preference trade-offs. This could be

studied using a piecewise-smooth dynamical system with more than three dimensions (or by using a fast-slow dynamical system) and which could have more than one switching manifold. Moreover, the switching manifolds might intersect with each other. Such a generalisation would thus be very interesting (and challenging) to study from both biological and mathematical perspectives. From a biological viewpoint, this generalisation could be used to test a possible mechanistic explanation for the patterns seen in the Lake Constance data, such as the relatively constant total biomass contrasting with the highly variable biomasses of individual species [128]. From a mathematical viewpoint, this generalisation has potential utility in developing a general methodology for bifurcations in piecewise-smooth dynamical systems that arise from intersections of switching manifolds when the ambient space has more than three dimensions.

5.1.2 Smooth 1 predator-2 prey models

The ecological motivation for reformulating our piecewise-smooth dynamical system as a smooth dynamical system is based on relaxing the assumption of a discontinuous switch. On the one hand, it is not clear whether there exist predators that instantaneously change their diet. On the other hand, it is not clear which of the many possible smooth approximations best describes prey switching. Therefore, we regularised the piecewise-smooth system in two different ways.

First, we "smoothed out" the piecewise-smooth model using hyperbolic tangent functions which allowed us to express a continuous change in the predator feeding behaviour based on prey abundances. In doing so, we added one parameter to the system (i.e., k) that represents the steepness of the continuous switch. We analysed

the resulting smooth model I using a combination of linear stability analysis and numerical computations. The equilibrium of the smooth analog of the piecewise-smooth system constructed using tanh functions can be solved numerically. For a sufficiently steep hyperbolic tangent, the dynamical behaviour (i.e., settling to a steady state or periodic orbit) of the piecewise-smooth system and its smooth analog I are the same. For a shallow hyperbolic tangent function, the smooth system I (4.1) predicts that the predator and the two prey also coexist at steady state levels (instead of oscillating) in the parameter regime, where the piecewise-smooth system predicts all population densities oscillate. Finally, we fitted the new parameter k to data collected for two different types of predator species that can be categorised roughly based on their feeding behaviour. As a result, our parameter fitting suggests that prey switching of a more selective predator would be best represented with a steeper tanh function that that of a less selective predator.

Second, we regularised the piecewise-smooth system by increasing the dimensionality of the system and reformulated the three-dimensional piecewise-smooth system as a four-dimensional smooth dynamical system. The two vector fields on each side of the discontinuity in the piecewise-smooth system describe the predator's two different feeding modes: It feeds on the preferred prey type on one side and on the alternative prey type on the other. Hence, there is an abrupt change in the predator's desire to consume the preferred prey across the discontinuity. When reformulating our second smooth system from such a piecewise-smooth system, we considered the desire to consume the preferred prey as a system variable (i.e., as a variable that changes on a comparable time scale than that of the population densities) and constructed an equation for its temporal evolution according to the piecewise-smooth system. Our construction is similar to fitness-gradient dynamics,

which have previously given insight into rapid adaptation and predator-prey interaction in plankton [17]. However, in contrast to how fitness-gradient dynamics is applied in [17], we assumed that the predator fitness is equivalent to the switching condition we obtained in the formulation of the piecewise-smooth system using optimal foraging theory in Chapter 3. We made this decision to guarantee that the smooth analog II reduces to the piecewise-smooth system at the extremes of the two different feeding modes, and thus, enables us to carry out a fair comparison between the two systems and their behaviour.

We analysed the resulting four-dimensional system (4.13) using linear stability analysis. Indeed, the steady state, where population densities are nonzero, is equivalent in both systems. However, the four eigenvalues (i.e., two pairs of complex conjugates) of the equilibrium in the smooth system II (4.13) have both positive and negative real parts, except for a point at which the slope of the preference trade-off is equal to the preference towards the alternative prey (i.e., $a_q = q_2$). Then, all four eigenvalues of the steady state have a zero real part. This is different from the piecewise-smooth system where there is a complex conjugate pair of eigenvalues, and thus, the real part of the eigenvalues have the same sign everywhere. Finally, we fitted the smooth system II to data in order to find a suitable perturbation from the steady state that yields oscilllations similar to the recurring pattern of increases and declines in the ciliate predator population in Lake Constance in spring.

The characteristic equation for the eigenvalues of the steady state, where the populations coexist, is more challenging to analyse in the case of the two smooths analogs than in the case of the original piecewise-smooth system. In fact, for the smooth system I (4.1), the characteristic equation is difficult to solve analytically

because we obtain only a numerical solution to the steady state. In the case of the smooth system II (4.13), the characteristic equation involves solving a fourth order equation which complexifies a possible future bifurcation analysis. Thereby, an alternative approach for regularising the piecewise-smooth without increasing the dimensions of the system would be to reformulate the piecewise-smooth system as a *fast-slow dynamical system* according to the method originally developed in [118], and later surveyed in [123].

Fast-slow dynamical systems are systems in which two time scales are present [71]. Such a difference in time scales can arise in several different ways. For example, fast-slow dynamics can occur in electrical circuits or in the communication between cells through abrupt changes in a potential across a cell membrane [71]. Indeed, the classical examples of fast-slow systems are the Van der Pol [132] and Fitzhugh-Nagumo equations [31,98]. The former describes the dynamics of an electrical circuit with an amplifying valve, whereas the latter is a simplified version of the Hodgkin-Huxley nerve axon model [52]. In addition to engineering and neuroscience applications, fast-slow dynamical systems have been used to give insight into pattern formation between a slowly diffusing activator and an inhibitor with a fast diffusion time scale [44], slow storage followed by a rapid release of elastic energy in opening and closing of plant leaves [32], and ocean circulation in which saline transport is assumed to be slower than thermal transport [69]. In theoretical ecology, fast-slow systems have been useful for understanding the effects of rapid evolutionary change of traits on predator-prey interaction [17, 62]. However, we note that in the latter example, the fast-slow system is not obtained as a result of regularising a given piecewise-smooth system.

The formal construction of a smooth system from a piecewise-smooth system

enables a comparison between the two different modelling frameworks, both from a biological and mathematical perspective. However, without additional data on the functional form of prey switching (collected from a controlled laboratory experiment, for example), it is difficult to say with the data we currently have which of the three models—the piecewise-smooth system with a "discontinuous" predator or the two smooth systems with a gradully adapting predator—provides a better putative mechanistic explanation for the observations of plankton dynamics in spring in Lake Constance. Based on the parameter fitting we carried out for the smooth system, the simplistic assumption of a discontinous predator we made in Chapter 3 is justified at least in the case of a selective predator. Above all, the construction of models using alternative modelling approaches allows us to gain more insight into the dynamics exhibited by the models. Furthermore, we can use this knowledge and compare different models against each other and validate them in order to construct prey-switching models for predator-prey interaction in organisms besides plankton, as long as the assumptions of large population size, well-mixed environment, and the use of community-integrated parameters are justified.

Appendix A

Defining and nondegeneracy conditions of the adding-sliding bifurcation

The 1 predator-2 prey system in Equation (3.4) exhibits a novel centre to two-part periodic orbit ("C2PO") bifurcation that we discovered and studied numerically in Section 3.4. The C2PO bifurcation differs from the standard adding-sliding bifurcation in the way that the periodic orbit is born. In the C2PO bifurcation, there is a family of entirely sliding centres at the bifurcation point. In the standard adding-sliding bifurcation, however, there exists one entirely sliding periodic orbit that grows to encompass a non-sliding segment as the distance to the bifurcation point increases. However, as we are about to show, the C2PO bifurcation satisfies both the defining (i.e., equality) and nondegeneracy (i.e., inequality) conditions that specify the standard adding-sliding bifurcation [23]. This result enables us to take advantage of the existing normal form map for the adding-sliding bifurcation in the process of deriving a normal form to describe the C2PO bifurcation

analytically.

In addition to Filippov's convex method (see Section 2.1.2.3), the sliding flow at the discontinuity boundary h can also be formulated using *Utkin's equivalent control method* [131]. According to Utkin's method, the sliding flow is a sum of the mean of the two vector fields and a control $\gamma(x)$ in the direction of the difference between the vector fields:

$$f_{s_U} = \frac{f_+ + f_-}{2} + \frac{f_- - f_+}{2}\gamma(x)\,, \tag{A.1}$$

where

$$\gamma(x) = -\frac{\mathcal{L}_{f_+}h + \mathcal{L}_{f_-}h}{\mathcal{L}_{f_-}h - \mathcal{L}_{f_+}h} \in [-1, 1]\,. \tag{A.2}$$

Similar to Filippov's method, the sliding flow derived using Utkin's control method is tangent to h (i.e., $\mathcal{L}_{f_{s_U}}h = 0$). Utkin's and Filippov's methods are related using $\gamma = 2\alpha - 1$. If $\gamma = -1$, then the sliding flow is governed by f_+. For the 1 predator-2 prey system (3.4), the control $\gamma(x)$ is given by

$$\gamma(x) = \frac{p_1(-2r_1 + z) + a_q p_2(2r_2 - z)}{z(p_1 + a_q p_2)}\,. \tag{A.3}$$

The three defining conditions for all four principal sliding bifurcation scenarios (i.e., adding-sliding, grazing-sliding, crossing-sliding, and switching-sliding) state that the intersection point x^* at which the critical trajectory involved in the bifurcation intersects with the boundary of the sliding region (1) has to belong to the switching manifold, which (2) has to be well-defined. In addition, the intersection point (3) has to be located on the boundary of the sliding and crossing regions [23]. In the case of the 1 predator-2 prey piecewise-smooth system (3.4), the intersection point is the cusp $x^* = (p_1^*, p_2^*, z^*) = (m/(eq_1), m/(eq_1 a_q), r_1 - r_2)$

between f_+ and the switching boundary (see Section 3.3.4). For the cusp x^*, we have (as the first defining condition of an adding-sliding bifurcation)

$$h(x^*) = p_1^* - a_q p_2^* = \frac{m}{eq_1} - \frac{a_q m q_1}{eq_1 a_q} = 0\,. \tag{A.4}$$

Thus, the cusp is located on the manifold $h = p_1 - a_q p_2$. The second defining condition also holds because h is well-defined:

$$\left.\frac{dh}{d\mathbf{x}}\right|_{x^*} = \begin{bmatrix} 1 & -a_q & 0 \end{bmatrix} \neq 0\,. \tag{A.5}$$

In addition, the third defining condition is satisfied because the intersection point x^* lies on the boundary of the sliding region

$$\gamma(x^*) = \frac{p_1^*(-2r_1 + z^*) + a_q p_2^*(2r_2 - z^*)}{z^*(p_1^* + a_q p_2^*)} = \frac{-(r_1 - r_2)}{r_1 - r_2} = -1\,, \tag{A.6}$$

$$f_+(x^*) = (r_1 - z^*)p_1^* - a_q r_2 p_2^* = \frac{r_1 m - m(r_1 - r_2) - m r_2}{eq_1} = 0\,. \tag{A.7}$$

The nondegeneracy condition applicable to all four sliding bifurcation cases requires that in the neighbourhood of x^*, the vector field f_- is pointing towards, and does not graze, the switching boundary. This can be shown for the 1 predator-2 prey system (3.4) at x^*, at which

$$\mathcal{L}_{f_-} h(x^*) = r_1 p_1^* - a_q(r_2 - z^*)p_2^* = \frac{2m}{eq_1}(r_1 - r_2) > 0\,. \tag{A.8}$$

The aforementioned three defining (A.4)–(A.7) and one nondegeneracy (A.8) conditions are the same in each of the four principal sliding bifurcation cases. However, the second nondegeneracy condition is specific to the adding-sliding bifurcation and requires an additional defining condition. This defining condition states that there

must be a point of tangency between the sliding flow and the boundary between the crossing and sliding regions at the bifurcation point. This occurs when

$$\mathcal{L}_{f_+}\gamma(x^*) := \gamma_x f_+(x^*) = \begin{bmatrix} \frac{-r_2}{(r_1-r_2)\left(\frac{m}{eq_1}\right)} & \frac{a_q r_2}{(r_1-r_2)\frac{m}{eq_1}} & \frac{2}{r_1-r2} \end{bmatrix} \begin{bmatrix} \frac{r_2 m}{eq_1} \\ \frac{r_2 m}{eq_1 a_q} \\ 0 \end{bmatrix} = 0\,, \tag{A.9}$$

where

$$\gamma_x = \begin{bmatrix} \frac{\partial\gamma}{\partial p_1} & \frac{\partial\gamma}{\partial p_2} & \frac{\partial\gamma}{\partial z} \end{bmatrix}. \tag{A.10}$$

The second nondegeneracy condition, which is specific to the adding-sliding bifurcation, thereby requires that the sliding flow reaches its local minimum in terms of the control γ. This is satisfied when

$$(\mathcal{L}_{f_+})^2\gamma(x^*) := \gamma_x(x^*)f_{+_x}(x^*)f_+(x^*) + \gamma_{xx}(x^*)f_+(x^*)^2 > 0\,. \tag{A.11}$$

For Equation (3.4), the first term in the second nondegeneracy condition (A.11) becomes

$$\gamma_x(x^*)f_{+_x}(x^*)f_+(x^*) = \begin{bmatrix} \frac{-r_1 eq_1}{(r_1-r_2)m} & \frac{a_q r_2 eq_1}{(r_1-r_2)m} & \frac{1}{r_1-r_2} \end{bmatrix} \begin{bmatrix} \frac{r_2^2 m}{eq_1} \\ \frac{f_2^2 m}{eq_1 a_q} \\ r_2 m(r_1-r_2) \end{bmatrix} = r_2 m\,. \tag{A.12}$$

Using

$$\gamma_{xx} = \begin{bmatrix} \frac{\partial^2\gamma}{\partial p_1^2} & \frac{\partial^2\gamma}{\partial p_2^2} & \frac{\partial^2\gamma}{\partial z^2} \end{bmatrix}, \tag{A.13}$$

for Equation (3.4), the second term in the second nondegeneracy condition (A.11)

becomes

$$\gamma_{xx}(x^*)f_+(x^*)^2 = \begin{bmatrix} \frac{1}{(r_1-r_2)\left(\frac{m}{eq_1}\right)^2} & \frac{-a_q^2}{(r_1-r_2)\left(\frac{m}{eq_1}\right)^2} & \frac{-2}{(r_1-r_2)^2} \end{bmatrix} \left(\frac{m}{eq_1}\right)^2 \begin{bmatrix} r_2^2 \\ \left(\frac{r_2}{a_q}\right)^2 \\ 0 \end{bmatrix} = 0\,. \tag{A.14}$$

Finally, by combining the result in (A.12) and (A.14), we find that the second nondegeneracy condition (A.11) holds in the case of the 1 predator-2 prey system (3.4)

$$\gamma_x(x^*)f_{+_x}(x^*)f_+(x^*) + \gamma_{xx}(x^*)f_+(x^*)^2 = r_2 m + 0 > 0\,. \tag{A.15}$$

Appendix B

Parameter fitting

There are several approaches available for parameter estimation of ODE models. For example, COPASI [56] and Berkeley Madonna [86] are programme packages, and PottersWheel [88] is a MATLAB toolbox, that feature optimisation methods for searching an ODE's parameter space and minimising an objective function. In addition to these software packages, approximate Bayesian computation (ABC) methods can be used to infer parameter values and to distinguish between competing ODE models (see [7] for a review). We use ABC combined with a sequential Monte Carlo (SMC) method because the fitting results can be assessed by studying the posterior parameter distribution rather than just a single value that gives the best fit as a result of an optimisation method. In addition, this approach allows us to code every step of the algorithm on our own. We can thereby be more aware of the possible sources of error in the fitting process than when providing input and analysing an output of an available software package.

In the case of the 1 predator-2 prey piecewise-smooth model (3.4), we compare the scaled prey exhibited by the model with that calculated from the Lake Constance data (see Section 3.4.7). Because the model captures the periodicity in the

scaled prey ratio better than the amplitude, we calculate and use the periodicity exhibited in the data as our objective function in the ABC method. Thus, we look for a set of parameter values of the growth rate of the preferred and alternative prey (i.e., r_1 and r_2, respectively) and the predator mortality rate (i.e., m) that yield a periodicity of the model (3.4) as close as possible to the periodicity exhibited in the data. We introduce the ABC method [129] in Section B.1. We then use it for estimating the prey growth rate in a standard 1 predator-1 prey Lotka-Volterra model (1.1) as an example case in Section B.2.1 before presenting the results for the parameter fitting of the piecewise-smooth model (3.4) in Section B.2.2.

B.1 Bayesian inference and Monte Carlo methods

In the parameter-fitting process, we assume that the data are noisy observations of a simulation of the piecewise-smooth 1 predator-2 prey model (3.4) with unknown parameters collectively denoted by $\theta = (r_1, r_2, m)$. We then use a Bayesian approach to infer the parameters and to indicate the uncertainty of the results. In the present study, we have some information about the parameters of the piecewise-smooth system—for example, $r_1, r_2, m > 0$ and additionally $0 < a_q < q_2/q_1$ for the adding-sliding periodic orbit to be present. This information is included in the prior distribution $\pi(\theta)$. As we consider the data, which are represented in this case by the scaled prey ratio calculated from the Lake Constance data, our knowledge about the parameter θ changes. Thus, we calculate the posterior distribution

$P(\theta|D)$ using Bayes' rule

$$P(\theta|D) = \frac{P(D|\theta)\pi(\theta)}{P(D)}, \tag{B.1}$$

where $P(D|\theta)$ is the probability of the data given θ and $P(D) = \int_\theta P(D|\theta)\pi(\theta)d\theta$ is the normalising constant. In most applications, equation (B.1) does not have a closed-form solution because $P(D|\theta)$ or the integral in the denominator are unknown. However, the Monte Carlo (MC) simulation methods can be used to estimate θ by repeatedly drawing random samples distributed according to $P(\theta|D)$.

In using the Monte Carlo method for fitting parameters of the piecewise-smooth model to Lake Constance data, we first sample a candidate parameter set θ^* from $\pi(\theta)$, which for each element in θ is a uniform distribution within the appropriate range. We have used simulations and literature (e.g., [39, 128]) to help determine the upper limit of this range for r_1, r_2 and m. We then simulate the piecewise-smooth model (3.4) with θ^* and compare the simulation with the data by calculating the squared difference $d^2(D, D^*)$ between the periodicity in the scaled prey ratio exhibited in the simulation (D^*) and the periodicity in the prey ratio exhibited by the data (D). That is,

$$d^2(D, D^*) = (D - D^*)^2. \tag{B.2}$$

After calculating $d^2(D, D^*)$ for every θ^*, we examine the results by studying θ^* sampled in the MC simulation and the corresponding differences $d^2(D, D^*)$. To discriminate between parameter values according to the goodness of the fit, we use a tolerance $\epsilon_1 > 0$ to determine the level of agreement between the simulation and the data. We consider the sampled parameters that yield a difference below

this tolerance as accepted parameter values and study the resulting distribution of them.

B.2 ABC implementations

First, we implement a simple ABC rejection algorithm (as used in [105]), which proceeds as follows:

I Sample a candidate parameter set θ^* from $\pi(\theta)$.

II Simulate the model to create a simulation data set and calculate the error between the periodicity in the scaled prey ratio in the data and that produced by the model.

III Accept or reject θ^* depending on whether or not the difference in the periodicity lies within a desired range. That is, accept θ^* if and only if $d^2(D, D^*) < \epsilon_1$.

IV Repeat the algorithm until a required number of candidate samples are accepted. For example, choose ϵ_1 such that 10% of the initial candidates are accepted.

We use the ABC rejection algorithm to obtain estimates for $d^2(D, D^*)$ in a run where first 10% and then 5% of the initial candidates were accepted. In other words, we simulate N candidates, calculate the distance for each candidate, put the candidates in order based on their value for $d^2(D, D^*)$, and accept 10% (or 5%) of them that give the smallest value for $d^2(D, D^*)$. We then choose the largest distance generated by the accepted candidates as the desired tolerance level $\epsilon_{1,10\%}$ (and $\epsilon_{L,5\%}$, where L is the number of tolerance levels). We construct a decreasing

sequence of L tolerance levels $\{\epsilon_{1,10\%}, ..., \epsilon_{L,5\%}\}$ and apply these tolerance levels to the ABC scheme based on the sequential Monte Carlo (ABC SMC) method introduced in [129].

In ABC SMC, N candidate parameters $\{\theta^{(1)}, ..., \theta^{(N)}\}$ are sampled from $\pi(\theta)$. The algorithm incorporates a decreasing sequence of L tolerance levels—for example, $\{\epsilon_{1,10\%}, ..., \epsilon_{L,5\%}\}$, where $\epsilon_{1,10\%}$ is the largest distance between the period exhibited in the simulation and in the data when 10% of the N candidates sampled are accepted in the ABC rejection method and $\epsilon_{L,5\%}$ is the largest distance between the period exhibited in the simulation and in the data when 5% of the N candidates sampled are accepted in the ABC rejection method. Initially, we sample θ^* from $\pi(\theta)$. Then, at every iteration, we sample the candidate parameters among the candidates that were accepted in the previous step. The tolerance level is stricter at each step. Thus, the ABC SMC algorithm propagates through the sequence of tolerance levels as it proceeds gradually towards the distribution obtained at the last step [129]. The ABC SMC method proceeds as follows [129]:

1. Initialize the decreasing sequence of tolerance levels $\{\epsilon_1, ..., \epsilon_L\} = \{\epsilon_{1,10\%}, ..., \epsilon_{L,5\%}\}$. Set tolerance level indicator $l = 1$.

2. Set candidate indicator $i = 1$.

3. In the first iteration ($l = 1$), sample a candidate θ^* from $\pi(\theta)$. If $t \neq 1$, sample θ^* from $\{\theta_{l-1}^{(i)}\}$ with weights w_{l-1}. Perturb the candidate according to the perturbation kernel K_l to obtain θ^{**}, where θ^* denotes a candidate before the perturbation and θ^{**} denotes a candidate after the perturbation. For simplicity, we chose K_l to be a normal distribution centred on θ^* with variance 0.1.

4. Simulate the piecewise-smooth system (3.4) with θ^{**}, calculate the periodicity in the scaled prey ratio exhibited in the simulation, and determine the squared difference $d^2(D, D^*)$ for the periodicity in the prey ratio exhibited in the data. If $d^2(D, D^*) > \epsilon_l$, return to step 3.

5. Set $\theta_l^{(i)} = \theta^{**}$ and calculate the weight for the $\theta_l^{(i)}$ candidate:

$$w_l^{(i)} = \begin{cases} 1 & , \text{if } l = 0 \\ \frac{\pi\left(\theta_l^{(i)}\right)}{\sum_{j=1}^{N} w_{l-1}^{(j)} K_l\left(\theta_{l-1}^{(j)}, \theta_l^{(i)}\right)} & , \text{if } l > 0. \end{cases} \tag{B.3}$$

6. If $i < N$, set $i = i + 1$ and return step 3.

7. If $l < L$, set $l = l + 1$ and return step 2.

A problem with the ABC rejection algorithm as a stand-alone sampling method is its low acceptance rate if there is a large difference between the prior and posterior distributions. To overcome this problem, ABC can be used together with Markov chain MC simulations (ABC MCMC) which is guaranteed to converge to the target (approximate) posterior distribution [89]. As a disadvantage, the samples in the ABC MCMC are not entirely independent, and as a result, there is a risk that the algorithm dwells or gets stuck in parameter regions that have a low probability of being accepted. Thus, ABC SMC has been developed to avoid these problems with the ABC rejection and ABC MCMC algorithms. Even though a similar guarantee of convergence to ABC MCMC does not exist for the ABC SMC [129], the goodness of the posterior distribution can be assessed through analysing the intermediate distributions and the number of proposals that are required to obtain a given number of accepted proposals [129].

B.2.1 Implementation of the ABC SMC method for the 1 predator-1 prey Lotka-Volterra system in Equation (1.1)

Before carrying out parameter fitting with Lake Constance data, we want to test our ABC rejection and ABC SMC implementations with the 1 predator-1 prey Lotka-Volterra model (1.1). We first generate data as a simulation of the model (1.1) with noise following a normal distribution with standard deviation $\sigma = 0.5$ added. We then infer the employed parameter value for prey growth rate $r = 1$ with the ABC SMC method. To calculate the squared distance, we choose nonnegative prey densities among 30 points we select uniformly at random generated by adding noise to the simulation (see Figure B.1 top left). We define the squared distance as

$$d^2(P) = \sum_i (P_{\text{data}}(i) - P_*(i))^2 \,, \tag{B.4}$$

where $P_{\text{data}}(i)$ denotes the prey density at the ith selected data point in the generated data and $P_*(i)$ denotes the prey density predicted by the model at the same point. As our prior distribution, we assume $r \sim \mathcal{U}(0, 10)$. As we expect, the squared distance shows a minimum at $r = 1$ (see Figure B.1, top right) and the probability density estimates obtained in the ABC SMC method (steps 1–7) approach a distribution that has a peak near $r = 1$ (see Figure B.1, bottom).

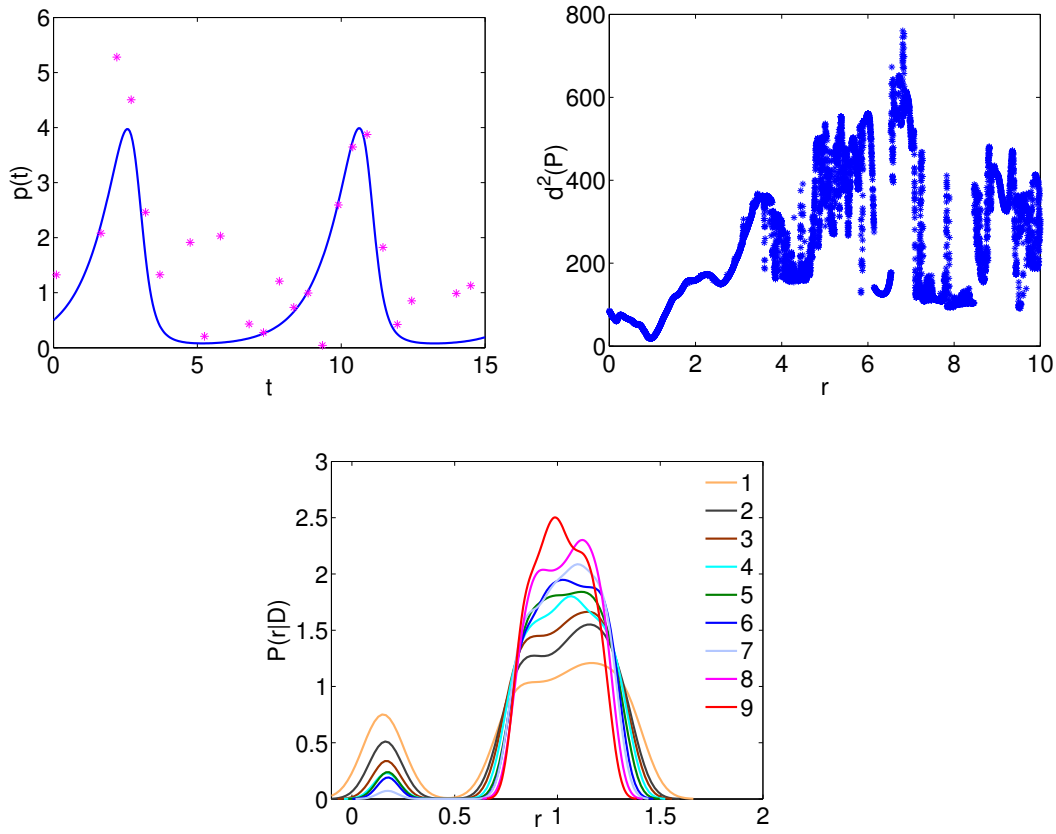

Figure B.1: Estimating prey growth rate ($r = 1$) of the Lotka-Volterra model (1.1) using (top) ABC rejection (steps I–VI) and (bottom) ABC SMC method (steps 1–7). (Top left) Solid curve denotes the prey density of a simulation of the Lotka-Volterra model (1.1) with $(\beta, e, m) = (1, 1, 1)$ and $(p(0), z(0)) = (0.5, 0.1)$. Asterisks denote the data points we select uniformly at random from the prey density of (1.1) after the addition of noise from a normal distribution with $\sigma = 0.5$. For these data points we calculate the squared distance between the generated data and the model simulation. (Top right) Squared distance $d^2(P)$ between the simulation (i.e., solid curve in top left) and the generated data (i.e., asterisks in top left) as a function of prey growth rate r after 10000 iterations of the ABC rejection algorithm (steps I–VI). (Bottom) Smooth probability density estimates calculated using MATLAB's `ksdensity` function illustrate how the ABC SMC (steps 1–7) propagates towards the target distribution in red. In the ABC SMC method ($L = 9$, $N = 1000$), we construct the sequence of tolerance levels ϵ_i ($i = 1, ..., 9$) linearly spaced between when 10% ($\epsilon_1 \approx 52.6$) and when 5% ($\epsilon_9 \approx 36.9$) of the candidate samples θ^* are accepted in the ABC rejection method (steps I–VI) for the Lotka-Volterra system (1.1).

B.2.2 Parameter fitting of the 1 predator-2 prey piecewise-smooth system in Equation (3.4) to Lake Constance data

To have an estimate for the periodicity in the prey ratio exhibited in the Lake Constance data, we calculate the mean data for the prey ratio p_1/p_2 in spring in Lake Constance over the period 1979–1999. For p_1 and p_2, we select the same prey species as in the comparison between the piecewise-smooth model (3.4) and the Lake Constance data (see Figure 3.12). Similarly to the data comparison in Section 3.4.7, we obtain the processed data by subtracting a least-squares fit of a straight line to the mean of the data. The equation for this line is $y = 0.03x + 0.95$, where the norm of the residual is 4.39. We calculate the period of the prey ratio oscillations in spring as the mean difference between consecutive peaks in the prey ratio (i.e., March 27, March 31, April 26, May 11, May 12, and May 15). We choose these peaks based on visual inspection, and we calculate 11 period estimates from them. With our choice of consecutive peaks, we obtain a period of about 21.82 ± 4.30 days. We use this period as our data, to which we fit the growth rate of the preferred (r_1) and alternative (r_2) prey, and the predator death rate (m) of the piecewise-smooth model (3.4).

For the ABC rejection algorithm (steps I–II) that we carry out for 1000 iterations, we assume the following uniform distributions as our prior distributions for the parameters: $r_1 \sim \mathcal{U}(1,3)$, $r_2 \sim \mathcal{U}(0.01, 0.8)$, $m \sim \mathcal{U}(0.1, 1)$. We chose these distributions by studying the literature (for example, [128]) and by simulating the piecewise-smooth system numerically. We simulate the piecewise-smooth model (3.4) with $(q_1, q_2, \beta_1, \beta_2, e, a_q) = (1, 0.5, 1, 1, 0.25, 0.4)$ and $(p_1(0), p_2(0), z(0)) =$

$(1, 1, 1)$ for 500 days of which we discard the first one-third as a transient based on visual inspection and numerical simulations of the model (3.4). As a result of our ABC rejection algorithm, we obtain the best fit to the period calculated from the data (i.e., 21.82 days) with $(r_1, r_2, m) = (1.50, 0.12, 0.10)$ and the period of the prey ratio produced by the model (3.4) is about 21.9 days.

In the ABC SMC method ($L = 9$, $N = 30$), we construct the sequence of tolerance levels ϵ_l ($l = 1, ..., 9$) equally spaced from when 10% ($\epsilon_1 \approx 51.4$) and to when 5% ($\epsilon_9 \approx 20.8$) of the candidate samples $\theta^* = (r_1^*, r_2^*, m^*)$ are accepted in the ABC rejection method. We simulate the piecewise-smooth model (3.4) with $(q_1, q_2, \beta_1, \beta_2, e, a_q) = (1, 0.5, 1, 1, 0.25, 0.4)$ and $(p_1(0), p_2(0), z(0)) = (1, 1, 1)$ for 750 days of which we discard the first one-third as a transient based on visual inspection and numerical simulations of the model (3.4). As a result of our ABC SMC method, the mean of the accepted samples at the final iteration (i.e., $l = 9$) is $(r_1^*, r_2^*, m^*) = (1.33, 0.48, 0.14)$ and the period of the prey ratio then produced by the model (3.4) is about 20.66 days. For the smooth probability density functions of r_1, r_2, and m at each iteration (i.e., $l = 1, \ldots, 9$), see Figure B.2.

B.2.3 Parameter fitting of the 1 predator-2 prey smooth system I in Equation (4.1) and II in Equation (4.13) to Lake Constance data

To have an estimate for the predator density in the Lake Constance data in years 1991 and 1998, we first normalise both the data points ($P_{\text{data}}(i)$) and the model prediction ($P_*(i)$) for the predator density z by L_2-norm (i.e., the Euclidean dis-

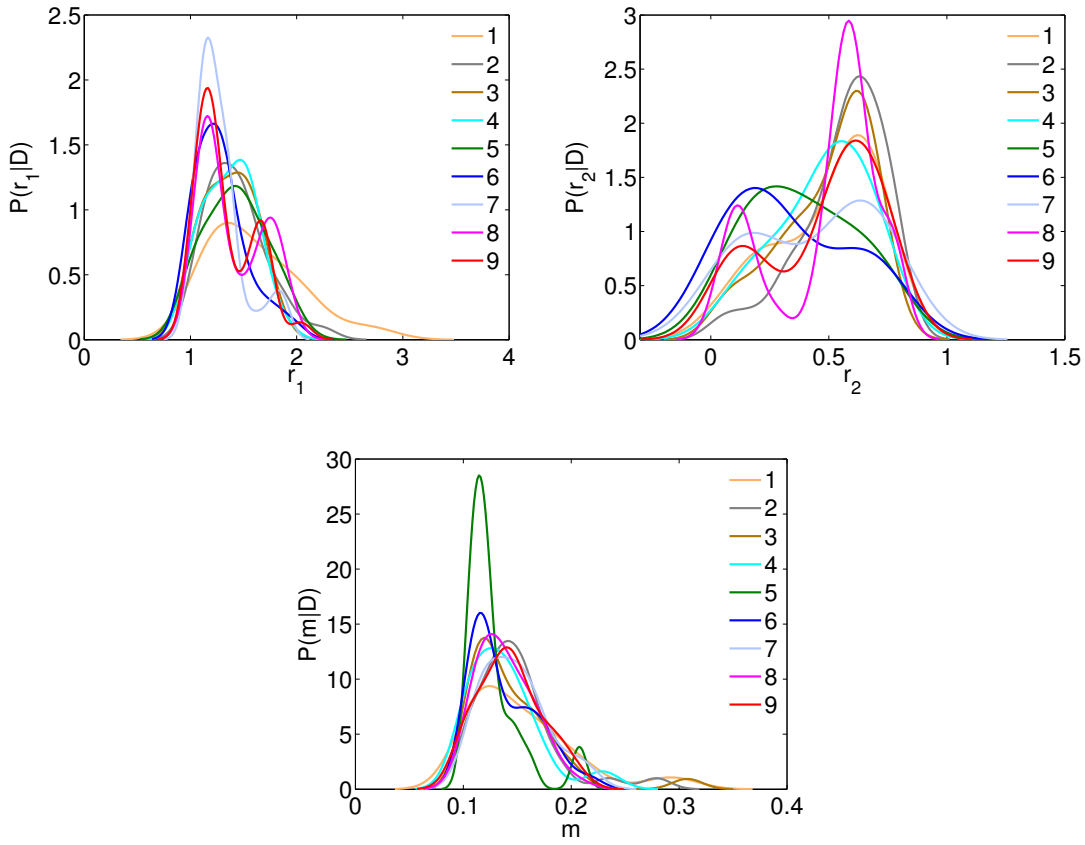

Figure B.2: Smooth probability density estimates calculated using MATLAB's `ksdensity` function for (top left) the growth rate of the preferred prey (r_1), (top right) the growth rate of the alternative prey r_2, and (bottom) the predator death rate (m) in the 1 predator-2 prey piecewise-smooth model (3.4) using the ABC SMC method [129] (steps 1–7). In the ABC SMC method ($L = 9$, $N = 30$), we construct the sequence of tolerance levels ϵ_l ($l = l, ..., 9$) linearly spaced between when 10% ($\epsilon_1 \approx 51.4$) and when 5% ($\epsilon_9 \approx 20.8$) of the candidate samples θ^* are accepted in the ABC rejection method (steps I–VI) for the piecewise-smooth model (3.4).

tance)

$$L_{2_{P_{\text{data}/*}}} = \sqrt{\sum_i \left|P_{\text{data}/*}(i)\right|^2}. \tag{B.5}$$

In the parameter fitting for the data comparison in Section 4.2.3, we choose data points between March 1 and June 15. We restrict the time window of comparison to spring, as it has been suggested that predator-prey feeding interactions are an important factor in explaining the ciliate-algal dynamics in Lake Constance in that season [128] and that such interactions have larger relative importance than environmental conditions [116]. In year 1991, there are 31 data points in the chosen time window for the selective ciliate predator *Balanion planctonicum* and 19 data points for the unselective ciliate predator *Rimostrombidum lacustris*. In year 1998, there are 15 data points for both the selective ciliate predator *Balanion planctonicum* and unselective ciliate predator *Rimostrombidum lacustris*. In the case of the smooth system II, we fit the model to the total predator abundance calculated as the sum of the unselective and selective predator abundances. After normalising these data points and the model prediction for these data points by L_2-norm in Equation (B.5), we align the peak abundances both in the data and in the model simulation before calculating the squared distance (B.4) between the data and the model prediction.

For the ABC rejection algorithm (steps I–II) that we carry out for 1000 iterations, we assume the following uniform distributions as our prior distributions for the parameters: $r_1 \sim \mathcal{U}(1,3)$, $r_2 \sim \mathcal{U}(0.01,0.8)$, $m \sim \mathcal{U}(0.1,1)$, $a_q \sim \mathcal{U}(0.01,2)$, and $k \sim \mathcal{U}(2,100)$. In the case of the smooth system II, we assume $m \sim \mathcal{U}(0.05,1)$ and $\nu \sim \mathcal{U}(1.1,5)$, where ν represents the initial perturbation from the steady state V. That is, we start simulations of the smooth system II at $z(0) = \nu\tilde{z}$. We chose these distributions by studying the literature (for example, [128]) and by simu-

lating the smooth systems I and II numerically. We simulate the smooth model I (4.1) with $(q_1, q_2, \beta_1, \beta_2, e) = (1, 0.5, 1, 1, 0.25)$ and $(p_1(0), p_2(0), z(0)) = (1, 1, 1)$ for 457 (i.e., twice the lenght of the "spring" we chose to start March 1 and end June 15) days of which we discard the first three months (i.e., 61 days) as a transient based on visual inspection and numerical simulations of the model (4.1). In the case of the smooth system II, we simulate the model (4.13) with $(r_1, r_2, \beta_1, \beta_2, e, q_2, a_q) = (1, 0.4, 1, 1, 0.25, 0.5, 0.5)$ and $(p_1(0), p_2(0), z(0), q(0)) = (a_q m(r_1 + r_2)/(e(a_q r_1 + q_2 r_2)), m(r_1 + r_2)/(e(a_q r_1 + q_2 r_2)), \nu(r_1 + r_2), r_1/(r_1 + r_2))$, which for p_1, p_2, and q corresponds to the steady state IV of the smooth system II (4.13). Similarly to the smooth system I, we simulate the smooth system II for 457 days of which we discard the first three months (i.e., 61 days) as a transient based on visual inspection and numerical simulations of the model (4.13).

In the ABC SMC method ($L = 10$, $N = 50$) for the smooth system I, we construct the sequence of tolerance levels ϵ_l $(l = 1, ..., 10)$ equally spaced from when 5% and to when 1% (in year 1991), and when 10% and to when 1% (in year 1998), of the candidate samples $\theta^* = (r_1^*, r_2^*, m^*, a_q^*, k^*)$ are accepted in the ABC rejection method. We simulate the smooth model I (4.1) with $(q_1, q_2, \beta_1, \beta_2, e) = (1, 0.5, 1, 1, 0.25)$ and $(p_1(0), p_2(0), z(0)) = (1, 1, 1)$ for 457 days of which we discard the first three months (i.e., 61 days) as a transient based on visual inspection and numerical simulations of the model (4.1).

In the ABC SMC method ($L = 10$, $N = 50$) for the smooth system II, we construct the sequence of tolerance levels ϵ_l $(l = 1, ..., 10)$ equally spaced from when 10% and to when 1% of the candidate samples $\theta^* = (m^*, \nu)$ are accepted in the ABC rejection method. We simulate the smooth model II (4.13) with $(r_1, r_2, \beta_1, \beta_2, e, q_2, a_q) = (1, 0.4, 1, 1, 0.25, 0.5, 0.5)$ and $(p_1(0), p_2(0), z(0), q(0)) =$

$(a_q m(r_1+r_2)/(e(a_q r_1+q_2 r_2)), m(r_1+r_2)/(e(a_q r_1+q_2 r_2)), \nu(r_1+r_2), r_1/(r_1+r_2))$, for 457 days of which we discard the first three months (i.e., 61 days) as a transient based on visual inspection and numerical simulations of the model (4.13).

As a result of our ABC SMC method for the smooth system I, the mean of the accepted samples at the final iteration (i.e., $l = 10$) is $(r_1^*, r_2^*, m^* a_q^*, k^*) = (1.56, 0.61, 0.17, 0.080, 62)$ for the selective predator fitted to the 1991 data. The mean distance to the data produced by the model (4.1) is 0.35. For the unselective predator fitted to the 1991 data, the mean of the accepted samples at the final iteration (i.e., $l = 10$) is $(r_1^*, r_2^*, m^*, a_q^*, k^*) = (1.41, 0.66, 0.41, 0.16, 54)$ and the mean distance to the data produced by the model (4.1) is 0.35. For the smooth probability density functions of r_1, r_2, m, a_q, and k at each iteration (i.e., $l = 1, \ldots, 10$), see Figures B.3 and B.4, for the selective and unselective predator, respectively.

In the case of year 1998, we obtain with our ABC SMC implementation that the mean of the accepted samples at the final iteration (i.e., $l = 10$) for the selective predator is $(r_1^*, r_2^*, m^*, a_q^*, k^*) = (1.45, 0.65, 0.52, 0.17, 76)$ and the mean distance to the data produced by the model (4.1) is 0.23. For the unselective predator, the mean of the accepted samples at the final iteration (i.e., $l = 10$) is $(r_1^*, r_2^*, m^*, a_q^*, k^*) = (1.89, 0.66, 0.66, 0.17, 36)$ and the mean distance to the data produced by the model (4.1) is 0.27, when fitted to the data from 1998. For the smooth probability density functions of r_1, r_2, m, a_q, and k at each iteration (i.e., $l = 1, \ldots, 10$), see Figures B.5 and B.6, for the selective and unselective predator, respectively.

As a result of our ABC SMC method for the smooth system II, the mean of the accepted samples at the final iteration (i.e., $l = 10$) is $(m^*, \nu^*) = (0.29, 4.4)$

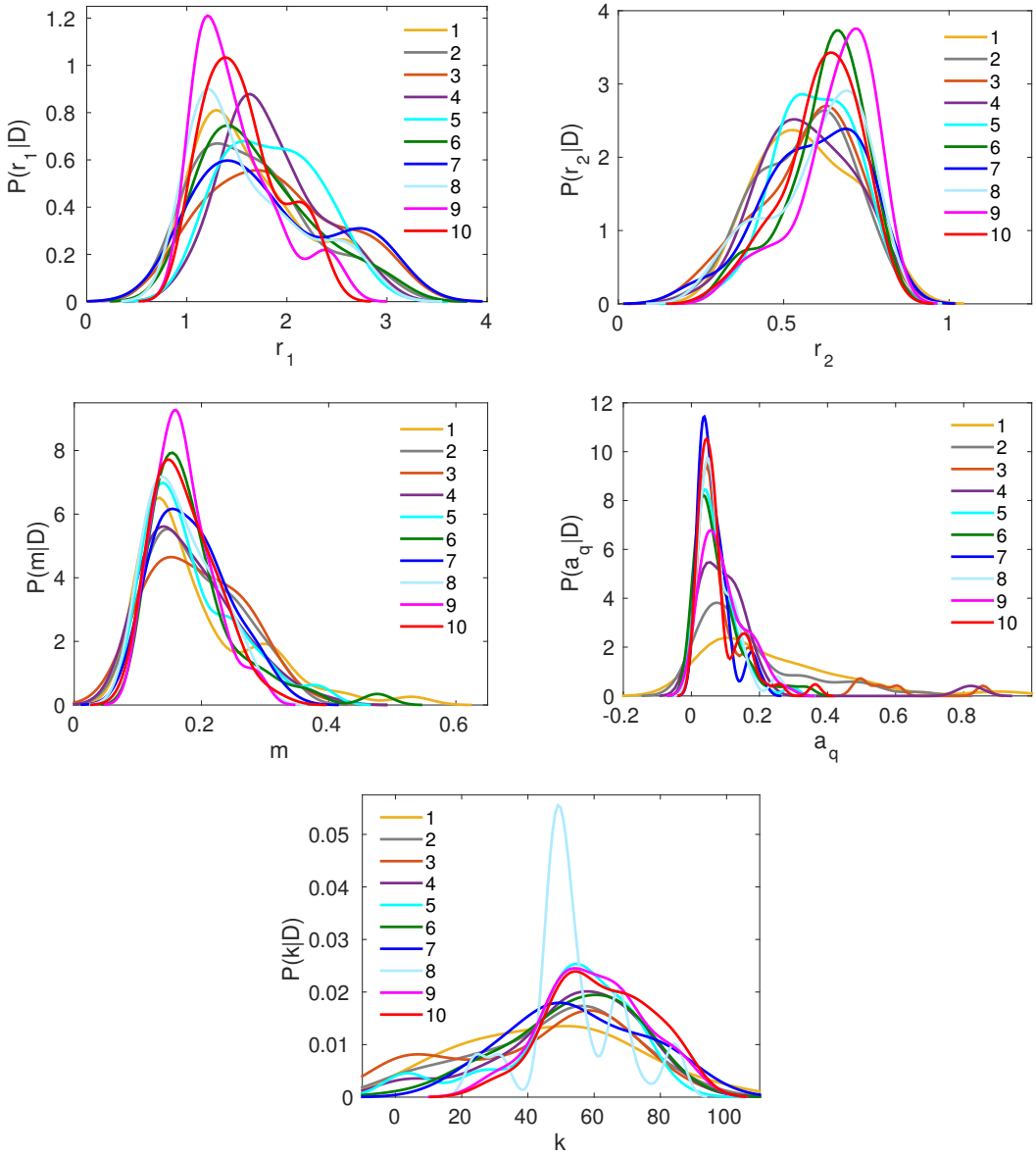

Figure B.3: Smooth probability density estimates calculated using MATLAB's `ksdensity` function for (top left) the growth rate of the preferred prey, (top right) the growth rate of the alternative prey, (middle left) the predator death rate, (middle right) the slope of the preference trade-off, and (bottom) the steepness of the tanh function of the selective predator in the smooth model I (4.1) using the ABC SMC method [129] (steps 1–7) and 1991 data. In the ABC SMC method ($L = 10$, $N = 50$), we construct the sequence of tolerance levels ϵ_l ($l = l, ..., 10$) linearly spaced between when 5% ($\epsilon_1 \approx 0.60$) and when 1% ($\epsilon_{10} \approx 0.46$) of the candidate samples θ^* are accepted in the ABC rejection method (steps I–VI) for the smooth model I (4.1).

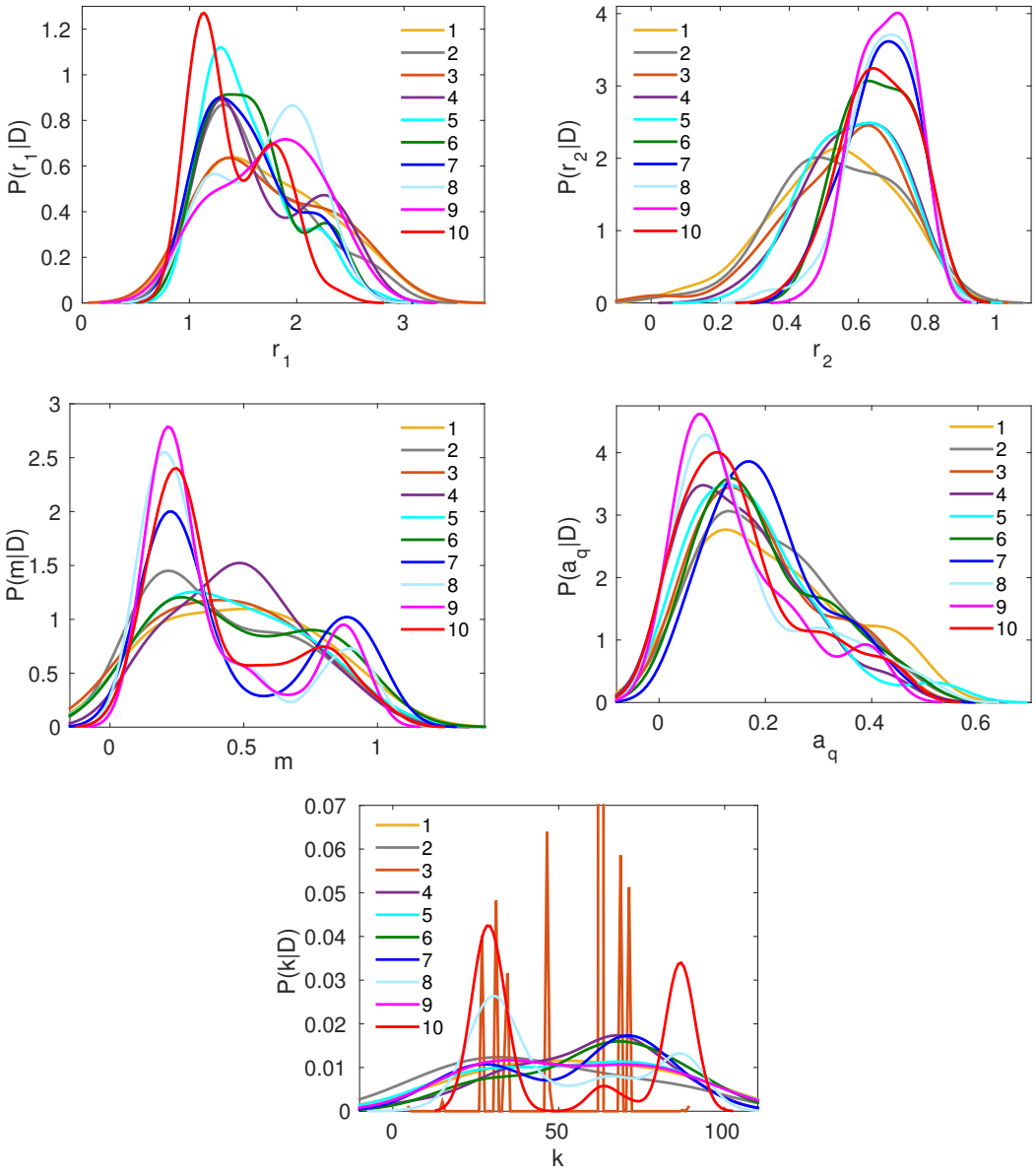

Figure B.4: Smooth probability density estimates calculated using MATLAB's `ksdensity` function for (top left) the growth rate of the preferred prey, (top right) the growth rate of the alternative prey, (middle left) the predator death rate, (middle right) the slope of the preference trade-off, and (bottom) the steepness of the tanh function of the unselective predator in the smooth model I (4.1) using the ABC SMC method [129] (steps 1–7) and 1998 data. In the ABC SMC method ($L = 10$, $N = 50$), we construct the sequence of tolerance levels ϵ_l ($l = l, ..., 10$) linearly spaced between when 5% ($\epsilon_1 \approx 0.57$) and when 1% ($\epsilon_{10} \approx 0.43$) of the candidate samples θ^* are accepted in the ABC rejection method (steps I–VI) for the smooth model I (4.1).

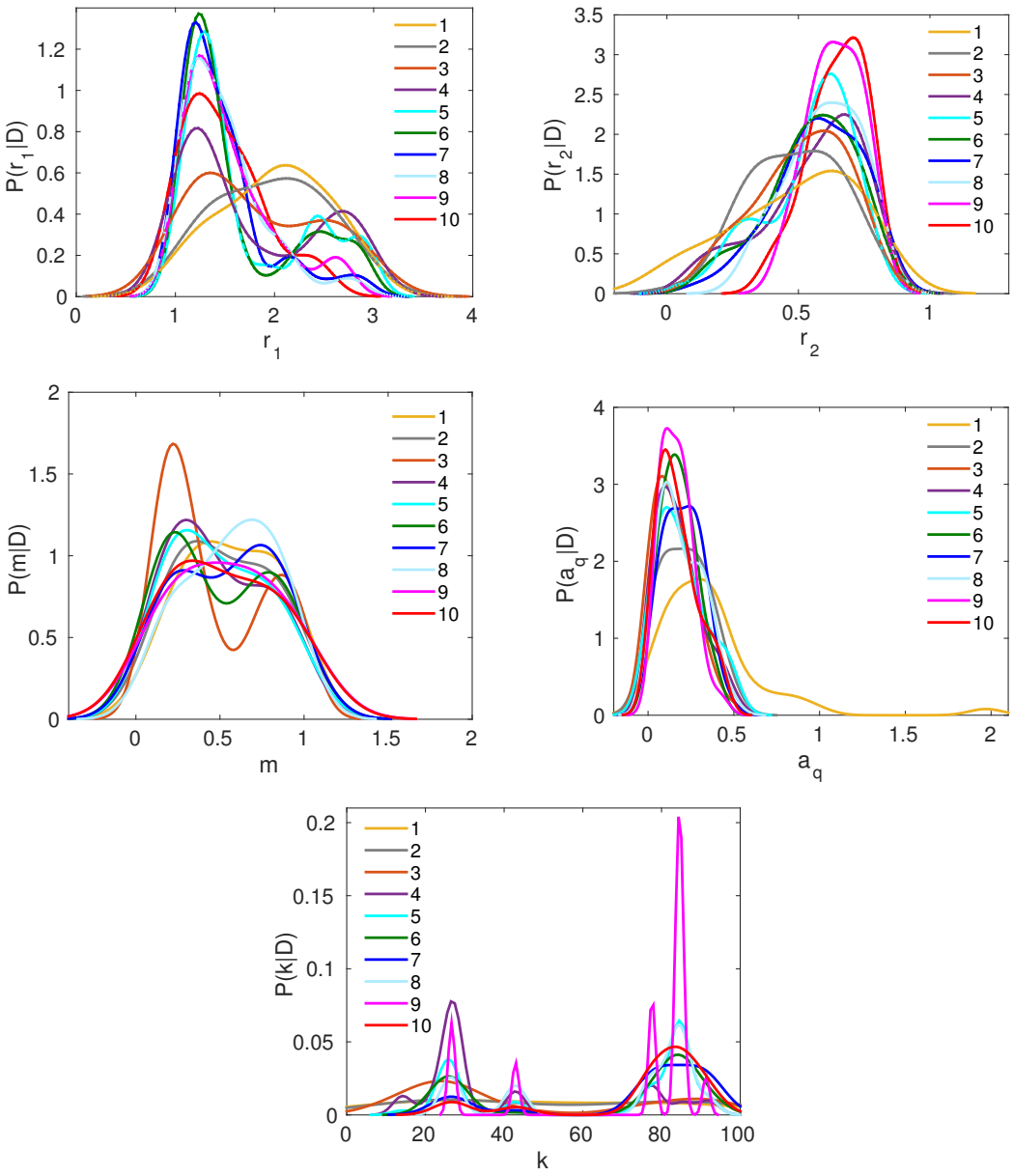

Figure B.5: Smooth probability density estimates calculated using MATLAB's `ksdensity` function for (top left) the growth rate of the preferred prey, (top right) the growth rate of the alternative prey, (middle left) the predator death rate, (middle right) the slope of the preference trade-off, and (bottom) the steepness of the tanh function of the selective predator in the smooth model I (4.1) using the ABC SMC method [129] (steps 1–7) and 1998 data. In the ABC SMC method ($L = 10$, $N = 50$), we construct the sequence of tolerance levels ϵ_l ($l = l, ..., 10$) linearly spaced between when 10% ($\epsilon_1 \approx 0.71$) and when 1% ($\epsilon_{10} \approx 0.32$) of the candidate samples θ^* are accepted in the ABC rejection method (steps I–VI) for the smooth model I (4.1).

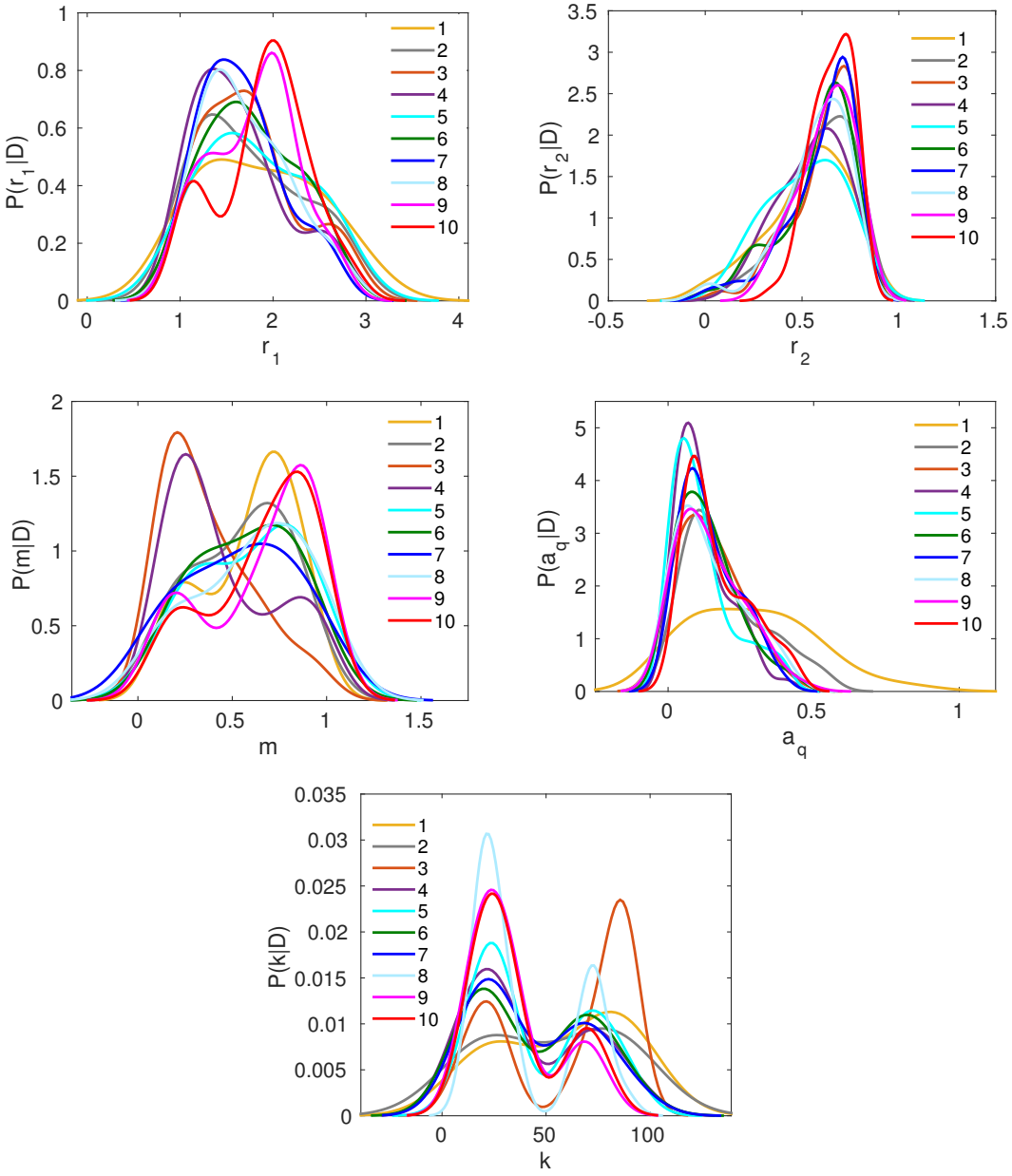

Figure B.6: Smooth probability density estimates calculated using MATLAB's `ksdensity` function for (top left) the growth rate of the preferred prey, (top right) the growth rate of the alternative prey, (middle left) the predator death rate, (middle right) the slope of the preference trade-off, and (bottom) the steepness of the tanh function of the unselective predator in the smooth model I (4.1) using the ABC SMC method [129] (steps 1–7) and 1998 data. In the ABC SMC method ($L = 10$, $N = 50$), we construct the sequence of tolerance levels ϵ_l ($l = l, ..., 10$) linearly spaced between when 10% ($\epsilon_1 \approx 0.60$) and when 1% ($\epsilon_{10} \approx 0.35$) of the candidate samples θ^* are accepted in the ABC rejection method (steps I–VI) for the smooth model I (4.1).

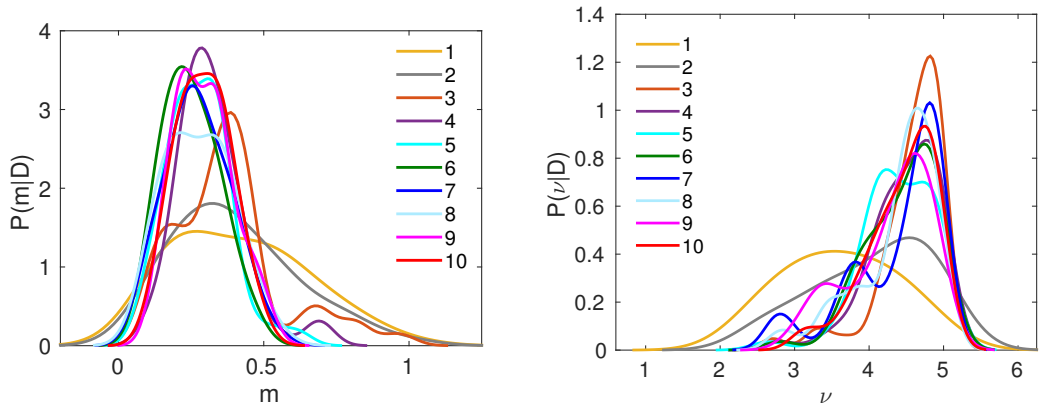

Figure B.7: Smooth probability density estimates calculated using MATLAB's `ksdensity` function for (left) the total predator death rate and (right) the perturbation from the steady state IV of the total predator population (i.e., $z(0) = \nu\tilde{z}$) in the smooth model II (4.13) using the ABC SMC method [129] (steps 1–7) and 1991 data. In the ABC SMC method ($L = 10$, $N = 50$), we construct the sequence of tolerance levels ϵ_l ($l = l, ..., 10$) linearly spaced between when 10% ($\epsilon_1 \approx 0.71$) and when 1% ($\epsilon_{10} \approx 0.32$) of the candidate samples θ^* are accepted in the ABC rejection method (steps I–VI) for the smooth model II (4.13).

for the total predator population fitted to the total predator 1991 data. The mean distance to the data produced by the model (4.13) is 0.32. For the smooth probability density functions of m and ν at each iteration (i.e., $l = 1, \ldots, 10$), see Figure B.7.

In the case of year 1998, we obtain with our ABC SMC implementation that the mean of the accepted samples at the final iteration (i.e., $l = 10$) for the total predator population in 1998 is $(m^*, \nu^*) = (0.66, 2.2)$, and the mean distance to the data produced by the model (4.13) is 0.20. For the smooth probability density functions of m and ν at each iteration (i.e., $l = 1, \ldots, 10$), see Figure B.8.

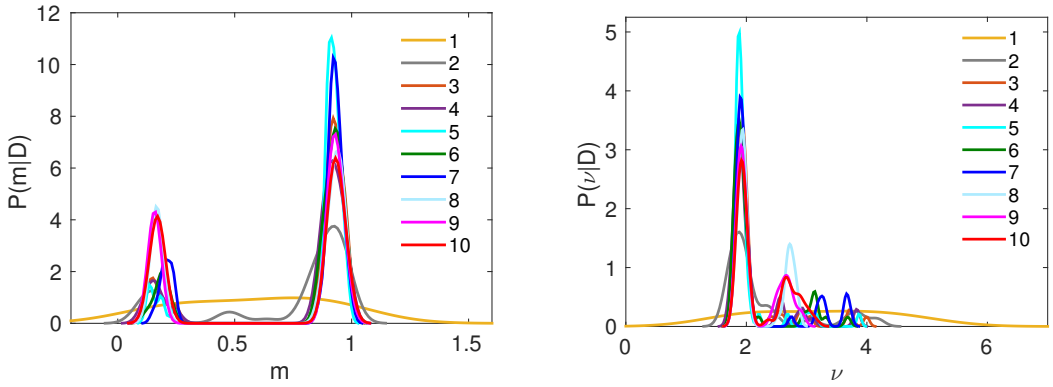

Figure B.8: Smooth probability density estimates calculated using MATLAB's `ksdensity` function for (left) the total predator death rate and (right) the perturbation from the steady state IV of the total predator population (i.e., $z(0) = \nu\tilde{z}$) in the smooth model II (4.13) using the ABC SMC method [129] (steps 1–7) and 1998 data. In the ABC SMC method ($L = 10$, $N = 50$), we construct the sequence of tolerance levels ϵ_l ($l = l, ..., 10$) linearly spaced between when 10% ($\epsilon_1 \approx 0.31$) and when 1% ($\epsilon_{10} \approx 0.21$) of the candidate samples θ^* are accepted in the ABC rejection method (steps I–VI) for the smooth model II (4.13).

References

[1] P. A. Abrams. The evolution of predator-prey interactions: Theory and evidence. *Annual Review of Ecology and Systematics*, 31:79–105, 2000.

[2] P. A. Abrams and H. Matsuda. Positive indirect effects between prey species that share predators. *Ecology*, 77:610–616, 1996.

[3] P. A. Abrams and H. Matsuda. Population dynamical consequences of reduced predator switching at low total prey densities. *Population Ecology*, 45:175–185, 2003.

[4] T. R. Anderson. Plankton functional type modelling: Running before we can walk? *Journal of Plankton Research*, 27:1071–1081, 2005.

[5] D. Avitabile, M. Homer, A. R. Champneys, J. C. Jackson, and D. Robert. Mathematical modelling of the active hearing process in mosquitoes. *Journal of The Royal Society Interface*, 7:105–122, 2010.

[6] E. Bäurle and U. Gaedke. *Lake Constance—characterization of an ecosystem in transition*, volume 53 of *Archiv für Hydrobiologie Special Issues in Advances in Limnology*. E. Schweizerbartische Verlagsbuchhandlung, 1999.

[7] M. A. Beaumont. Approximate Bayesian Computation in evolution and ecology. *Annual Review of Ecology, Evolution, and Systematics*, 41:379–406, 2010.

[8] L. Becks, S. P. Ellner, L. E. Jones, and N. G. Hairston Jr. Reduction of adaptive genetic diversity radically alters eco-evolutionary community dynamics. *Ecology Letters*, 13:989–997, 2010.

[9] R. Black. "Plankton decline across oceans as waters warm". BBC News Science and Environment, 2010. `http://www.bbc.co.uk/news/science-environment-10781621` Accessed: 12-06-2013.

[10] B. J. M. Bohannan and R. E. Lenski. Linking genetic change to community evolution: Insights from studies of bacteria and bacteriophage. *Ecology Letters*, 3:362–377, 2000.

[11] D. S. Boukal and V. Křivan. Lyapunov functions for lotka-volterra predator-prey models with optimal foraging behavior. *Journal of Mathematical Biology*, 39:493–517, 1999.

[12] D. G. Boyce, M. R. Lewis, and B. Worm. Global phytoplankton decline over the past century. *Nature*, 466:591–596, 2010.

[13] F. Brauer and C. Castello-Chávez. *Mathematical Models in Population Biology and Epidemiology*. Springer, 2012.

[14] G. Casey, H. De Jong, and Gouzé J.-L. Piecewise-linear models of genetic regulatory networks: Equilibria and their stability. *Journal of Mathematical Biology*, 52:27–56, 2006.

[15] A. R. Champneys and M. di Bernardo. *Piecewise smooth dynamical systems.* Scholarpedia 3(9):4041, 2008. `http://www.scholarpedia.org/article/Piecewise_smooth_dynamical_systems/` Accessed: 12-06-2013.

[16] A. Colombo, M. di Bernardo, S. J. Hogan, and M. R. Jeffrey. Bifurcations of piecewise smooth flows: Perspectives, methodologies and open problems. *Physica D*, 241:1845–1860, 2012.

[17] M. H. Cortez and S. P. Ellner. Understanding rapid evolution in predator-prey interactions using the theory of fast-slow dynamical systems. *The American Naturalist*, 176:E109–E127, 2010.

[18] R. Cropp and J. Norbury. Parameterizing plankton functional type models: Insights from a dynamical systems perspective. *Journal of Plankton Research*, 31:939–963, 2009.

[19] D. H. Cushing. The seasonal variation in oceanic production as a problem in population dynamics. *Journal du Conseil/Conseil Permanent International pour l'Exploration de la Mer*, 24:455–464, 1959.

[20] V. Dakos, E. Beninca, E. H. van Nes, C. J. Philippart, M. Scheffer, and J. Huisman. Interannual variability in species composition explained as seasonally entrained chaos. *Proceedings of the Royal Society of London. Series B: Biological Sciences*, 276:2871–2880, 2009.

[21] C. R. Darwin. *The Origin of Species.* John Murray, 1859.

[22] F. Dercole, A. Gragnani, and S. Rinaldi. Bifurcation analysis of piecewise-smooth ecological models. *Theoretical Population Biology*, 72:197–213, 2007.

[23] M. di Bernardo, C. J. Budd, A. R. Champneys, and P. Kowalczyk. *Piecewise-Smooth Dynamical Systems*. Springer, 2008.

[24] J. M. Drake and B. D. Griffen. Early warning signals of extinction in deteriorating environments. *Nature*, 467:456–459, 2010.

[25] M. Edwards, G. Beaugrand, D.G. Johns, P. Helaouet, P. Licandro, A McQuatters-Gollop, and M. Wootton. Ecological Status Report: Results from the CPR survey 2009/2010. SAHFOS Technical Report 8:1-8, Sir Alister Hardy Foundation for Ocean Science, Plymouth U.K., 2011.

[26] G. T. Evans. A framework for discussing seasonal succession and coexistence of phytoplankton species. *Limnology and Oceanography*, 33:1027–1036, 1988.

[27] P. G. Falkowski, M. E. Katz, A. H. Knoll, A. Quigg, J. A. Raven, O. Schofield, and F. J. R. Taylor. The evolution of modern eukaryotic phytoplankton. *Science*, 305:354–360, 2004.

[28] M. J. R. Fasham, H. W. Ducklow, and S. M. McKelvie. A nitrogen-based model of plankton dynamics in the oceanic mixed layer. *Journal of Marine Research*, 48:591–639, 1990.

[29] A. F. Filippov. *Differential Equations with Discontinuous Righthand Sides*. Kluwer Academic Publishers Dordrecht, The Netherlands, 1988.

[30] FAO Fisheries and Aquaculture Department. *The state of world fisheries and aquaculture 2012*. Food and Agriculture Organization of the United Nations, 2012. `http://www.fao.org/docrep/016/i2727e/i2727e.pdf` Accessed: 12-06-2013.

[31] R. FitzHugh. Impulses and physiological states in models of nerve membranes. *Biophysical Journal*, 1:445–466, 1961.

[32] Y. Forterre. Slow, fast and furious: Understanding the physics of plant movements. *Journal of Experimental Botany*, 64:4745–4760, 2013.

[33] P. S. J. Franks. NPZ models of plankton dynamics: Their construction, coupling to physics and application. *Journal of Oceanography*, 58:379–387, 2002.

[34] E. Freire, E. Ponce, and J. Ros. The focus-center-limit cycle bifurcation in symmetric 3D piecewise linear systems. *SIAM Journal on Applied Mathematics*, 65:1933–1951, 2005.

[35] J. A. Freund, S. Mieruch, B. Scholze, K. Wiltshire, and U. Feudel. Bloom dynamics in a seasonally forced phytoplankton–zooplankton model: Trigger mechanisms and timing effects. *Ecological Complexity*, 3:129–139, 2006.

[36] N. Fuentes, H. Güde, M. Wessels, and D. Straile. Allochthonous contribution to seasonal and spatial variability of organic matter sedimentation in a deep oligotrophic lake (Lake Constance). *Limnologica–Ecology and Management of Inland Waters*, 43:122–130, 2013.

[37] G. F. Fussmann, S. P. Ellner, K. W. Shertzer, and N. G. Hairston Jr. Crossing the Hopf bifurcation in a live predator-prey system. *Science*, 290:1358–1360, 2000.

[38] G. F. Fussmann, M. Loreau, and P. A. Abrams. Eco-evolutionary dynamics of communities and ecosystems. *Functional Ecology*, 21:465–477, 2007.

[39] U. Gaedke, 2012. personal communication.

[40] M. Gao, H. Shi, and Z. Li. Chaos in a seasonally and periodically forced phytoplankton–zooplankton system. *Nonlinear Analysis: Real World Applications*, 10:1643–1650, 2009.

[41] R. A. Gatenby, J. Brown, and T. Vincent. Lessons from applied ecology: Cancer control using an evolutionary double bind. *Cancer Research*, 69:7499–7502, 2009.

[42] G. F. Gause, N. P. Smaragdova, and A. A. Witt. Further studies of interaction between predators and prey. *Journal of Animal Ecology*, 5:1–18, 1936.

[43] S. A. H. Geritz, E. Kisdi, G. Meszena, and J. A. J. Metz. Evolutionarily singular strategies and the adaptive growth and branching of the evolutionary tree. *Evolutionary Ecology*, 12:35–57, 1998.

[44] A. Gierer and H. Meinhardt. A theory of biological pattern formation. *Kybernetic*, 12:30–39, 1972.

[45] L. Glass. Classification of biological networks by their qualitative dynamics. *Journal of Theoretical Biology*, 54:85–107, 1975.

[46] P. R. Grant and B. R. Grant. Unpredictable evolution in a 30-year study of Darwin's finches. *Science*, 296:707–711, 2002.

[47] J. Guckenheimer. *Bifurcation.* Scholarpedia 2(6):1517, 2007. `http://www.scholarpedia.org/article/Bifurcation` Accessed: 01-05-2014.

[48] J. Guckenheimer and P. Holmes. *Nonlinear Oscillations, Dynamical Systems, and Bifurcations of Vector Fields.* Springer, 1996.

[49] N. G. Hairston, S. P. Ellner, M. A. Geber, T. Yoshida, and J. A. Fox. Rapid evolution and the convergence of ecological and evolutionary time. *Ecology Letters*, 8:1114–1127, 2005.

[50] N. G. Hairston, Jr., W. Lampert, C. E. Cáceres, C. L. Holtmeier, L. J. Weider, U. Gaedke, J. M. Fischer, J. A. Fox, and D. M. Post. Lake ecosystems: Rapid evolution revealed by dormant eggs. *Nature*, 401:446, 1999.

[51] A. G. Haldane and R. M. May. Systemic risk in banking ecosystems. *Nature*, 469:351–355, 2011.

[52] A. L. Hodgkin and A. F. Huxley. A quantitative description of membrane current and its application to conduction and excitation in nerve. *Journal of Physiology*, 117:500–544, 1952.

[53] C. S. Holling. The functional response of predators to prey density and its role in mimicry and population regulation. *Memoirs of the Entomological Society of Canada*, 97:5–60, 1965.

[54] R. D. Holt. Predation, apparent competition and the structure of prey community. *Theoretical Population Biology*, 12:197–229, 1977.

[55] R. R. Hood, E. A. Laws, and R. A. Armstrong. Pelagic functional group modeling: Progress, challenges and prospects. *Deep-Sea Research II*, 53:459–512, 2006.

[56] S. Hoops, S. Sahle, R. Gauges, C. Lee, J. Pahle, N. Simus, M. Singhal, L. Xu, P. Mendes, and U. Kummer. COPASI–a COmplex PAthway SImulator. *Bioinformatics*, 22:3067–3074, 2006.

[57] F. Hoppensteadt. *Predator-prey model*. Scholarpedia 1(10):1563, 2006. `http://www.scholarpedia.org/article/Predator-prey_model` Accessed: 24-04-2014.

[58] A. Huppert, B. Blasius, R. Olinky, and L. Stone. A model for seasonal phytoplankton blooms. *Journal of Theoretical Biology*, 236:276–290, 2005.

[59] A. Huppert, B. Blasius, and L. Stone. A model of phytoplankton blooms. *The American Naturalist*, 159:156 –171, 2002.

[60] M. R. Jeffrey and S. J. Hogan. The geometry of generic sliding bifurcations. *SIAM Review*, 53:505–525, 2011.

[61] L. E. Jones, L. Becks, S. P. Ellner, N. G. Jr Hairston, T. Yoshida, and G. F. Fussmann. Rapid contemporary evolution and clonal food web dynamics. *Philosophical Transactions of the Royal Society of London B: Biological Sciences*, 364:1579 –1591, 2009.

[62] L. E. Jones and S. P. Ellner. Effects of rapid prey evolution on predator-prey cycles. *Journal of Mathematical Biology*, 55:541–573, 2007.

[63] S. A. Kelly, T. M. Panhuis, and A. M. Stoehr. Phenotypic plasticity: Molecular mechanisms and adaptive significance. *Comprehensive Physiology*, 2:1417–1439, 2012.

[64] A. I. Khibnik and A. S. Kondrashov. Three mechanisms of red queen dynamics. *Proceedings of the Royal Society of London. Series B: Biological Sciences*, 264:1049–1056, 1997.

[65] C. A. Klausmeier. Successional state dynamics: A novel approach to modeling nonequilibrium foodweb dynamics. *Journal of Theoretical Biology*, 262:584–595, 2010.

[66] J. M. Kneitel and J. M. Chase. Trade-offs in community ecology: Linking spatial scales and species coexistence. *Ecology Letters*, 7:69–80, 2004.

[67] M. Kondoh. Foraging adaptation and the relationship between food-web complexity and stability. *Science*, 299:1388–1391, 2003.

[68] A. Korobeinikov and G. C. Wake. Global properties of the three-dimensional predator-prey Lotka-Volterra system. *Journal of Applied Mathematics and Decision Sciences*, 3:155–162, 1999.

[69] P. Kowalczyk and P. Glendinning. Boundary-equilibrium bifurcations in piecewise-smooth slow-fast systems. *Chaos*, 21(2), 2011.

[70] V. Křivan. Optimal foraging and predator-prey dynamics I. *Theoretical Population Biology*, 49:265–290, 1996.

[71] C. Kuehn. *Multiple Time Scale Dynamics*. Preprint version, 2014/2015.

[72] Y. A. Kuznetsov. *Elements of Applied Bifurcation Theory*. Springer, 1998.

[73] Y. A. Kuznetsov, S. Rinaldi, and A. Gragnani. One-parameter bifurcations in planar Filippov systems. *International Journal of Bifurcation and Chaos*, 13:2157–2188, 2003.

[74] V. Křivan. Dynamic ideal free distribution: Effects of optimal patch choice on predator-prey dynamics. *The American Naturalist*, 149:167–178, 1997.

[75] V. Křivan and J. Eisner. Optimal foraging and predator-prey dynamics, III. *Theoretical Population Biology*, 63:269–279, 2003.

[76] V. Křivan and J. Eisner. The Lotka-Volterra predator-prey model with foraging-predation risk trade-offs. *The American Naturalist*, 170:771–782, 2007.

[77] V. Křivan and A. Sikder. Optimal foraging and predator-prey dynamics II. *Theoretical Population Biology*, 55:111–126, 1999.

[78] W. Lampert and U. Sommer. *Limnoecology: The Ecology of Lakes and Streams*. Oxford University Press, 2007.

[79] R. Lande. A quantitative genetic theory of life history evolution. *Ecology*, 63:607–615, 1982.

[80] O. Larink and W. Westheide. *Coastal Plankton. Photo Guide for European Seas*. Verlag Dr. Friedrich Pfeil, 2011.

[81] C. Le Quéré. Reply to horizons article "Phytoplankton functional type modelling: Running before we can walk?" I. Abrupt changes in marine ecosystems? *Journal of Plankton Research*, 28:871–872, 2006.

[82] S. A. Levin and J. D. Udovic. A mathematical model of coevolving populations. *The American Naturalist*, 111:657–675, 1977.

[83] E. Litchman and C. A. Klausmeier. Trait-based community ecology of phytoplankton. *Annual Review of Ecology, Evolution, and Systematics*, 39:615–639, 2008.

[84] E. Litchman, C. A. Klausmeier, O. M. Schofield, and P. G. Falkowski. The role of functional traits and trade-offs in structuring phytoplankton communities: Scaling from cellular to ecosystem level. *Ecology Letters*, 10:1170–1181, 2007.

[85] A. J. Lotka. Undamped oscillations derived from the law of mass action. *Journal of the American Chemical Society*, 42:1595–1599, 1920.

[86] R. Macey, G. Oster, and T. Zahley. *Berkeley Madonna*. `http://www.berkeleymadonna.com/` Accessed: 25-04-2014, 2000.

[87] D. L. Mackas. Does blending of chlorophyll data bias temporal trend? *Nature*, 472:E4–E5, 2011.

[88] T. Maiwald and J. Timmer. Dynamical modeling and multi-experiment fitting with PottersWheel. *Bioinformatics*, 24:2037–2043, 2008.

[89] P. Marjoram, J. Molitor, V. Plagnol, and S. Tavaré. Markov chain monte carlo without likelihoods. *Proceedings of the National Academy of Sciences*, 100:15324–15328, 2003.

[90] MATLAB. *Version 8.1.0.604 (R2013a)*. The MathWorks Inc., Natick, Massachusetts, 2013.

[91] B. J. McGill, B. J. Enquist, E. Weiher, and M. Westoby. Rebuilding community ecology from functional traits. *Trends in Ecology and Evolution*, 21:178–185, 2006.

[92] A. McQuatters-Gollop, P. C. Reid, M. Edwards, P. H. Burkill, C. Castellani, S. Batten, W. Gieskes, D. Beare, R. R. Bidigare, E. Head, R. Johnson,

M. Kahru, J. A. Koslow, and A. Pena. Is there a decline in marine phytoplankton? *Nature*, 472:E6–E7, 2011.

[93] A. Merico, J. Bruggeman, and K.W. Wirtz. A trait-based approach for downscaling complexity in plankton ecosystem models. *Ecological Modelling*, 220:3001–3010, 2009.

[94] H. Müller and A. Schlegel. Responses of three freshwater planktonic ciliates with different feeding modes to cryptophyte and diatom prey. *Aquatic Microbial Ecology*, 17:49–60, 1999.

[95] W. W. Murdoch. Switching in general predators: Experiments on prey specificity and stability of prey populations. *Ecological Monographs*, 39:335–354, 1969.

[96] J. Murdock. *Unfoldings*. Scholarpedia 1(12):1904, 2006. `http://www.scholarpedia.org/article/Unfoldings` Accessed: 19-05-2014.

[97] J. D. Murray. *Mathematical Biology: I. An Introduction*. Springer, 2002.

[98] J. Nagumo, S. Arimoto, and S. Yoshizawa. An active pulse transmission line simulating nerve axon. *Proceedings of the Institute of Radio Engineers*, 50:2061–2070, 1962.

[99] A. B. Nordmark. Non-periodic motion caused by grazing incidence in an impact oscillator. *Journal of Sound and Vibration*, 145:279–297, 1991.

[100] F. Pelletier, T. Clutton-Brock, J. Pemberton, S. Tuljapurkar, and T. Coulson. The evolutionary demography of ecological change: Linking trait variation and population growth. *Science*, 315:1571–1574, 2007.

[101] P. Piiroinen and Y. A. Kuznetsov. An event-driven method to simulate Filippov systems with accurate computing of sliding motions. *ACM Transactions on Mathematical Software*, 34:13:1–13:24, 2008.

[102] S. H. Piltz, M. A. Porter, and P. K. Maini. Prey switching with a linear preference trade-off. *SIAM Journal on Applied Dynamical Systems*, 13:658–682, 2014.

[103] T. Platt, G. N. White III, L. Zhai, S. Sathyendranath, and S. Roy. The phenology of phytoplankton blooms: Ecosystem indicators from remote sensing. *Ecological Modelling*, 220:3057–3069, 2009.

[104] D. M. Post, M. E. Conners, and D. S. Goldberg. Prey preference by a top predator and the stability of linked food chains. *Ecology*, 81:8–14, 2000.

[105] J. K. Pritchard, M. T. Seielstad, A. Perez-Lezaun, and M. W. Feldman. Population growth of human Y chromosomes: A study of Y chromosome microsatellites. *Molecular Biology and Evolution*, 16:1791–1798, 1999.

[106] D. J. Rapport. An optimization model of food selection. *The American Naturalist*, 105:575–587, 1971.

[107] P. C. Reid, G. Gorick, and M. Edwards. Climate change and European Marine Ecosystem Research. Technical report, Sir Alister Hardy Foundation for Ocean Science, Plymouth U.K., 2011.

[108] A. C. Revkin. "On plankton, warming and whiplash". The New York Times, 2011. `http://dotearth.blogs.nytimes.com/2011/04/26/on-plankton-warming-and-whiplash/` Accessed: 12-06-2013.

[109] M. L. Rosenzweig and R. H. MacArthur. Graphical representation and stability conditions of predator-prey interaction. *The American Naturalist*, 97:209–223, 1963.

[110] R. R. Rykaczewski and J. P. Dunne. A measured look at ocean chlorophyll trends. *Nature*, 472:E5–E6, 2011.

[111] M. Scheffer, S. Rinaldi, Y. Kuznetsov, and E. H. van Nes. Seasonal dynamics of Daphnia and algae explained as a periodically forced predator-prey systems. *Oikos*, 80:519–532, 1997.

[112] M. Shimada, Y. Ishii, and Harunobu Shibao. Rapid adaptation: A new dimension for evolutionary perspectives in ecology. *Population Ecology*, 52:5–14, 2010.

[113] D. J. W. Simpson and R. Kuske. Stochastically perturbed sliding motion in piecewise-smooth systems. arXiv:1204.5792, 2012. Submitted.

[114] D. J. W. Simpson and J. D. Meiss. Andronov-Hopf bifurcations in planar, piecewise-smooth, continuous flows. *Physics Letters A*, 371:213–220, 2007.

[115] L. B. Slobodkin. *Growth and Regulation of Animal Populations*. Holt, Rinehart, and Winston, 1961.

[116] U. Sommer, R. Adrian, L. De Senerpont Domis, J. J. Elser, U. Gaedke, B. Ibelings, E. Jeppesen, M. Lurling, J. C. Molinero, W. M. Mooij, E. van Donk, and M. Winder. Beyond the Plankton Ecology Group (PEG) model: Mechanisms driving plankton succession. *Annual Review of Ecology, Evolution, and Systematics*, 43:429–448, 2012.

[117] U. Sommer, Z. M. Gliwicz, W. Lampert, and A. Duncan. The PEG-model of seasonal succession of planktonic events in freshwaters. *Archiv für Hydrobiologie*, 106:433–471, 1986.

[118] J. Sotomayor and M. A. Teixeira. Regularization of discontinuous vector fields. In *International Conference on Differential Equations, Lisboa, Equadiff 95, 1996*, pages 207–223, 1996.

[119] C. F. Steiner, A. S. Schwaderer, V. Huber, C. A. Klausmeier, and E. Litchman. Periodically forced food-chain dynamics: Model predictions and experimental validation. *Ecology*, 90:3099–3107, 2009.

[120] D. W. Stephens and J. R. Krebs. *Foraging Theory*. Princeton University Press, 1986.

[121] S. H. Strogatz. *Nonlinear Dynamics and Chaos*. Westview, 1994.

[122] J. Sun, E. M. Bollt, M. A. Porter, and M. S. Dawkins. A mathematical model for the dynamics and synchronization of cows. *Physica D*, 240:1497–1509, 2011.

[123] M. A. Teixeira and P. R. da Silva. Regularization and singular perturbation techniques for non-smooth systems. *Physica D*, 241:1948–1955, 2012.

[124] E. Teramoto, K. Kawasaki, and N Shigesada. Switching effect of predation on competitive prey species. *Journal of Theoretical Biology*, 79:303–315, 1979.

[125] K. Tirok and U. Gaedke. Spring weather determines the relative importance of ciliates, rotifers and crustaceans for the initiation of the clear-water phase in a large, deep lake. *Journal of Plankton Research*, 28:361–373, 2006.

[126] K. Tirok and U. Gaedke. Regulation of planktonic ciliate dynamics and functional composition during spring in Lake Constance. *Aquatic Microbial Ecology*, 49:87–100, 2007.

[127] K. Tirok and U. Gaedke. The effect of irradiance, vertical mixing and temperature on spring phytoplankton dynamics under climate change: Long-term observations and model analysis. *Oecologia*, 150:625–642, 2007.

[128] K. Tirok and U. Gaedke. Internally driven alternation of functional traits in a multispecies predator-prey system. *Ecology*, 91:1748–1762, 2010.

[129] T. Toni, D. Welch, N. Strelkowa, A. Ipsen, and M. P. Stumpf. Approximate Bayesian computation scheme for parameter inference and model selection in dynamical systems. *Journal of the Royal Society Interface*, 6:187–202, 2009.

[130] J. Truscott and J. Brindley. Ocean plankton populations as excitable media. *Bulletin of Mathematical Biology*, 56:981–998, 1994.

[131] V. I. Utkin. *Sliding Modes in Control Optimization*. Springer-Verlag, 1992.

[132] B. van der Pol. A theory of the amplitude of free and forced triode vibrations. *Radio Review*, 1:701–710, 1920.

[133] E. van Leeuwen, Å. Brännström, V. A. A. Jansen, U. Dieckmann, and A. G. Rossberg. A generalized functional response for predators that switch between multiple prey species. *Journal of Theoretical Biology*, 328:89–98, 2013.

[134] E. van Leeuwen, V. A. A. Jansen, and P. W. Bright. How population dynamics shape the functional response in a one-predator-two-prey system. *Ecology*, 88:1571–1581, 2007.

[135] E. H. van Nes and M. Scheffer. What minimal models cannot tell: A comment on a model of phytoplankton blooms. *The American Naturalist*, 163:924–926, 2004.

[136] P. Verity. Feeding in planktonic protozoans: Evidence for nonrandom acquisition of prey. *The Journal of Protozoology*, 38:69–76, 1991.

[137] V. Volterra. Variations and fluctuations of a number of individuals in animal species living together. In: Animal Ecology. pp. 409–448. McGraw Hill, New York, 1931. Translation by R. N. Chapman.

[138] R. J. Williams. Effects of network and dynamical model structure on species persistence in large model food webs. *Theoretical Ecology*, 1:141–151, 2008.

[139] M. Yamamichi, T. Yoshida, and A. Sasaki. Comparing the effects of rapid evolution and phenotypic plasticity on predator-prey dynamics. *The American Naturalist*, 178:287–304, 2011.

[140] T. Yoshida, L. E. Jones, S. P. Ellner, G. F. Fussman, and N. G. Hairston Jr. Rapid evolution drives ecological dynamics in a predator-prey system. *Nature*, 424:303–306, 2003.